PNNL-11211
UC-721

Ferrocyanide Safety Project
Ferrocyanide Aging Studies
Final Report

M. A. Lilga
R. T. Hallen
E. V. Alderson
M. O. Hogan
T. L. Hubler
G. L. Jones
D. J. Kowalski
M. R. Lumetta
W. F. Riemath
R. A. Romine
G. F. Schiefelbein
M. R. Telander

June 1996

Prepared for Westinghouse Hanford Company
Waste Tank Safety Program under
Contract DE-AC06-76RLO 1830
with the U.S. Department of Energy

Pacific Northwest National Laboratory
Operated for the U.S. Department of Energy
by Battelle

Battelle

PNNL-11211

PACIFIC NORTHWEST NATIONAL LABORATORY
operated by
BATTELLE
for the
UNITED STATES DEPARTMENT OF ENERGY
under Contract DE-AC06-76RLO 1830

Printed in the United States of America

Available to DOE and DOE contractors from the Office of Scientific and Technical Information, P.O. Box 62, Oak Ridge, TN 37831; prices available from (615) 576-8401.

Available to the public from the National Technical Information Service, U.S. Department of Commerce, 5285 Port Royal Rd., Springfield, VA 22161

PNNL-11211
UC-721

Ferrocyanide Safety Project
Ferrocyanide Aging Studies
Final Report

M. A. Lilga
R. T. Hallen
E. V. Alderson
M. O. Hogan
T. L. Hubler
G. L. Jones
D. J. Kowalski
M. R. Lumetta
W. F. Riemath
R. A. Romine
G. F. Schiefelbein
M. R. Telander

June 1996

Prepared for
Westinghouse Hanford Company
Waste Tank Safety Program
under Contract DE-AC06-76RLO 1830
with the U.S. Department of Energy

Pacific Northwest National Laboratory
Richland, Washington 99352

Summary

This final report gives the results of the work conducted by Pacific Northwest National Laboratory (PNNL) from FY 1992 to FY 1996 on the Ferrocyanide Aging Studies, part of the Ferrocyanide Safety Project. The Ferrocyanide Safety Project was initiated as a result of concern raised about the safe storage of ferrocyanide waste intermixed with oxidants, such as nitrate and nitrite salts, in Hanford Site single-shell tanks (SSTs). In the laboratory, such mixtures can be made to undergo uncontrolled or explosive reactions by heating dry reagents to over 200°C. In 1987, an Environmental Impact Statement (EIS), published by the U.S. Department of Energy (DOE), *Final Environmental Impact Statement, Disposal of Hanford Defense High-Level Transuranic and Tank Waste, Hanford Site, Richland, Washington*, included an environmental impact analysis of potential explosions involving ferrocyanide-nitrate mixtures. The EIS postulated that an explosion could occur during mechanical retrieval of saltcake or sludge from a ferrocyanide waste tank, and concluded that this worst-case accident could create enough energy to release radioactive material to the atmosphere through ventilation openings, exposing persons offsite to a short-term radiation dose of approximately 200 mrem. Later, in a separate study (1990), the General Accounting Office postulated a worst-case accident of one to two orders of magnitude greater than that postulated in the DOE EIS. The uncertainties regarding the safety envelope of the Hanford Site ferrocyanide waste tanks led to the declaration of the Ferrocyanide Unreviewed Safety Question (USQ) in October 1990.

A special Hanford Ferrocyanide Task Team was commissioned to address all technical aspects of tanks containing ferrocyanide wastes. The Hanford Ferrocyanide Task Team consisted of technical experts from Westinghouse Hanford Company (WHC), PNNL, and outside consultants. Their goals were to resolve the USQ by defining safety criteria, categorize the safety of the tank waste, and resolve the Ferrocyanide Safety Issue by ensuring that the waste is stored safely.

Numerous studies conducted by the Task Team defined safety criteria and resulted in closure of the USQ in March 1994. The potential for ferrocyanide reactions in Hanford Site SSTs was evaluated, and the energy released during these reactions was quantified. Dynamic X-ray diffraction was also used to identify specific reactions and to quantify reaction rates. In addition, a number of experimental and theoretical studies were conducted in an effort to analyze the thermal characteristics of the tanks and to investigate the likelihood of "hot spots" forming as a result of radiolytic heating.

Resolving the Ferrocyanide Safety Issue requires that tank contents meet the safety criteria and operations be conducted such that waste conditions fall within the criteria limits. Because the ferrocyanide sludge has been exposed for many years to other highly caustic wastes, as well as to elevated temperatures and both gamma and beta radiation, ferrocyanide decomposition has occurred in the tanks. As a result, the concentration of ferrocyanide is less than that predicted by tank inventory records. As such, C-Farm tanks have been re-categorized as safe, allowing resolution of the Ferrocyanide Safety Issue for these tanks.

The goal of the Ferrocyanide Aging Studies task of the Ferrocyanide Safety Project was to contribute to the resolution of the Ferrocyanide Safety Issue by defining the long-term chemical and radiolytic decomposition ("aging") of ferrocyanide materials under conditions found in the SSTs. Information from these studies has provided baseline data for comparison with actual SST waste samples as they are obtained and analyzed. The results of the Aging Studies have directly assisted in determining the strategy for safe storage of the ferrocyanide waste in the tanks and how the Ferrocyanide Safety Issue was to be resolved.

In the PNNL studies, ferrocyanide waste simulants were used instead of actual waste. The simulants used in these studies were primarily In-Farm simulants, prepared by WHC to mimic the waste generated when the In-Farm flowsheet was used to remove radiocesium from waste supernates in the SSTs. In the In-Farm flowsheet, nickel ion and ferrocyanide anion were added to waste supernate to precipitate sodium nickel ferrocyanide and co-precipitate radiocesium. Once the radiocesium was removed, supernates were pumped from the tanks and disposed to the ground via cribs. Later, new wastes from cladding removal processes and/or from evaporators were added. These new wastes were typically highly caustic, having hydroxide ion concentrations of over 1 *M* and as high as 4 *M*. The Aging Studies investigated possible reactions between this caustic waste and the precipitated ferrocyanide waste in a radiation field.

Over a 5-year period, these studies demonstrated and characterized the aging of ferrocyanide waste simulants through dissolution and hydrolysis processes. The experiments show the ultimate products are ammonia (which is slowly radiolyzed), carbonate, and oxides or hydroxides of iron and nickel. Thus, most of the fuel value in the solid phase is consumed in the process. Any ferrocyanide tank waste that contacted highly caustic waste also would undergo similar aging processes. The rate of aging is primarily a function of the waste temperature. Tank records indicate that most tanks were at a sufficiently high temperature for a long enough time that significant aging would be expected. Waste samples from C-Farm tanks contained very little, if any, ferrocyanide and may be the best evidence that aging occurs in ferrocyanide tanks.

The major results from the experimental work conducted for these studies are discussed below:

- Sodium nickel ferrocyanide, $Na_2NiFe(CN)_6$, in simulants was shown to dissolve in basic solutions, forming insoluble nickel hydroxide, $Ni(OH)_2$, and soluble sodium ferrocyanide, $Na_4Fe(CN)_6$. The influence on solubility of base concentration, sodium ion concentration, anions, and temperature was investigated. Destruction of ferrocyanide anion by hydrolysis to form ammonia and formate ion was promoted by temperature and gamma radiolysis. Increasing temperature and gamma dose rate increased the rate of hydrolysis, as indicated by the amount of ammonia formed with time. As an approximation, ammonia production with time was described as being linear. Rate constants for ammonia production followed an Eyring relationship and also increased linearly with increasing applied gamma dose rate. Rate constants for ammonia production under other conditions were predicted with use of the temperature and dose rate relationships.

- Ammonia and formate ion were destroyed in the gamma environment at 90°C. The measured ammonia destruction rate constants were 1.1×10^{-3} *M*/day at an applied dose rate of 1×10^{5} rad/h and 2.1×10^{-4} *M*/day at 9×10^{3} rad/h. Formate ion destruction occurred at a faster rate than ammonia destruction. At an applied dose rate of 1×10^{5} rad/h and at 90°C, a rate constant for formate radiolysis of 6.15×10^{-3} *M*/day was measured. Nuclear magnetic resonance experiments show that carbonate is cleanly formed. These results are consistent with observations that the formate concentrations are much lower than the ammonia concentrations in hydrolyzed solutions.

- Nickel, initially precipitated as $Ni(OH)_2$, redissolved as the tetracyanonickelate anion, $Ni(CN)_4^{-2}$, as identified by Fourier transform infrared spectroscopy analysis of supernate solutions. The $Ni(CN)_4^{-2}$, hydrolyzed at the same rate as ferrocyanide anion in a gamma field. The presence of nitrate and nitrite ions in these solutions increased the rate of ammonia production by about a factor of 3 over the rate when these ions were not present.

- Hydrolysis occurred faster than expected at 60°C in a pH 10 solution with an applied gamma dose rate of 4.5×10^{4} rad/h, considering the low solubility of $Na_2NiFe(CN)_6$ at this pH. In the gamma field, and without accounting for ammonia radiolysis, an ammonia yield of 18 mole% was obtained after 5.3 months. When total cyanide data were used, the actual percent destruction was 72%. The rate constant for ammonia production was reasonably approximated using temperature and dose rate relationships developed from experiments with soluble ferrocyanide anion conducted in 2 *M* NaOH. These results indicate that even ferrocyanide sludge that did not come into direct contact with highly basic wastes should also have aged significantly.

Acknowledgments

The authors would like to thank S. R. Gano, J. W. Brothers, and M. A. Gerber of Pacific Northwest National Laboratory for reviewing this document and for making many valuable suggestions. We also acknowledge the contributions of S. A. Bryan, K. H. Pool, M. W. Goheen, R. E. Brinson, S. J. Bos, R. D. Scheele, R. L. Sell, J. Liu, D. E. McCready, and J. R. Coleman, who performed a variety of analyses. Special thanks go to R. J. Cash, J. E. Meacham, and H. Babad of Westinghouse Hanford Company for support, encouragement, and direction on this project.

Abbreviations

AA	atomic absorption spectroscopy
DOE	U.S. Department of Energy
EDS	energy dispersive spectroscopy
EDTA	ethylenediaminetetraacetic acid
en	ethylenediamine
EIS	Environmental Impact Statement
ESEM	environmental scanning electron microscopy
FECN-14	PNNL-prepared cesium nickel ferrocyanide material
FTIR	Fourier transform infrared spectroscopy
IC	ion chromatography
IF-1A	In-Farm-1A, Rev. 4, WHC-prepared flowsheet ferrocyanide material
IF-1B	In-Farm-1B, Rev. 7, WHC-prepared flowsheet ferrocyanide material
ISE	ion selective electrode
NMR	nuclear magnetic resonance spectroscopy
PNNL	Pacific Northwest National Laboratory
SSTs	single-shell storage tanks
USQ	unreviewed safety question
"vendor" material	unwashed ferrocyanide simulant containing $Na_2NiFe(CN)_6$, Na_2SO_4, and 4.5 H_2O, as determined by chemical analysis, prepared by an outside vendor
WHC	Westinghouse Hanford Company
XRD	X-ray diffraction spectroscopy

Contents

Figures

Tables

1.0 Introduction

The research performed for the Ferrocyanide Aging Studies was part of an effort begun in the mid-1980s to characterize the materials stored in the single-shell waste storage tanks (SSTs) at the U.S. Department of Energy's (DOE) Hanford Site. Various radioactive wastes from defense operations have accumulated at the Hanford Site in underground waste storage tanks since the early 1940s. During the 1950s, additional tank storage space was required to support the defense mission. Hanford Site scientists developed two procedures to obtain this additional storage volume within a short time period without constructing more storage tanks. One procedure involved the use of evaporators to concentrate the waste by removing water. The other procedure involved developing precipitation processes for scavenging radiocesium and other soluble radionuclides from tank waste liquids.

In the radiocesium scavenging processes, waste solutions were adjusted to a pH between 8 and 10; and sodium or potassium ferrocyanide and nickel sulfate were added to co-precipitate cesium with the insoluble alkali-metal nickel ferrocyanide. Because waste solutions had high nitrate and radiolytically produced nitrite concentrations, these ions became incorporated into the precipitates. After the radioactive precipitates settled, the decontaminated solutions were pumped to disposal cribs, thereby providing the additional tank storage volume. Much later, some of the tanks were "stabilized" against leakage when pumpable liquids were removed from the tanks, leaving behind a wet solid (sludge) residue containing the ferrocyanide precipitates (Burger et al. 1991). In implementing this process, approximately 140 metric tons of ferrocyanide [calculated as $Fe(CN)_6^{-4}$] were added to waste that was later routed to 20 large (500,000- to 750,000-million-gal) underground SSTs. Records at Hanford show 18 SSTs received at least 200 kg (1000 g-mol) of ferrocyanide precipitates. The ferrocyanide received by the individual tanks range from 200 kg up to possibly 16,600 kg in Tank BY-104 (Borsheim and Simpson 1991).

Three flowsheets were used to scavenge the radiocesium from aqueous wastes. The T-Plant flowsheet, used to treat first-cycle waste from the bismuth phosphate process, generated about 8% of the total ferrocyanide waste. The U-Plant flowsheet treated "metal waste" dissolved in nitric acid after the uranium had been recovered using the tributyl phosphate process. The U-Plant flowsheet produced about 66% of the total ferrocyanide waste. The third process, the In-Farm flowsheet, treated the basic supernate waste from recovery of uranium after the solids had been allowed to settle. This process produced the remaining 26% of the total ferrocyanide waste.

Unlike the In-Farm flowsheet waste, T-Plant and U-Plant flowsheet waste contained substantial metal concentrations that precipitated when neutralized with sodium hydroxide. The ferrocyanide was thereby diluted, assuming that the solids-settling behaviors of the metal species and ferrocyanides were approximately the same. Although the In-Farm flowsheet produced only about a quarter of the ferrocyanide waste, the concentration of ferrocyanide in this waste was significantly higher than that in the T-Plant and U-Plant waste. Prepared In-Farm and U-Plant flowsheet simulants, which are representative of these wastes, contain about 25 wt% and 8 wt% ferrocyanide ion (on a dry basis), respectively.

As part of waste management operations, after the ferrocyanide waste was precipitated and the supernate removed, aluminum cladding waste and/or evaporator bottoms from the concentration of reprocessing wastes were added to the tanks (Anderson 1990). These solutions were generally quite alkaline, containing NaOH concentrations of 1 to 2 *M*, with occasional additions of up to 4 *M* NaOH.

Concern has been raised about the safe storage of ferrocyanide waste intermixed with oxidants, such as nitrate and nitrite salts. In the laboratory, such mixtures can be made to undergo uncontrolled or explosive reactions by heating dry reagents to over 200°C. For example, mixtures of cesium zinc ferrocyanide and nitrate explode when heated (Hepworth et al. 1957). The 1987 Environmental Impact Statement (EIS), *Final Environmental Impact Statement, Disposal of Hanford Defense High-Level Transuranic and Tank Waste, Hanford Site, Richland, Washington* (DOE 1987), included an environmental impact analysis of potential explosions involving ferrocyanide-nitrate mixtures. The EIS postulated that an explosion could occur during mechanical retrieval of saltcake or sludge from a ferrocyanide waste tank. The EIS concluded that this worst-case accident could create enough energy to release radioactive material to the atmosphere through ventilation openings, exposing persons offsite to a short-term radiation dose of approximately 200 mrem. A General Accounting Office study (Peach 1990) postulated a greater worst-case accident, with independently calculated doses of one to two orders of magnitude greater than that postulated in the DOE EIS. Uncertainties regarding the safety envelope of the Hanford Site ferrocyanide waste tanks led to the declaration of the Ferrocyanide Unreviewed Safety Question (USQ) in October 1990 (Deaton 1990).

A special Hanford Ferrocyanide Task Team was commissioned to address all technical aspects of tanks containing ferrocyanide wastes. The Hanford Ferrocyanide Task Team was composed of technical experts from Westinghouse Hanford Company (WHC), Pacific Northwest National Laboratory (PNNL),[a] and outside consultants. Their goals were to resolve the USQ by defining safety criteria, categorize the safety of the tank waste, and resolve the Ferrocyanide Safety Issue by ensuring that the waste is stored safely.

Numerous studies conducted by the Task Team defined safety criteria and resulted in closure of the USQ in March 1994 (Postma et al. 1994; Sheridan 1994). The potential for ferrocyanide reactions in Hanford Site SSTs was evaluated, and the energy released during these reactions was quantified (Burger 1984; Burger and Scheele 1988, 1991; Cady 1993; Hallen et al. 1992; Scheele and Cady 1992; Scheele et al. 1991, 1992). Dynamic X-ray diffraction (XRD) was also used to identify specific reactions and to quantify reaction rates (Dodds and Thompson 1994). In addition, a number of experimental and theoretical studies were conducted in an effort to analyze the thermal characteristics of the tanks (Crowe et al. 1993; McLaren 1993, 1994; McLaren and Cash 1993) and to investigate the likelihood of "hot spots" forming as a result of radiolytic heating (Epstein et al. 1994; McGrail et al. 1993). The measured temperatures in these tanks continue to drop, and the highest temperature currently recorded is 52°C (Cash and Meacham 1996).

(a) Operated for the U.S. Department of Energy by Battelle under Contract DE-AC06-76RLO 1830.

Safety criteria for ferrocyanide waste were based on the concentration of ferrocyanide in the waste, the amount of free (unbound) water present, and the temperature of the waste. Waste is considered safe if it contains less than 8 wt% $Na_2NiFe(CN)_6$ (measured in dried waste with no free water), regardless of temperature, water content, or oxidant content. Ferrocyanide waste is said to be conditionally safe if it contains more than 8 wt% $Na_2NiFe(CN)_6$, contains up to 24 wt% free water, and is at a temperature less than 90°C. Tanks are categorized as unsafe if they contain higher ferrocyanide concentrations without adequate free water or contain waste at a temperature higher than 90°C.

Resolving the Ferrocyanide Safety Issue requires that tank contents meet the safety criteria and operations be conducted such that waste conditions fall within the criteria limits. Because the ferrocyanide sludge has been exposed for many years to other highly caustic wastes, as well as to elevated temperatures and both gamma and beta radiation, ferrocyanide decomposition has occurred in the tanks. As a result, the concentration of ferrocyanide is less than that predicted by tank inventory records. As such, C-Farm tanks have been re-categorized as safe, allowing resolution of the Ferrocyanide Safety Issue for these tanks (Meacham et al. 1996).

The goal of the Ferrocyanide Aging Studies task of the Ferrocyanide Safety Project was to contribute to the resolution of the Ferrocyanide Safety Issue by defining the long-term chemical and radiolytic decomposition ("aging") of ferrocyanide materials under conditions found in the SSTs. Information from these studies has provided baseline data for comparison with actual SST waste samples as they are obtained and analyzed. The results of the Aging Studies have directly assisted in determining the strategy for safe storage of the ferrocyanide waste in the tanks and how the Ferrocyanide Safety Issue was to be resolved.

This final report summarizes the research conducted for this task from FY 1992 to FY 1996. It is a compilation and comprehensive evaluation of data reported previously (Lilga et al. 1992-1995) and new data collected in FY 1996. Ferrocyanide aging studies utilized a variety of ferrocyanide materials, including flowsheet simulants. Sodium nickel ferrocyanide, $Na_2NiFe(CN)_6$, comprising the bulk of the ferrocyanide material originally precipitated in cesium scavenging operations, was found to dissolve in caustic solutions to form soluble ferrocyanide anion, $Fe(CN)_6^{-4}$, and insoluble nickel hydroxide, $Ni(OH)_2$. Dissolution was studied under a variety of conditions. Destruction of $Fe(CN)_6^{-4}$ by hydrolysis was studied as a function of temperature, applied gamma dose rate, and added metal ions. A 5.3-month hydrolysis experiment was conducted at pH 10 and 60°C, conditions under which $Na_2NiFe(CN)_6$ is virtually insoluble. Also studied was the hydrolysis of tetracyanonickelate anion, $Ni(CN)_4^{-2}$, an important intermediate in the overall hydrolysis of ferrocyanide.

2.0 Work Accomplished

The Aging Studies task addressed issues regarding how ferrocyanides in tank waste have changed over decades of storage and after additions of other highly caustic wastes (evaporator bottoms or cladding waste). Aging, as used here, is any process that alters the chemical nature of the ferrocyanide waste. In these studies, the primary aging pathways that have been demonstrated and investigated are dissolution of alkali metal nickel ferrocyanides, shown in Eq. (1) for the sodium compound; hydrolysis of ferrocyanide ion, shown in Eq. (2) for one reported stoichiometry (Robuck and Luthy 1989); and hydrolysis of tetracyanonickelate ion, shown in Eq. (3), which forms during aging.

$$Na_2NiFe(CN)_{6\,(s)} + 2\,OH^- \rightleftarrows Fe(CN)_6^{-4} + 2\,Na^+ + Ni(OH)_{2\,(s)} \quad (1)$$

$$Fe(CN)_6^{-4} + 2\,OH^- + 11\,H_2O + 1/6\,O_2 \rightarrow 6\,NH_3 + 6\,HCO_2^- + 1/3\,Fe_3O_{4\,(s)} \quad (2)$$

$$Ni(CN)_4^{-2} + 2\,OH^- + 8\,H_2O \rightarrow 4\,NH_3 + 4\,HCO_2^- + Ni(OH)_{2\,(s)} \quad (3)$$

As discussed below, the dissolution stoichiometry in Eq. (1) is consistent with experimental Aging Studies results. However, the hydrolysis reactions in Eqs. (2) and (3) merely illustrate what has been observed by others and that the expected final products are ammonia, formate ion, and metal oxides and hydroxides. Although good cyanide balances have been obtained, the precise stoichiometries shown have not been observed in Aging Studies research for reasons discussed in this report. Mechanisms and the possible involvement of various reactive intermediates, such as cyanate and $\cdot NO_2$, have not been explicitly investigated in this work, but results do offer insight into likely reaction pathways.

The following sections describe the materials and methodologies used and the results of solubility and hydrolysis studies conducted for this task. Solubility studies investigated the effects of pH variation; ionic strength and sodium ion concentration; the presence of anions such as phosphate, carbonate, and nitrate; and temperature. A vendor-prepared ferrocyanide material; In-Farm-1A, Rev. 4 (IF-1A) flowsheet-prepared (WHC) $Na_2NiFe(CN)_6$; and FECN-14, a cesium nickel ferrocyanide material (PNNL), were used in the solubility studies. Contrary to the sodium analogs, cesium-containing phases were found to be insoluble in up to 4 *M* NaOH (typical concentration of evaporator bottoms). In addition, competition experiments were performed to investigate the rate of cesium ion exchange relative to the rate of dissolution of In-Farm flowsheet simulant.

Also reported is the destruction of ferrocyanide anion by hydrolysis in caustic solution, studied under conditions approximating those in SSTs. Most of the hydrolysis studies used the In-Farm simulant, In-Farm-1B, Rev 7 (IF-1B). Tests were also conducted with T-Plant-24 and U-Plant-2-19 simulants. Simulants were prepared by WHC to mimic the composition and properties of SST wastes as they were originally precipitated (Jeppson and Wong 1993). The influence of applied gamma dose rate and temperature on hydrolysis in 2 *M* NaOH was examined. Experiments were also conducted in

the presence of metal ion additives, including an aluminum coating waste simulant. A series of experiments were completed in which hydrolysis was carried out over a 5.3-month period at pH 10 and 60°C in a gamma field. Other studies included radiolysis of ammonia and formate ion, both of which are cyanide hydrolysis products. The presence of $Ni(CN)_4^{-2}$ was verified by Fourier transform infrared spectroscopy (FTIR) analysis. This ion apparently forms when the free cyanide ion, which is liberated as $Fe(CN)_6^{-4}$ is destroyed, reacts with solid $Ni(OH)_2$ (Eqs. 4 and 5). Hydrolysis of the $Ni(CN)_4^{-2}$ anion, an important intermediate in $Na_2NiFe(CN)_6$ aging, was investigated separately.

$$Fe(CN)_6^{-4} + x\,L^n \rightleftarrows Fe(CN)_{6-x}L^{-4+x(n+1)} + x\,CN^- \quad (4)$$
$L^n = OH^-, H_2O$, etc.

$$Ni(OH)_{2\,(s)} + 4\,CN^- \rightleftarrows Ni(CN)_4^{-2} + 2\,OH^- \quad (5)$$

2.1 Experimental

This section describes the materials and experimental methodology used in the dissolution and hydrolysis studies. It also includes a discussion of the gamma facility, the gamma dose rate cross section experienced by irradiated solutions, and the analytical methods used.

2.1.1 Materials and Methodology for Dissolution Studies

Dissolution studies were conducted on three alkali metal nickel ferrocyanide-containing materials. The first material investigated was the so-called "vendor" material, with an approximate composition of $Na_2NiFe(CN)_6 \cdot Na_2SO_4 \cdot 4.5\ H_2O$; it was used as supplied by Atomergic Chemetals Corp., a commercial vendor. Two cesium-containing ferrocyanide materials were later investigated as they became available: FECN-14, a PNNL-prepared ferrocyanide material containing $Cs_2NiFe(CN)_6$, and dried IF-1A, the top layer of the WHC-prepared In-Farm flowsheet material. Table 2.1 shows the compositions of these materials as determined by atomic absorption (AA) and FTIR spectroscopic analyses of samples dissolved in 5 wt% ethylenediamine/5 wt% ethylenediamine tetraacetic acid (en/EDTA).

Table 2.1. Moles of Analyte/Gram Ferrocyanide Material Used in Dissolution Experiments. Analyses of Cs, Fe, Ni, and Na by AA and $Fe(CN)_6^{-4}$ by FTIR for Materials Dissolved in en/EDTA.

Analyte	moles/g Vendor	moles/g FECN-14	moles/g IF-1A
Cs	--	3.06×10^{-3}	2.96×10^{-5}
Fe	1.93×10^{-3}	1.33×10^{-3}	6.56×10^{-4}
Ni	2.00×10^{-3}	1.51×10^{-3}	1.00×10^{-3}
Na	7.36×10^{-3}	3.35×10^{-4}	1.02×10^{-2}
$Fe(CN)_6^{-4}$	1.86×10^{-3}	1.30×10^{-3}	7.13×10^{-4}

In a typical dissolution experiment, 1 g of the vendor material was stirred in 50 mL of an aqueous base solution in a Teflon round-bottom flask. Solution samples were periodically taken and analyzed for total iron by AA. In these experiments and with these materials, all of the soluble iron is in the form of ferrocyanide anion. At the conclusion of the experiment, the final pH was measured and the soluble and insoluble reaction products were identified with use of FTIR, powder XRD, and energy dispersive spectroscopies (EDS) combined with environmental scanning electron microscopy (ESEM).

2.1.2 Materials and Methodology for Hydrolysis Studies

The ferrocyanide flowsheet materials used in the hydrolysis studies were the bottom layer In-Farm-1B, Rev 7 (IF-1B) and T-Plant-24 and U-Plant-2-19 flowsheet materials prepared by WHC (Jeppson and Wong 1993). The wet sludges were dried to constant weight in a vacuum oven at 60°C and stored in a desiccator. The wet IF-1B material was found to contain 47.2 wt% water when dried under these conditions. The T-Plant and U-Plant materials contained 63% and 60% water, respectively.

Samples of the dried IF-1B material were characterized by stirring in 2 *M* NaOH or aqueous en/EDTA, and the supernates analyzed. Table 2.2 summarizes room temperature analyte concentrations based on AA analyses for iron (corresponding to soluble ferrocyanide), cesium, nickel, NO_3^-, and NO_2^-, and FTIR analysis for $Fe(CN)_6^{-4}$. The en/EDTA solvent dissolved all of the IF-1B starting material, while the NaOH solution did not. Appropriately, the iron, cesium, and nickel concentrations in the NaOH solution were found to be lower than in the en/EDTA solution. As discussed in more detail below, aqueous NaOH does not dissolve "$Cs_2NiFe(CN)_6$" or other phases containing cesium (Bryan et al. 1993; Lilga et al. 1993), accounting for the different concentrations in the two media.

Table 2.2. Analysis of IF-1B Dissolved in 2 *M* NaOH and en/EDTA at Room Temperature

	moles Analyte/g IF-1B	
Analyte	**2 *M* NaOH**	**en/EDTA**
Fe	6.35×10^{-4}	9.56×10^{-4}
Cs	$< 7.31 \times 10^{-7}$	3.69×10^{-5}
Ni	1.49×10^{-5}	8.78×10^{-4}
NO_3^-	5.01×10^{-3}	5.64×10^{-3}
NO_2^-	1.48×10^{-3}	1.16×10^{-3}
$Fe(CN)_6^{-4}$	5.65×10^{-4}	8.48×10^{-4}

The extent of dissolution (solubility) as a function of temperature was determined because aging experiments were conducted at elevated temperatures. Results at 70°C and 100°C in 2 *M* NaOH are shown in Table 2.3. In a typical hydrolysis experiment, 0.5 g of IF-1B was dissolved in 25 mL of 2 *M*

Table 2.3. Analyte Concentrations in Solutions of IF-1B Dissolved in 2 *M* NaOH at 70°C and 100°C

	moles Analyte/g IF-1B	
Analyte	**70°C**	**100°C**
Fe	7.72×10^{-4}	8.61×10^{-4}
Cs	1.24×10^{-6}	4.89×10^{-6}
Ni	4.26×10^{-6}	1.70×10^{-5}
NO_3^-	5.09×10^{-3}	5.33×10^{-3}
NO_2^-	1.69×10^{-3}	2.43×10^{-3}

NaOH. The ferrocyanide (total Fe) concentrations in such solutions as a function of temperature are shown in Figure 2.1, and initial concentrations at temperatures other than 70°C and 100°C were determined by interpolation of these data. For example, at 90°C, the starting ferrocyanide ion concentration for 0.5 g of IF-1B dissolved in 25 mL of 2 *M* NaOH was about 0.0166 *M*.

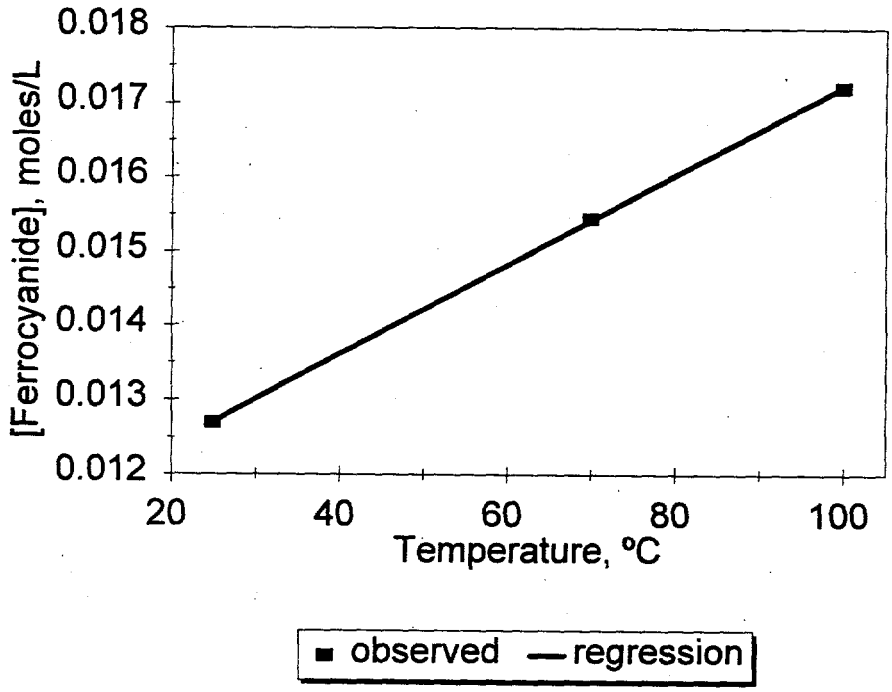

Figure 2.1. Temperature Dependence of Ferrocyanide Concentration When IF-1B Dissolves in 2 *M* NaOH

The cesium-containing phase that remains insoluble also prevents dissolution of a fraction of the $Na_2NiFe(CN)_6$ phase. The Fe/Cs molar ratio in the solids that are insoluble in 2 *M* NaOH at room temperature is calculated to be 8.9, which is much higher than if all of the cesium were present as "$Cs_2NiFe(CN)_6$" (Fe/Cs = 0.5) or "$CsNaNiFe(CN)_6$" (Fe/Cs = 1.0). Similarly, this ratio at 70°C and 100°C is 5.2 and 3.0, respectively. The insoluble material must contain the soluble $Na_2NiFe(CN)_6$ phase imbedded within the less-soluble cesium phase. The decrease in the Fe/Cs molar ratio shows that more of the soluble material is released at higher temperatures.

The solubilities of T-Plant and U-Plant (Jeppson and Wong 1993) simulants used in this study were those reported previously for the dried starting materials. T-Plant simulant contained 2.78×10^{-4} moles $Fe(CN)_6^{-4}$/g dry simulant (5.92 wt%), and U-Plant-2 contained 2.6×10^{-4} moles $Fe(CN)_6^{-4}$/g dry simulant (5.6 wt%).

In a typical hydrolysis experiment, identical Inconel vessels (0.23-cm wall thickness) were charged with the dried ferrocyanide flowsheet material and argon-purged caustic solution and sealed. Vessels were pressurized and vented two times with argon (to remove air), then pressure-checked with argon and vented to atmospheric pressure. Vessels were lowered into separate tubes in the gamma pit (see Section 2.1.3) for irradiation and brought to the desired temperature. Placement of the vessels in the gamma pit tubes was adjusted to give gamma dose rates as consistent as possible for each of the vessels. Temperature controllers were used with heating tape wrapped around each vessel to maintain a stable, consistent temperature. Heatup to 90°C took about 2 h. Temperatures and pressures were monitored and recorded with use of a Campbell Scientific 21X datalogger with battery backup utilizing an AM416 multiplexer, 107 Temperature probe, and Toshiba 3000 portable computer. Solutions were not stirred.

Reaction vessels were individually removed from the gamma pit, usually after 2, 6, 12, 16, and 19 days. Control experiments, which were prepared and treated identically but did not undergo gamma irradiation, were normally terminated after 12 and 19 days of reaction. Vessels were cooled to room temperature (cooling period 3 to 6 h), and a gas sample taken with a 75-mL evacuated sample vessel for mass spectral analysis. A GasTech ammonia sensing tube (colorimetric NH_3 determination) was used to estimate the gas-phase ammonia. Because the gas-phase ammonia was an insignificant fraction of the total ammonia produced (Section 2.1.4), the readings from the sensing tubes were used as qualitative indicators only. The reaction vessel was then sealed and returned to the laboratory for further analysis (Section 2.1.4). The supernate was sampled (5 mL, unfiltered) and analyzed for solution NH_3. Another 5 to 7 mL were filtered through a 0.45-μm Gelman Acrodisc syringe filter for AA, ion chromatography (IC), and FTIR analyses. The remaining supernate was filtered through a 0.47-μm magna nylon millipore filter, and the precipitate washed with de-ionized water. Precipitates were dried at 100°C.

Hydrolysis experiments investigating the effect of added metal ions that are found in SST waste were conducted in essentially the same manner with the following variations. The time dependence of hydrolysis was not investigated; experiments containing metal ions were usually run for 13 days. The

Inconel vessels used had a smaller inside diameter and a thicker wall (0.93-cm wall thickness) than those used in the experiments described above. As a result, the geometry of the 25 mL of solution in the gamma field was different and the thicker vessel wall attenuated the gamma field to a larger extent than in the thin-wall vessels. The effects of different cross sections and attenuation were minimal, however, since the gamma dependence of aging was found to be small relative to the temperature dependence. Geometry had a larger effect on the temperature gradient through the unstirred solution column, which significantly affected the extent of the hydrolysis. Convective solution mixing in the thin-wall vessels (35-mm column height) was quite different than in the thick-wall vessels (117-mm column height). Therefore, while metal ion testing experiments are internally consistent, the results are not directly comparable to the normal hydrolysis experiments described above. However, experiments conducted in the thick-wall vessels without metal ion additives, run for varying lengths of time, established the baseline hydrolysis behavior for comparison.

In long-term (5.3 months) hydrolysis experiments conducted at 60°C with pH 10 solutions in a gamma field, Monel vessels were used. The vessel wall thickness was 0.55 cm.

Three different vessel styles were used in the three different series of hydrolysis experiments described above. Different vessels were used because the number of experimental parameters requiring examination and the length of time required for each test necessitated concurrent, rather than sequential, testing. Experiments within each series were performed consistently, and results are directly comparable. Because of the length of time required for each experiment and gamma facility scheduling, not all experiments could be duplicated. Two independent sets of duplicate experiments were run, as described below, to gain a sense of the reproducibility of these experiments. Both sets indicated an overall relative standard deviation of 10-11% for the ammonia production data.

2.1.3 Description of the Gamma Facility, Gamma Dose Rate Cross Sections for Irradiated Solutions, and Estimation of Integrated Dose

The Gamma Irradiation Facility (gamma pit) operated by PNNL contains 37 stainless steel irradiation tubes positioned in a 2.1-m-diameter (7-ft) by 4.2-m-deep (13-ft 8-in.) stainless steel tank. Two arrays of ^{60}Co with a combined inventory of 32 kCi are located near the bottom of the tank. For radiation shielding purposes, the tank is completely filled with water. A concrete wall, 1.1 m (3.5 ft) in height, surrounds the top of the tank. The irradiation tubes, which are sealed on the bottom, vary in length from 4.9 to 5.5 m (16 to 18 ft) and in diameter from 46 to 150 mm (1.8 to 6 in.). The irradiation flux of the tubes ranges from 2×10^2 to 2×10^6 rad/h. The uniform flux region varies from about 150 mm (6 in.) for the tubes closest to the sources to greater than 305 mm (12 in.) for the tubes farthest away from the sources. All flux measurements in the tubes are traceable to the National Institute of Standards and Technology.

Materials, capsules, and test systems are lowered into the irradiation tubes, manually or by using a half-ton crane, to a depth giving the desired flux. They are left in the tubes for the required time, and, because there is no activation associated with the gamma irradiation, materials are transported to other facilities for examination after removal from the tubes.

Figure 2.2 illustrates how the flux changes with depth in a typical gamma tube used in the hydrolysis experiments. The flux data shown are for February 1994. Over the course of the Aging Studies task, the flux in each tube decreased by about 20% because of the natural decay of the ^{60}Co sources. Also shown on the graph is the position of the top and bottom of a reaction solution in a thin-wall vessel within the tubes and the associated flux experienced by the solutions.

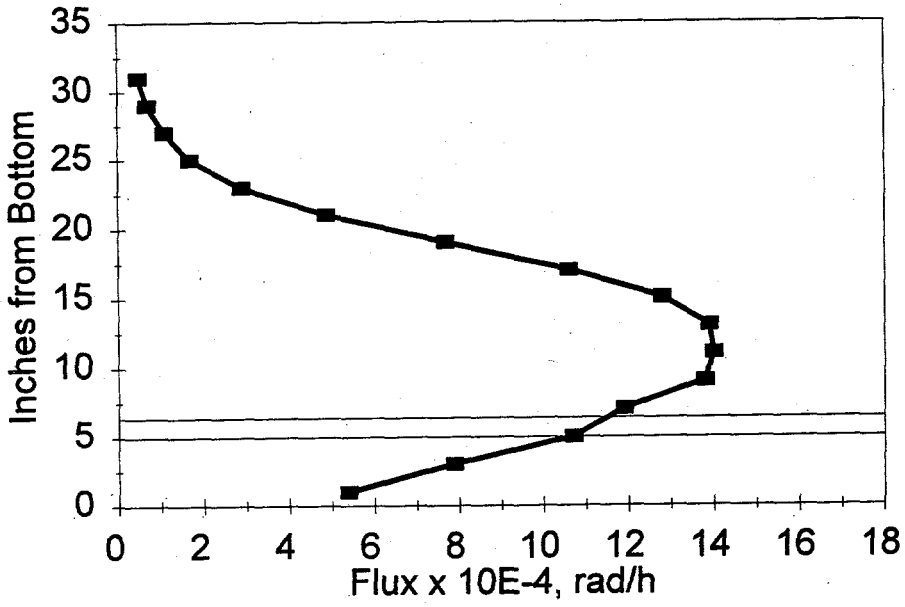

Figure 2.2. Gamma Dose Rate Cross Section for a Typical Tube Used in Hydrolysis Experiments Conducted at an Average Dose Rate of 1 x 10^5 rad/h and Position of a Solution Within the Tube

Integrated doses for samples irradiated at a flux of 9 x 10^3, 4 x 10^4, and 1 x 10^5 rad/h are estimated in Table 2.4. The integrated dose received in the gamma pit experiments is comparable to the calculated average gamma dose received by tank wastes, which is on the order of 3 x 10^7 to 5 x 10^8 rad (Parra 1994). The gamma dose rate, of course, is much lower in the SSTs, currently ranging from about 20 to 200 rad/h, than in these experiments (10^4 to 10^5 rad/h).

Table 2.4. Estimation of Integrated Gamma Dose in Hydrolysis Experiments at Various Dose Rates for the First and Last Samples Taken

	Integrated Gamma Dose (rad)	
Flux (rad/h)	**Sample 1, 2 days**	**Sample 6, 19 days**
1 x 10^5	4.8 x 10^6	4.6 x 10^7
4 x 10^4	1.9 x 10^6	1.8 x 10^7
9 x 10^3	4.3 x 10^5	4.1 x 10^6

2.1.4 Analytical Methods

Several different analytical methods were used to identify and quantitate dissolution and hydrolysis products. Gas samples from the headspace of the hydrolysis reaction vessels were obtained with an evacuated 75-mL sample vessel through a specially prepared gas sampling/pressure monitoring panel.

The gas sampling lines were first evacuated, then the sample vessel was allowed to equilibrate with the reaction vessel for 5 min before sealing. Gas samples were analyzed on a high-sensitivity Finnigan MAT-271 mass spectrometer for several gases, including argon, hydrogen, nitrogen, oxygen, and nitrogen oxides. The estimate of precision is better than 0.1 mole%.

Syringe-filtered hydrolysis supernates were analyzed by AA for total soluble iron, nickel, and cesium. These analyses are accurate to within 10%. The supernates were also analyzed for NO_3^-, NO_2^-, and HCO_2^- by IC, which is accurate to 5%. Supernates from solubility experiments were analyzed for total iron by AA. Soluble and insoluble reaction products were identified with use of FTIR, XRD, and ESEM/EDS.

Analyses of the free cyanide ion concentration were attempted using IC. However, it was later found that ethylenediamine was used in the IC method; ethylenediamine is reported to displace about 80% of the cyanide bound to nickel in $Ni(CN)_4^{-2}$ (Rocklin and Johnson 1983). Because of this displacement, free cyanide ion concentrations, as determined by IC, in solutions containing this anion are an order of magnitude larger than expected from equilibrium data. The observed concentrations can be rationalized by assuming 60% displacement of nickel-bound cyanide under the analysis conditions used, in good agreement with the literature. More realistic free CN^- concentrations were provided by ion selective electrode (ISE), which does not require dilution or sample pretreatment and does not detect $Ni(CN)_4^{-2}$ or other metal cyanide complexes.

Gas-phase ammonia was estimated with use of GasTech ammonia sensing tubes. Tubes were connected to the reaction vessel with a gas-tight seal; the plunger on the supplied pump was pulled to the 50- or 100-mL position, drawing gas through the sensing tube. A color change in the sensing material indicates the presence of ammonia; the position of the line of demarcation between the reacted and unreacted sensing material indicates the concentration, which is read off the calibrated tube in ppm. The concentration was adjusted for the change in pressure that occurred when the volume was increased by pulling the plunger.

Dissolved ammonia was determined with use of an Orion 720A pH/ISE meter equipped with an Orion 95-12 NH_3 ISE. Before the reaction solution $[NH_3]$ was determined, the accuracy of the ISE was checked using a standard NH_4Cl solution made basic by addition of an NaOH solution. Calibration measurements were typically within 3% of the actual concentration. Aluminum in reaction solutions was found to suppress the measured ammonia concentrations, as discussed in Section 2.7.1.

Experiments were performed to check the accuracy and suitability of the ISE method for dissolved ammonia analysis in which a known amount of NH_3 was generated by adding various amounts of a

standard 0.1 *M* NH_4Cl solution to 25 mL of 2 *M* NaOH in the reaction vessels. The range of ammonia concentrations generated was from 0.001 to 0.075 *M*, which is representative of the range of ammonia concentrations observed in the hydrolysis experiments (see Sections 2.4 through 2.10). Vessels were quickly sealed and heated to 90°C for 2 days without gamma irradiation. The vessels were cooled to room temperature and treated exactly like a vessel in a hydrolysis experiment; i.e., a 75-mL gas sample was taken (and later discarded), a gas sample was drawn through a GasTech ammonia sensing tube, and the vessel was sealed and returned to the laboratory for solution ammonia determination. As shown in Figure 2.3, the measured solution ammonia concentrations correlate well with the concentrations generated (data points); the least squares fit to the data (line) has a slope of 1.02 and intercept of 0.00. In addition, the number of moles of ammonia in the gas phase (10^{-8} to 10^{-6} moles), as estimated with the GasTech sensor, was at least 10^3 times lower than the number of moles in solution (10^{-5} to 10^{-3} moles). This ratio is consistent with that calculated using Henry's law (Edwards et al. 1978; Norton and Pederson 1994). These experiments demonstrate that ammonia concentrations can be accurately measured with the sampling scheme used; that adsorption of ammonia on the stainless steel vessel and tubing is not significant under the reaction and sampling conditions; and that the solution concentration, in solutions cooled to room temperature, adequately accounts for all ammonia generated from hydrolysis.

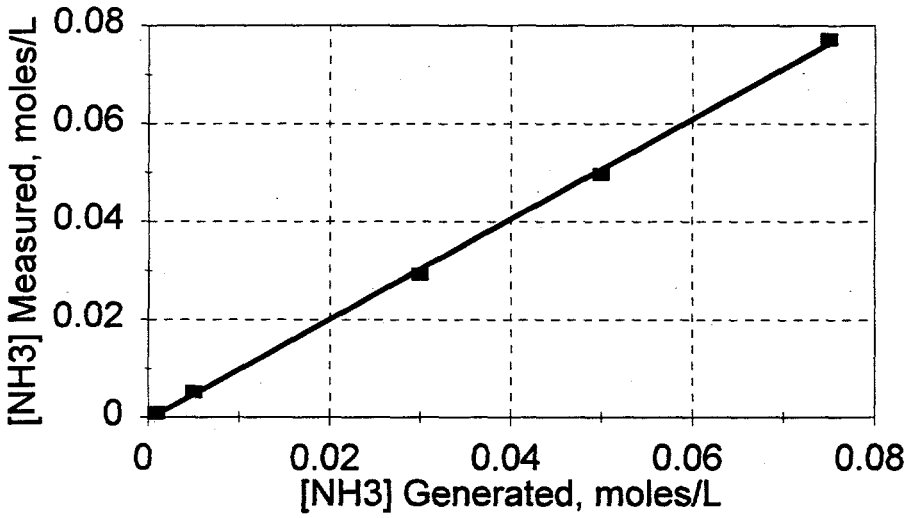

Figure 2.3. Measured Versus Generated Ammonia Concentration in Experiments Not Gamma Irradiated

2.2 Solubility of Ferrocyanide Waste Simulants

Factors affecting the dissolution of ferrocyanide anion from the vendor material, consisting primarily of $Na_2NiFe(CN)_6$; the two In-Farm flowsheet materials; and the FECN-14 material, containing $Cs_2NiFe(CN)_6$, were investigated. Results of these studies are reported in this section.

2.2.1 Solubility of Vendor-prepared Ferrocyanide Material

The effects of pH, sodium ion concentration, anion, and temperature on dissolution of the vendor material were investigated. Other experiments were also conducted in unstirred solution and with varying amounts of the vendor material. Table 2.5 is a summary of the experiments.

Table 2.5. Summary of Alkali Metal Nickel Ferrocyanide Solubility Experiments. Experiments were conducted using the vendor-prepared material, $Na_2NiFe(CN)_6 \cdot Na_2SO_4 \cdot 4.5\ H_2O$, except where noted.

I. pH Variation: pH = 12, 13, 14 at 25°C (vendor and FECN-14)

II. Sodium Ion Concentration Variation: pH 13, 25°C adjusted to 1 *M*, 4 *M*, and 6 *M* Na^+ with $NaNO_3$; pH 14, 25°C, adjusted to 2 *M* Na^+ with Na_2CO_3 and to 4 *M* Na^+ with $NaNO_3$ (vendor and IF-1A)

III. Anion Variation: pH 13, 25°C, adjusted to 1 *M* Na^+ with Sodium Salts of NO_3^-, PO_4^{3-}, SO_4^{2-}, CO_3^{2-}, and OH^-

IV. Temperature Variation: 25°C, 60°C, and 90°C at pH 13 and 1 *M* Na^+ (IF-1A)

V. Variation in $OH^-/Fe(CN)_6^{-4}$ ratio by varying amount of vendor material used

VI. Static Solubility Test: pH 13, 1 *M* Na^+, 25°C

Dissolution was found to occur according to Eq. (1), shown again below. Addition of base to solid $Na_2NiFe(CN)_6$ resulted in the dissolution of $Na_4Fe(CN)_6$ and the precipitation of $Ni(OH)_2$ at a rate that depended upon the solution composition. Product identification was supported by a variety of spectroscopic and analytical data, and the reaction was consistent with the measured change in solution pH.

$$Na_2NiFe(CN)_{6\,(s)} + 2\,OH^- \rightleftarrows Fe(CN)_6^{-4} + 2\,Na^+ + Ni(OH)_{2\,(s)} \qquad (1)$$

Figure 2.4 is a comparison of EDS micrographs from the analysis of the soluble and insoluble solids obtained from 0.1 *M* NaOH (pH 13) dissolution of the vendor-prepared $Na_2NiFe(CN)_6$. No nickel was found in the soluble fraction. An iron compound was the major species in this sample along with the SO_4^{-2} from the starting material. The EDS spectra show that nickel is found in the insoluble solids. The insoluble solids also contained iron because, as discussed below, the dissolution in pH 13 solution was not complete when the experiment was halted. Spectra of insoluble solids from pH 14 dissolution did not contain the iron peak.

Further identification of the reaction products comes from infrared spectra. Infrared spectra of supernates in the cyanide region typically gave a single absorbance at 2036 cm^{-1}, as did a commercial sample of $K_4Fe(CN)_6$. Therefore, soluble iron was in the form of $Fe(CN)_6^{-4}$. No soluble substitution

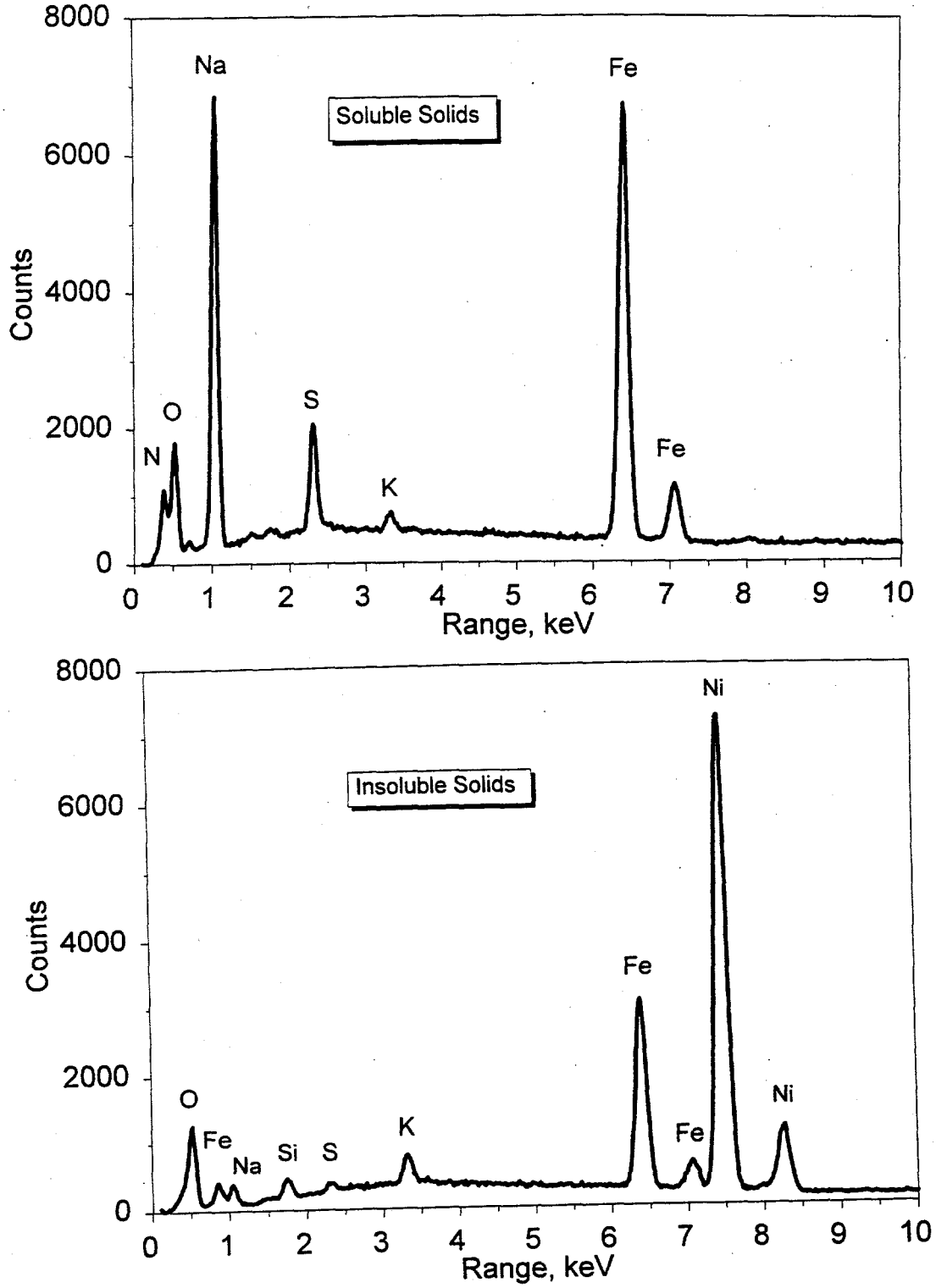

Figure 2.4. Comparison of EDS Micrographs of the Soluble and Insoluble Solids Obtained from pH 13 Dissolution of the Vendor-prepared $Na_2NiFe(CN)_6$

products were detected from solutions stirred at room temperature. Insoluble reaction products showed a peak at about 2090 cm^{-1}, a position consistent with sodium nickel ferrocyanide in the vendor-prepared starting material.

Figure 2.5 illustrates solid-state infrared spectra in the hydroxyl stretching region for soluble and insoluble solids, obtained from 0.1 *M* and 1.0 *M* NaOH dissolutions, and for laboratory-prepared $Ni(OH)_2$. The solids obtained from the supernates showed broad absorptions for water and NaOH, while the insoluble solids had an additional sharp band at 3630 cm^{-1}. This band corresponded well with that observed for $Ni(OH)_2$. Figure 2.6 shows the growth of this band in samples taken over the course of the 0.1 *M* NaOH dissolution experiment. The band was not easily resolved until after 24 h of reaction.

Figure 2.7 compares the XRD results for laboratory-prepared $Ni(OH)_2$ with the insoluble solids obtained from 0.1 *M* NaOH dissolution of the vendor-prepared $Na_2NiFe(CN)_6$. These data indicate that the insoluble material was $Ni(OH)_2$. XRD spectra of the soluble solids are consistent with an XRD reference library spectrum of $Na_4Fe(CN)_6$.

The effect of initial pH was studied with dissolution reactions performed at a starting pH of 12, 13, and 14 (0.01 *M*, 0.1 *M*, and 1.0 *M* NaOH, respectively) at room temperature. The rate of dissolution of $Na_2NiFe(CN)_6$ in aqueous base was found to increase with increasing pH, as displayed in Figure 2.8, which shows the change in total dissolved iron, $Fe(CN)_6^{-4}$, as determined by AA, as a function of time for the first hour of reaction. Dissolution was 95% complete after 0.5 h stirring at pH 14. The reaction at pH 12 was base-limited (OH^-/Fe mole ratio = 0.27), but equilibrium was rapidly reached within 0.1 h. At pH 13, a slight excess of base was present (OH^-/Fe mole ratio = 2.7). This dissolution proceeded rapidly at first then slowed to reach about 85% completion after 144 h, as shown in Figure 2.9. The pH 13 dissolution had not reached equilibrium when it was terminated.

Dissolution was suppressed when a pH 13 solution was adjusted to 1 *M* Na^+ ion by addition of Na_2SO_4. A greater suppression was observed when the solution was adjusted to 1 *M* Na^+ by addition of $NaNO_3$. However, adjustment to 1 *M* Na^+ by addition of Na_2CO_3, Na_3PO_4, or by a mixture of salts (SST simulant salts: $NaNO_3$, 80.47 wt%; $NaNO_2$, 4.37 wt%; Na_2CO_3, 1.52 wt%; NaOH, 3.12 wt%; Na_2SO_4, 1.48 wt%; Na_3PO_4, 9.04 wt%), simulating the composition of a typical SST, resulted in an enhancement of the rate of dissolution (Figure 2.10).

Ionic strength of the solutions does not seem to be a factor in these divergent results since no trend with extent of dissolution is seen and since both Na_2CO_3 and Na_2SO_4 have ionic strengths of 1.5 in these solutions, yet show quite different behavior. Buffering of the solutions by carbonate or phosphate also does not appear to be important since the reaction pH was well outside the buffer range of carbonate and, as will be seen later, the pH of both solutions dropped by about the amount expected for use of two equivalents of hydroxide per mole of ferrocyanide dissolved (Eq. 1).

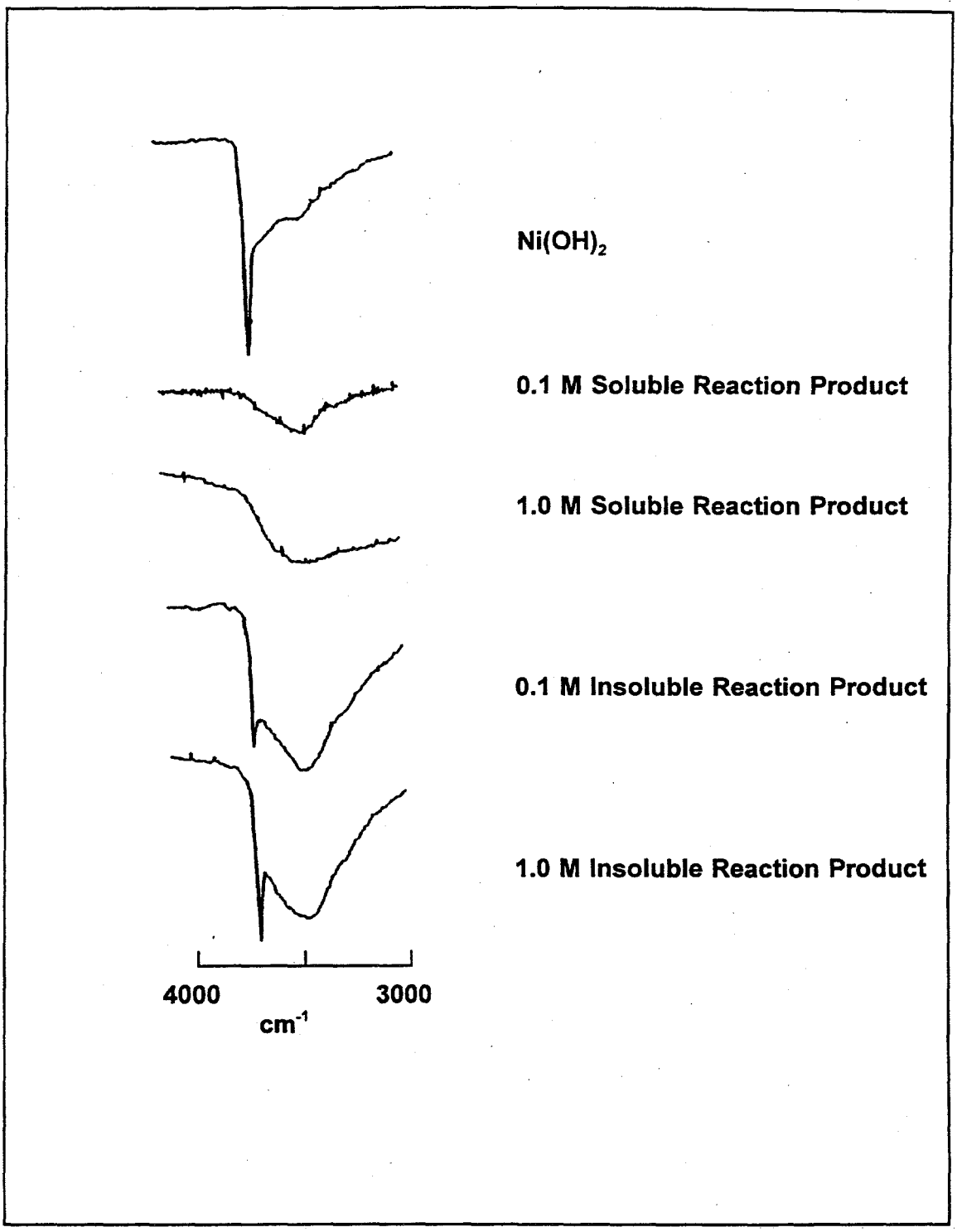

Figure 2.5. Infrared Spectra in the Hydroxyl Region for Dissolution Reaction Products

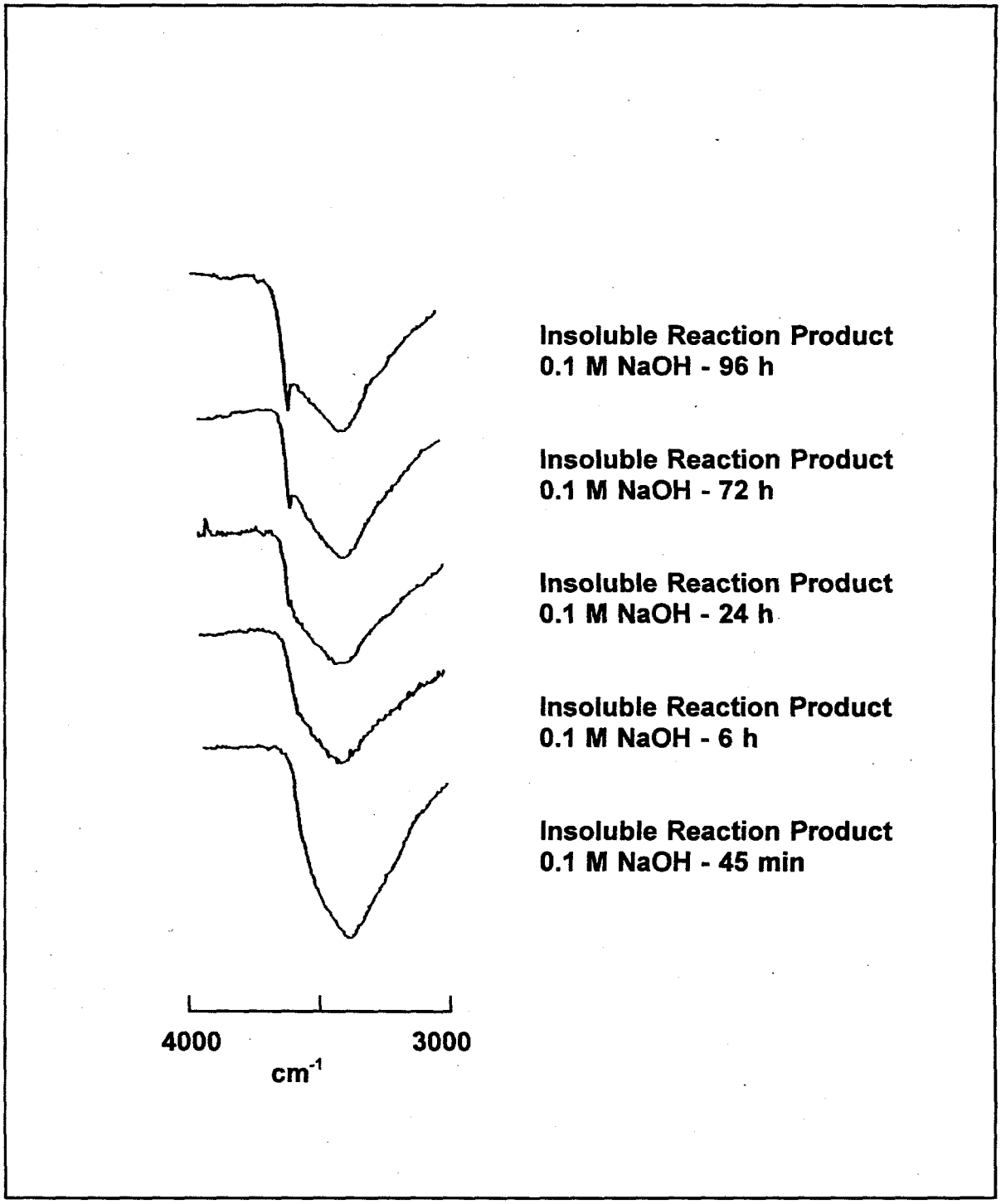

Figure 2.6. Infrared Spectra of Reaction Products in the Hydroxyl Region Over Time During Dissolution of Vendor-prepared $Na_2NiFe(CN)_6$ in 0.1 *M* NaOH

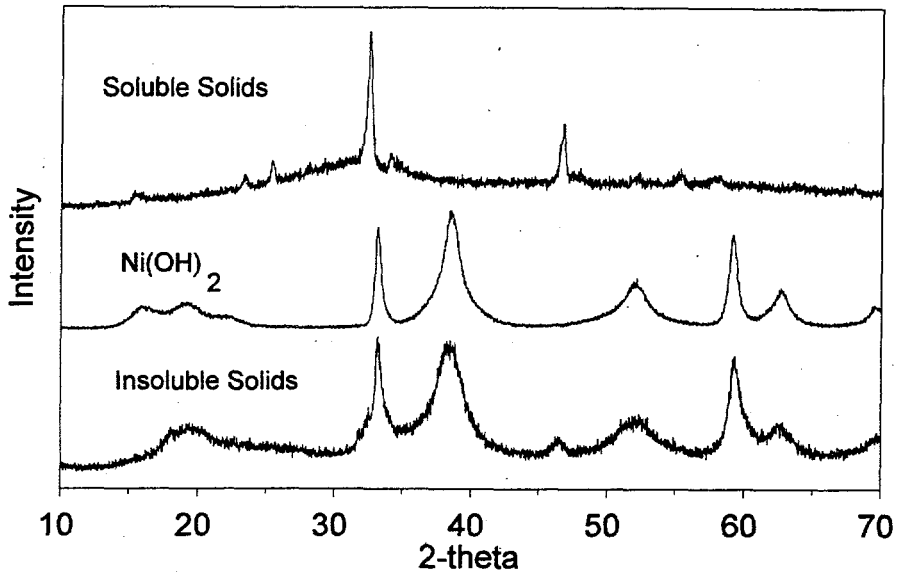

Figure 2.7. Comparison of XRD Results for Laboratory-prepared $Ni(OH)_2$ with the Soluble and Insoluble Solids Obtained from pH 13 Dissolution of the Vendor-prepared $Na_2NiFe(CN)_6$

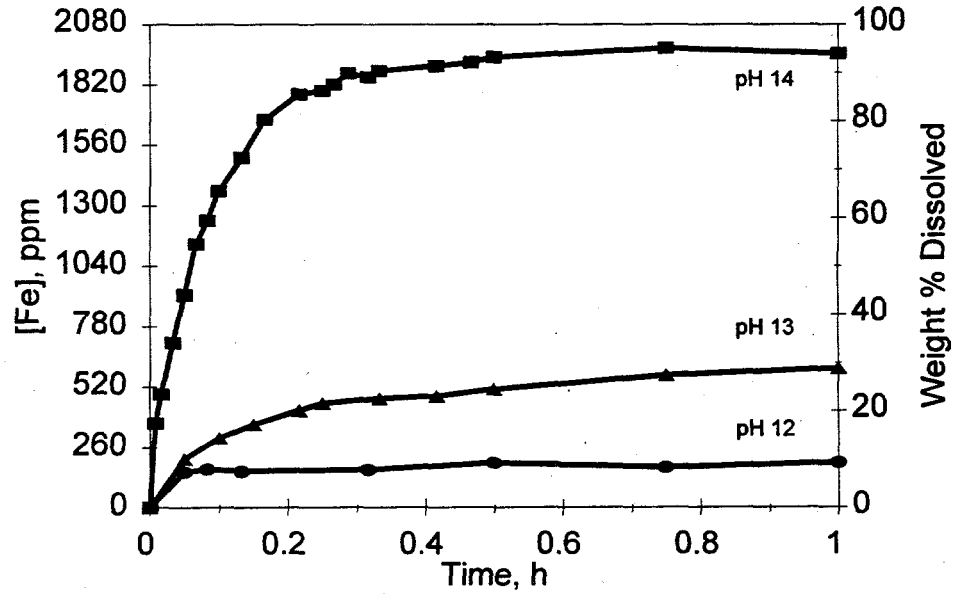

Figure 2.8. Solubility of Vendor-prepared $Na_2NiFe(CN)_6$ in NaOH as a Function of pH at 25°C, First Hour of Dissolution

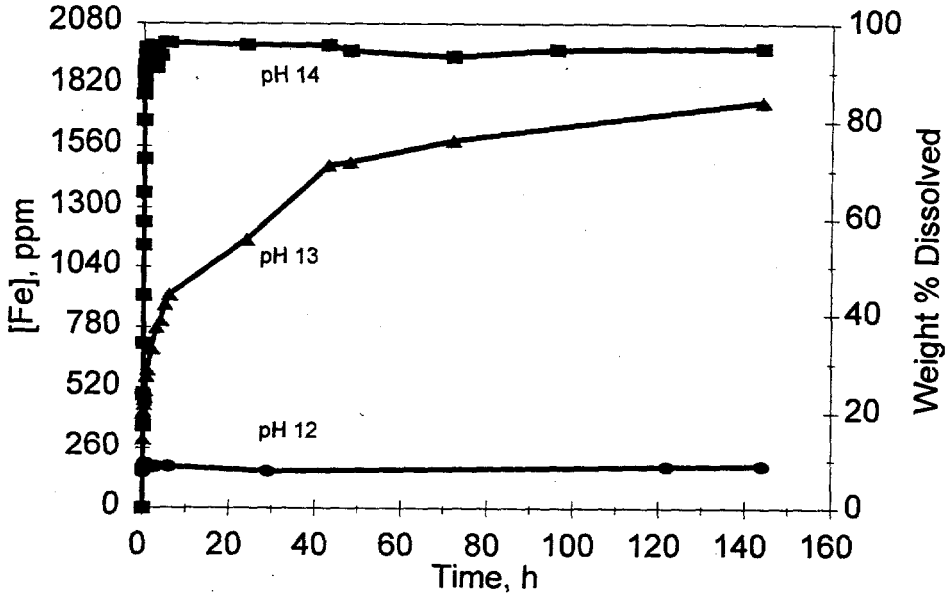

Figure 2.9. Solubility of Vendor-prepared $Na_2NiFe(CN)_6$ in NaOH as a Function of pH at 25°C, Extended Dissolution Time

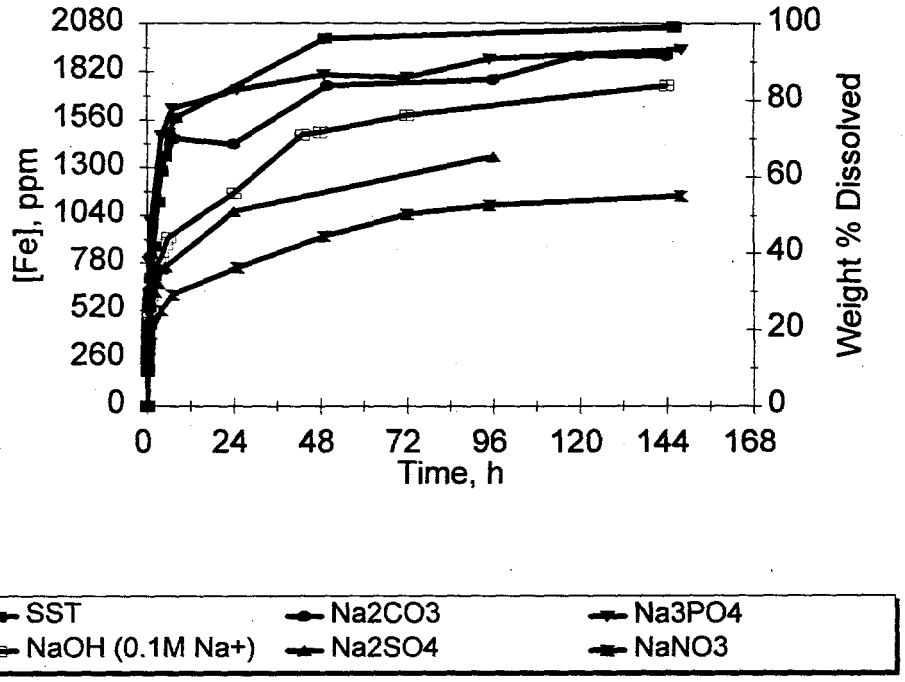

Figure 2.10. Solubility of Vendor Material in a pH 13 Solution Adjusted to 1 *M* Na^+ by Addition of Various Sodium Salts

The enhancement may result from an anion effect in which phosphate and carbonate accelerate dissolution by precipitating the highly insoluble nickel salts. Alternatively, these salts, precipitated on a particle surface, may have higher permeabilities to base compared with nickel hydroxide. However, neither nickel phosphate nor nickel carbonate could be positively identified spectroscopically. Absorption bands were observed in FTIR spectra that might be attributable to phosphate, but assignment to nickel phosphate was not possible. Laboratory-prepared nickel phosphate was found to be amorphous in XRD spectra. Nickel hydroxide was positively identified in the insoluble solids by FTIR and XRD.

Although AA data shown in Figure 2.10 indicate that the dissolution in carbonate media closely followed that in phosphate media, analysis of the insoluble reaction products indicated otherwise. From FTIR analysis, the insoluble fraction at the end of the phosphate dissolution was not the starting material but, rather, a reprecipitated iron-cyanide of unknown composition. From AA measurements, the reprecipitated material represented about 6% of the iron introduced. The remaining insoluble ferrocyanide fraction in the carbonate dissolution was primarily the expected unreacted vendor ferrocyanide containing only a small quantity of the reprecipitated material. Dissolution according to Eq. (1) was apparently more rapid in phosphate than in carbonate media, but the precipitation reaction gave the appearance, in plots of soluble iron as a function of time, that the rates were similar. The insoluble material from the SST simulant salt-containing experiment also showed a small amount of reprecipitated iron-cyanides.

Suppression of dissolution at pH 13 appeared to be related to the sodium ion activity, suggesting a common ion effect. The fastest dissolution at this pH was in the solution with no additional sodium ion ($[Na^+] = 0.1\ M$). As the sodium ion concentration was increased to 6 *M*, dissolution became slower and only about 30% of the ferrocyanide dissolved (Figure 2.11). In solutions with 1 *M* Na^+, discussed above, the rate and extent of dissolution in the presence of sodium sulfate may be greater than in the presence of sodium nitrate because sodium sulfate has a lower sodium ion activity. Association of sodium with the doubly charged sulfate ion decreases the effective sodium ion concentration.

Unlike the pH 13 solutions, the influence of sodium ion concentration and the presence of various anions was minimal in pH 14 solution. Figure 2.12 compares data from experiments at pH 14 with 1 *M* Na^+, as sodium hydroxide; 4 *M* Na^+, adjusted with sodium nitrate; and 2 *M* Na^+, adjusted with sodium carbonate. No effect of added sodium ion or anions was seen. Dissolution was over 90% complete within 1 h in each solution. The higher hydroxide ion concentration overcame any Na^+ ion inhibition.

The dependence of the rate of dissolution at pH 13 on initial quantity of vendor material present, which determines the $OH^-/Fe(CN)_6^{-4}$ mole ratio, was investigated. Figure 2.13 shows the results for the first 12 h of experiments using 1.0 g [$OH^-/Fe(CN)_6^{-4} = 2.7$], 0.25 g [$OH^-/Fe(CN)_6^{-4} = 10.8$], and 0.1 g [$OH^-/Fe(CN)_6^{-4} = 27$] vendor material, each in 50 mL of a pH 13 solution containing 1 *M* Na^+ adjusted with $NaNO_3$. Also shown are the pH 14 data in which 1 g of the vendor material in 50 mL of solution was used [$OH^-/Fe(CN)_6^{-4} = 27$]. Normalized to a weight percent dissolved basis, more rapid

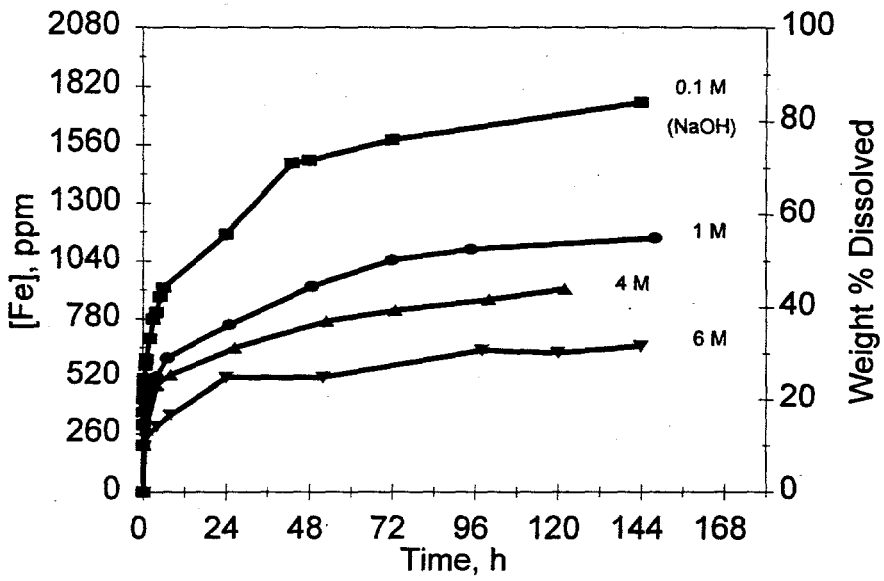

Figure 2.11. Solubility of Vendor Material at pH 13 as a Function of Sodium Ion Concentration (adjusted with $NaNO_3$)

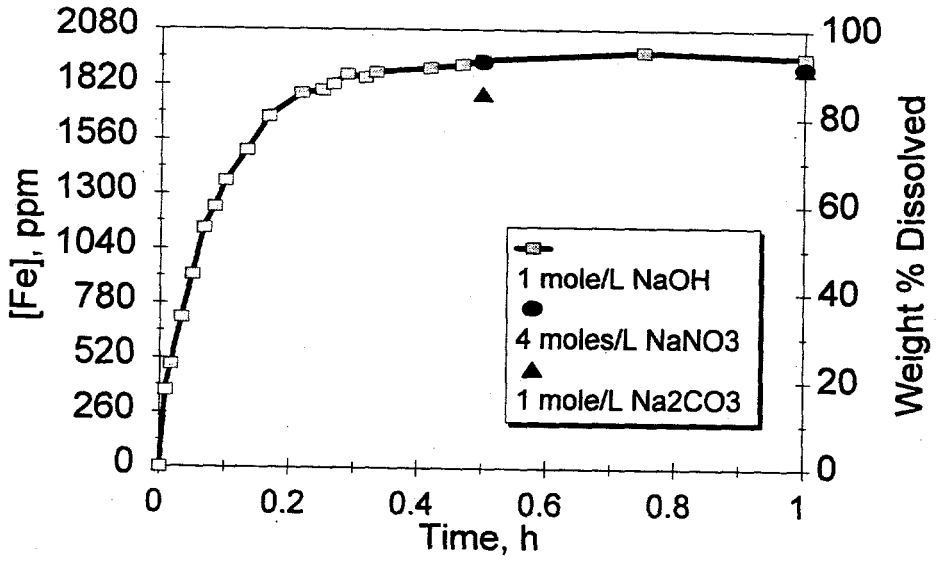

Figure 2.12. Dissolution of Vendor Material in pH 14 Solutions

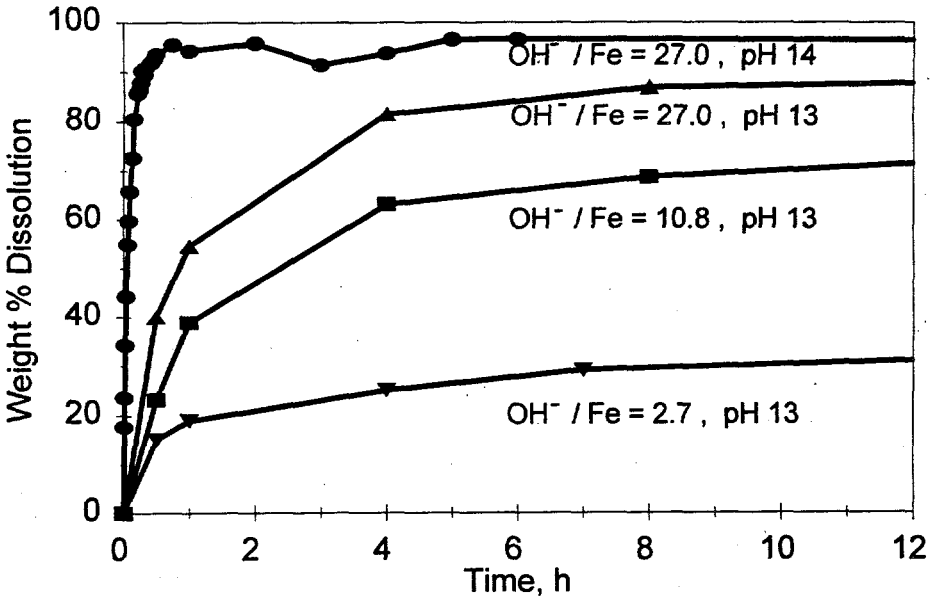

Figure 2.13. Solubility of Vendor Material as a Function of Hydroxide Ion to Ferrocyanide Ion Mole Ratio, 1 *M* Na^+

dissolution was observed when less ferrocyanide was present, i.e., when the hydroxide ion to ferrocyanide ion mole ratio was high. At longer reaction times in the pH 13 solution with the lowest $OH^-/Fe(CN)_6^{-4}$ ratio, the decrease in pH (0.2 to 0.4 pH units) may have contributed to the lower dissolution rate and extent of dissolution. However, at short reaction times this decrease was very small in each solution (calculated to be <0.5 pH units) and probably had an insignificant effect. At a hydroxide ion to ferrocyanide ion mole ratio of 27.0, the pH 14 dissolution was observed to be much more rapid than in pH 13 solution, indicating that the overall hydroxide ion concentration was still the major factor influencing the rate of dissolution.

An experiment was conducted investigating the dissolution of the vendor-prepared $Na_2NiFe(CN)_6$ in the presence of SST simulant salts under nearly static conditions, since the contents of actual SSTs are not mixed. The experiment was conducted at pH 13 with SST simulant salts added to give 1 *M* Na^+. The solution was sampled less frequently (24-h intervals) than the stirred solutions to minimize disturbance. Before each sampling, a 5-s stirring was required to ensure a homogeneous solution phase. Figure 2.14 illustrates the rate of dissolution in the static experiment compared with dissolution in a stirred solution with the same initial composition. As expected, the rate of dissolution was slower in the static solution and probably would have been slower if fewer samples had been taken. Nevertheless, appreciable dissolution occurred. About 40% was dissolved after 24 h, and 90% dissolution was observed after 6 days in the experiment conducted with minimal stirring.

Table 2.6 summarizes pH data taken during vendor material dissolution experiments. Moles of hydroxide consumed, as estimated from pH meter measurements (glass electrode), were ratioed against the moles of vendor material dissolved. Any inaccuracies in the measured pH values (0.1 units)

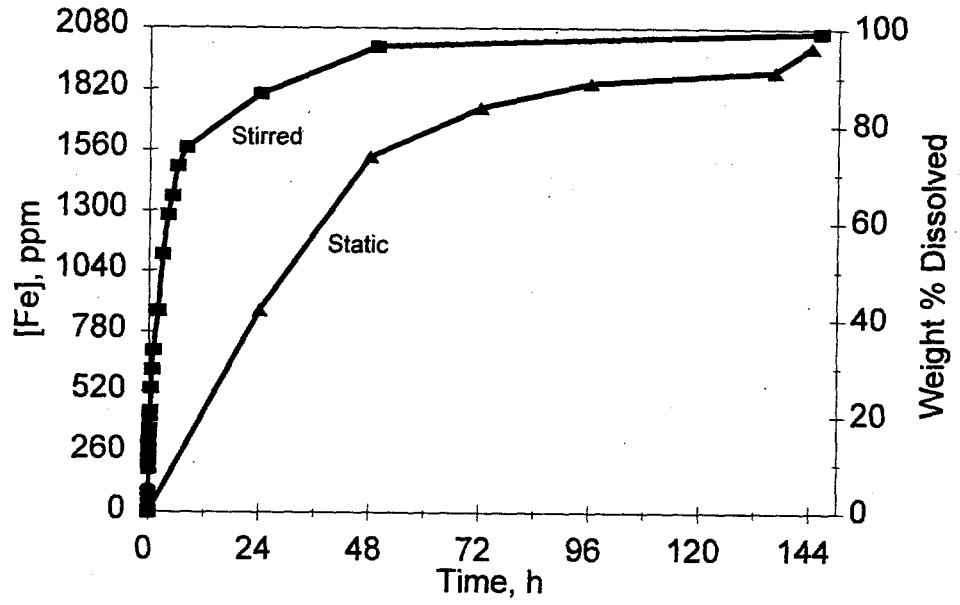

Figure 2.14. Comparison of Dissolution of Vendor Material Stirred and Static pH 13 Solutions Containing SST Simulant Salts

resulted in variations in the $OH^-/Fe(CN)_6^{-4}$ mole ratio of about 0.5 to 1; the calculated ratio is sensitive to the accuracy of the pH measurement. In most cases the $OH^-/Fe(CN)_6^{-4}$ ratio was approximately 2 as predicted from the stoichiometry of the dissolution reaction (Eq. 1). Ratios greatly different from 2 were observed in pH 14 solution and in cases where only a small amount of dissolution (small change in $[OH^-]$) had occurred, such as when 0.1 and 0.25 g of vendor material (as opposed to 1 g) were used. High sodium nitrate concentrations had relatively little effect on the calculated $OH^-/Fe(CN)_6^{-4}$ mole ratios, indicating that measured changes in pH may be accurate even though absolute pH values from glass electrode measurements in these high sodium solutions are uncertain.

2.2.2 Solubility of a $Cs_2NiFe(CN)_6$-containing Material

Dissolution tests were conducted with the PNNL-prepared material, FECN-14. Analyses indicated this material contained 2.3 moles Cs/mole ferrocyanide anion (Table 2.2) and had a Ni/Fe mole ratio of 1.14. Experiments showed that $Cs_2NiFe(CN)_6$ remained insoluble in 0.1 *M* to 4.0 *M* NaOH solutions after stirring for 144 h at room temperature. Infrared spectra indicated that the supernate solution consisted of $NaNO_3$ and NaOH, with no dissolved $Fe(CN)_6^{-4}$. Atomic absorption analyses also indicated that iron was not present in the supernate solution. The insoluble material remaining after 144 h had the same FTIR spectrum as the starting material. These results suggest that if a $Cs_2NiFe(CN)_6$ phase is present in ferrocyanide waste, it would not easily dissolve when contacted with caustic. These results also suggest that NaOH is not a suitable choice for dissolving ferrocyanide tank samples for subsequent analysis. The FECN-14 material dissolved readily in the en/EDTA solvent used for FTIR and AA analyses.

Table 2.6. Vendor Material Dissolution Data

Solution Composition	pH12	pH13	pH14	1 *M* Na^+ as Na_2SO_4[a]	1 *M* Na^+ as Na_2CO_3	1 *M* Na^+ as NaNO3		
Dissolution Time	**144h**	**144h**	**144h**	**144h**	**144h**	**73h**	**95h**	**148h**
% vendor dissolved	8.99	84.44	95.46	65.7	94.25	50.48	52.90	55.31
moles vendor dissolved	1.66E-4	1.56E-3	1.77E-3	1.22E-3	1.75E-3	9.35E-4	9.80E-4	1.02E-3
measured starting pH	12	12.9	14	12.9	12.95	12.9	12.9	12.9
starting moles NaOH	5.00E-4	3.97E-3	5.00E-2	3.97E-3	4.46E-3	3.97E-3	3.97E-3	3.97E-3
measured final pH	11.6	12.4	13.4	12.4	12.33	12.48	12.47	12.21
final moles NaOH	1.99E-4	1.26E-3	1.26E-2	1.26E-3	1.07E-3	1.51E-3	1.48E-3	8.11E-4
moles OH used	3.01E-4	2.72E-3	3.74E-2	2.72E-3	3.39E-3	2.46E-3	2.50E-3	3.16E-3
moles OH/moles FeCN	1.81	1.74	21.17	2.23	1.94	2.63	2.55	3.08

Solution Composition	4 *M* Na^+ as $NaNO_3$				6 *M* Na^+ as $NaNO_3$		1 *M* Na^+ as Na_3PO_4			
Dissolution Time	**8h**	**26.5h**	**53h**	**122h**	**120h**	**144h**	**7h**	**73h**	**95h**	**148h**
% vendor dissolved	25.51	31.35	37.20	44.20	36.71	37.92	78.36	86.38	91.26	93.67
moles vendor dissolved	4.73E-4	5.81E-4	6.89E-4	8.19E-4	6.80E-4	7.03E-4	1.45E-3	1.60E-3	1.69E-3	1.74E-3
measured starting pH	12.8	12.8	12.8	12.8	12.7	12.7	13	13	13	13
starting moles NaOH	3.15E-3	3.15E-3	3.15E-3	3.15E-3	2.51E-3	2.51E-3	5.00E-3	5.00E-3	5.00E-3	5.00E-3
measured final pH	12.3	12.37	12.32	12.2	11.87	11.5	12.9	12.65	12.6	12.4
final moles NaOH	9.98E-4	1.17E-3	1.04E-3	7.92E-4	3.71E-4	1.58E-4	3.97E-3	2.23E-3	1.99E-3	1.26E-3
moles OH used	2.16E-3	1.98E-3	2.11E-3	2.36E-3	2.14E-3	2.35E-3	1.03E-3	2.77E-3	3.01E-3	3.74E-3
moles OH/moles FeCN	4.56	3.41	3.06	2.88	3.14	3.34	0.71	1.73	1.78	2.16

Table 2.6. (contd)

Solution Composition	0.1g Vendor Material, 1 *M* Na^+ as $NaNO_3$					0.25g Vendor Material, 1 *M* Na^+ as $NaNO_3$			
Dissolution Time	**7h**	**24h**	**48h**	**72h**	**144h**	**8h**	**26.5h**	**53h**	**122h**
% vendor dissolved	86.96	91.79	94.69	99.52	99.52	68.79	81.93	89.47	87.54
moles vendor dissolved	1.61E-4	1.70E-4	1.75E-4	1.84E-4	1.84E-4	3.19E-4	3.79E-4	4.14E-4	4.05E-4
measured starting pH	12.9	12.9	12.9	12.9	12.9	12.9	12.9	12.9	12.9
starting moles NaOH	3.97E-3	3.97E-3	3.97E-3	3.97E-3	3.97E-3	3.97E-3	3.97E-3	3.97E-3	3.97E-3
measured final pH	12.53	12.63	12.72	12.52	12.42	12.49	12.54	12.5	12.42
final moles NaOH	1.69E-3	2.13E-3	2.62E-3	1.66E-3	1.32E-3	1.55E-3	1.73E-3	1.58E-3	1.32E-3
moles OH used	2.28E-3	1.84E-3	1.35E-3	2.32E-3	2.66E-3	2.43E-3	2.24E-3	2.39E-3	2.66E-3
moles OH/moles FeCN	14.14	10.81	7.68	12.56	14.41	7.62	5.90	5.77	6.55

(a) Sufficient amount of the sodium salt added to an aqueous solution of NaOH at the desired pH to yield [Na^+] shown.

The reason for the insolubility of $Cs_2NiFe(CN)_6$, in light of the solubility of the sodium analog, is unknown at this time. Possible explanations include a greater lattice energy than the sodium analog, a different crystal structure, and fewer defects or smaller channels through which base can enter the crystal lattice. The literature indicates that alkali metal nickel ferrocyanides are isomorphous regardless of composition, having cubic structures with unit cell parameters between 9.9 and 10.2Å (Loos-Neskovic et al. 1984, 1989; Loos-Neskovic and Federoff 1989). In a constant-sized unit cell, replacement of sodium with the larger cesium cation could block channels within the extended ferrocyanide structure and increase the lattice energy. Thus, there may be both thermodynamic and kinetic reasons the dissolution process is slow.

2.2.3 Solubility of In-Farm-1A, Rev. 4 Flowsheet Material

Upon drying to constant weight at 60°C under vacuum, dried IF-1A, the top-layer In-Farm flowsheet simulant (Jeppson and Wong 1993), lost 46% of its weight as water. Analytical results (iron, cesium, nickel, and sodium by AA, ferrocyanide anion by FTIR) for the dried simulant dissolved in en/EDTA solution were summarized in Table 2.1. This material contained 4.51×10^{-2} moles Cs/mole ferrocyanide (as determined from AA data). The Cs/Na mole ratio of 2.9×10^{-3} was smaller than the expected ratio of 9×10^{-3} based on the flowsheet recipe; more of the cesium was associated with the bottom ferrocyanide layer obtained in the flowsheet preparation (Table 2.2). Infrared and AA data were consistent for iron and ferrocyanide anion, giving a $Fe(CN)_6^{-4}/Fe$ ratio of 1.09, showing that iron was predominantly present in the form of ferrocyanide anion. The Ni/Fe ratio of 1.52 was greater than the stoichiometric ratio of 1.0 observed in the vendor material and in FECN-14. The IF-1A material either contained other nickel compounds, such as nickel phosphate, or contained ion-exchanged nickel within the ferrocyanide phase, $Ni_2Fe(CN)_6$.

Two dissolution experiments, one initially containing 1 *M* sodium ion at pH 13 ($NaNO_3$ used to adjust $[Na^+]$) and the other at pH 14 (1 *M* Na^+ as NaOH), were conducted in which 4.29 g of IF-1A were stirred in 75 mL of caustic solution. The quantities were chosen to give about the same final ferrocyanide ion concentration if all dissolved and to give the same $OH^-/FeCN_6^{-4}$ mole ratio as in previous experiments utilizing the vendor material. Iron and cesium concentrations in periodically drawn solution samples were determined by AA.

Dissolution (total dissolved iron concentration) as a function of time is shown in Figure 2.15, which compares the behavior of IF-1A with that of the vendor material under similar conditions. The rate of dissolution of IF-1A was generally suppressed relative to the vendor material; initial dissolution at pH 14 was rapid with a slow increase to about 85% dissolution after 144 h, while the vendor material was over 90% dissolved after 0.5 h. In pH 13 solution, the IF-1A material dissolved very slowly with only about 18% in solution after 144 h. None of the solution samples contained cesium; i.e., cesium was not solubilized even in pH 14 solution. Ferrocyanides are known to be good ion exchange materials for cesium sorption (Campbell et al. 1990; Loos-Neskovic and Fedoroff 1989), and it is likely that any cesium liberated by ferrocyanide dissolution would exchange back into the solid to form a $Cs_2NiFe(CN)_6$ or $NaCsNiFe(CN)_6$ phase.

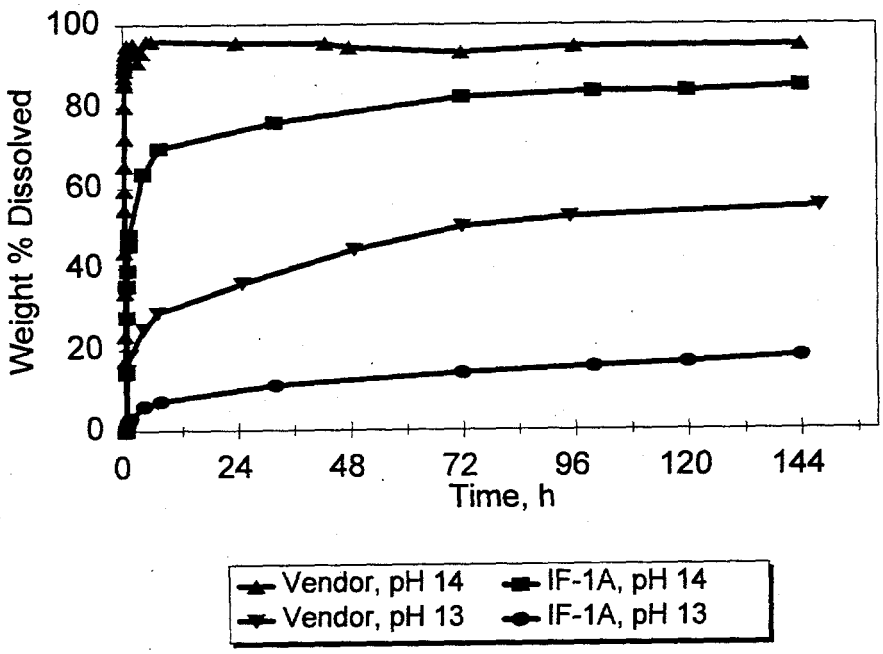

Figure 2.15. Vendor Material and In-Farm-1A Solubility at pH 13 and pH 14 with 1 *M* Na^+

The suppressed rates and lower solubilities were probably not a result of higher sodium ion concentrations arising from dissolution of salts from the IF-1A material (which would increase the [Na^+] about 0.5 *M*). The rate of dissolution of IF-1A in pH 13 solution was lower than that of the vendor material in a pH 13, 6 *M* Na^+ solution, which reached about 30% after 144 h (Figure 2.11). The rates were also suppressed in pH 14 solution, an effect not attributable to the Na^+ concentration (Figure 2.12). The lower rates and solubilities were more likely due to an accumulation of cesium at the particle surface, forming an insoluble phase. As cesium accumulation increases, the composition of this phase would tend to approach that of FECN-14, containing $Cs_2NiFe(CN)_6$, which was found to be insoluble in up to 4 *M* NaOH (Bryan et al. 1993; Lilga et al. 1993).

The temperature dependence of IF-1A dissolution was investigated at 60°C and 90°C using pH 13 solutions adjusted to 1 *M* sodium ion with $NaNO_3$. Figure 2.16 illustrates the increase in soluble iron (ferrocyanide ion) with time. The extent of dissolution increased with increasing temperature. At 25°C, after 144 h, about 18 wt% of the ferrocyanide had dissolved. At 60°C and 90°C, the reaction apparently approached equilibrium dissolution of about 52% and 60%, respectively. Atomic absorption analysis again showed no dissolved cesium in any of the reaction solutions.

2.2.4 Cesium Ion Exchange in Competition with Ferrocyanide Dissolution

In waste processing operations at the Hanford Site, ferrocyanides were precipitated to scavenge cesium; supernates were pumped off; and new waste was added on top of the ferrocyanide bed. The waste added was often highly caustic and also contained cesium. For example, neutralized current acid

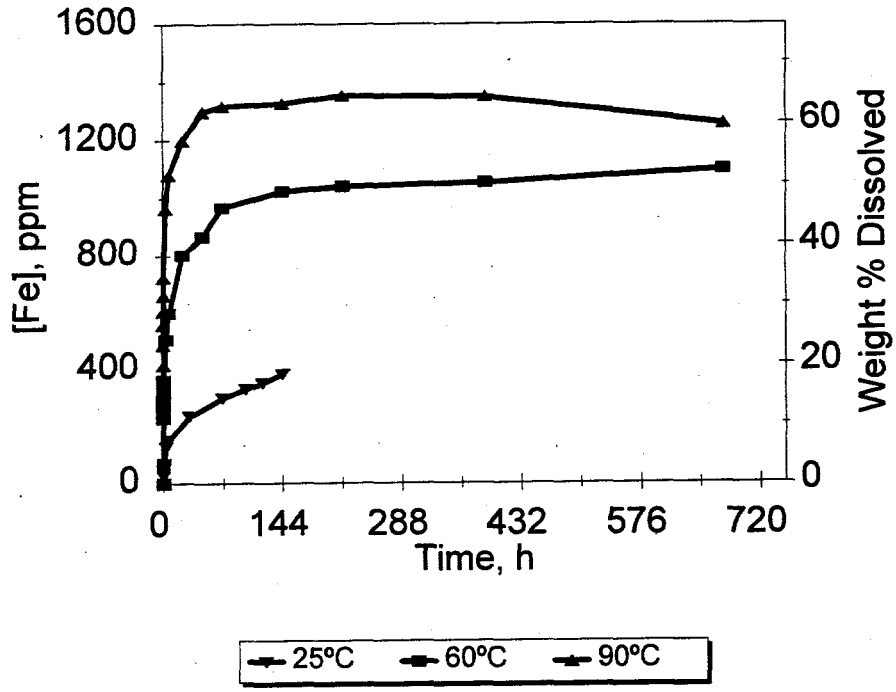

Figure 2.16. Temperature Dependence of In-Farm-1A Solubility at pH 13 with 1 *M* Na^+

waste contained about 5 Ci/L ^{137}Cs. If about 40% of the cesium was present as ^{137}Cs, the total cesium concentration was on the order of 1 x 10^{-3} *M* when added to the tanks. Assuming the waste contacted the ferrocyanide sludge, both dissolution and ion exchange processes could have occurred.

In previous solubility studies (Bryan et al. 1993; Lilga et al. 1993), a material containing $Cs_2NiFe(CN)_6$ (FECN-14, prepared in the absence of sodium ion) was found to be insoluble in up to 4 *M* NaOH at room temperature. Also, IF-1A, which contains cesium, dissolved to a lesser extent and at a slower rate than the vendor ferrocyanide material, $Na_2NiFe(CN)_6 \cdot Na_2SO_4 \cdot 4.5\ H_2O$, which does not contain cesium. Apparently, as the $Na_2NiFe(CN)_6$ in the IF-1A material dissolved, cesium became concentrated at the particle surface to form an insoluble cesium-rich phase, inhibiting dissolution. The actual chemical composition of the cesium-rich phase and the solubility of mixed Cs/Na phases, such as $NaCsNiFe(CN)_6$, have not been determined.

Solid sodium nickel ferrocyanide materials are also known to be excellent ion exchange materials for cesium (Loewenschuss 1982; Loos-Neskovic and Fedoroff 1989; Loos-Neskovic et al. 1976, 1990; Burgeson et al. 1994). Selectivity for cesium over sodium is very high (Campbell et al. 1990; Loos-Neskovic et al. 1976).

The extent of these two processes depends on their relative rates and the amount of mixing that occurred. If cesium uptake is relatively fast, all of the cesium could ion-exchange before the ferrocyanide exposed to the waste dissolves. If dissolution is fast relative to ion exchange, some of the cesium could be left in solution.

In the work conducted here, competition experiments were used to provide an indication of the rate of ion exchange relative to the rate of dissolution. Two room temperature experiments exploring vendor material dissolution (1 g) were conducted in the presence of 2.3 x 10^{-3} *M* $CsNO_3$ (50 mL), one containing 3 *M* NaOH, the other containing 4 *M* NaOH. The NaOH solution containing cesium was added to the solid vendor material, then stirred, and solution samples were periodically taken and analyzed for soluble iron (ferrocyanide anion) and cesium ion by AA. The results of both of these experiments were very similar, indicating an insensitivity to base strength, as illustrated in Figure 2.17. Dissolution, as determined by the soluble iron, was 70% to 80% complete within 2 min, reaching 85% to 90% after 24 h. Cesium uptake was also very rapid with 98% incorporation into the solid phase after 2 min when the first solution sample was taken.

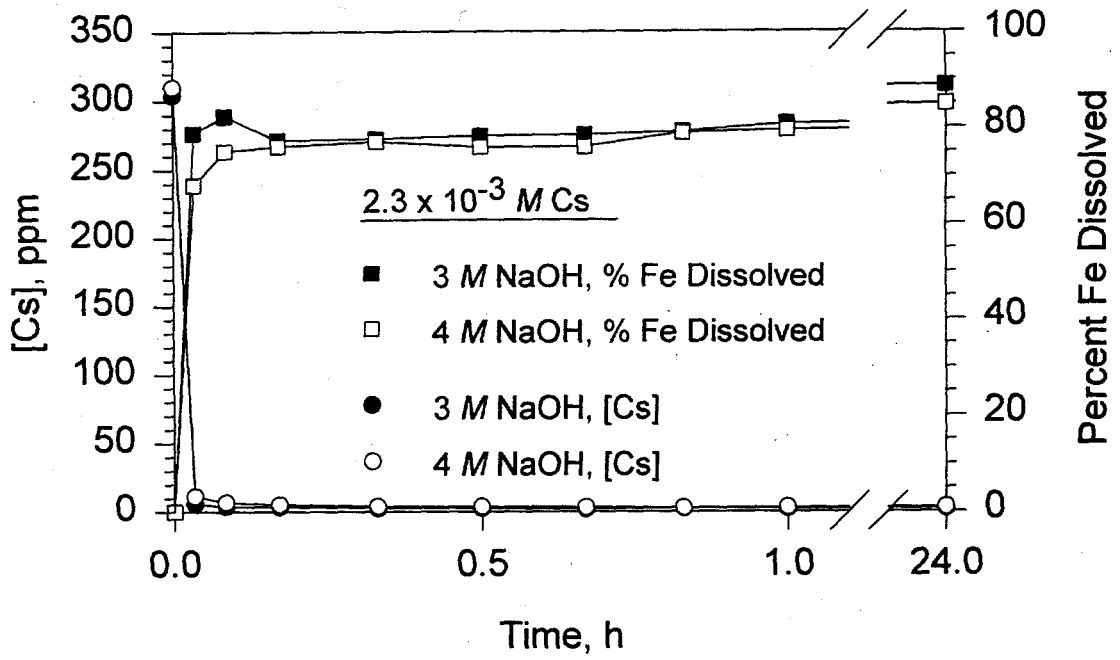

Figure 2.17. Dissolution and Cesium Ion Exchange in 3 and 4 *M* NaOH at an Initial [Cs] of 2.3 x 10^{-3} *M*

Figure 2.18 compares results of experiments conducted in 4 *M* NaOH with either 3 x 10^{-4} or 2.3 x 10^{-3} *M* cesium ion. Less dissolution is observed at the higher cesium concentration, with about 10% less dissolution under these conditions. At the higher cesium concentration, more cesium incorporation occurs, forming more of the insoluble cesium-containing ferrocyanide phase. The number of moles of cesium in 50 mL of the 3 x 10^{-4} *M* solution was not enough to measurably decrease the ferrocyanide solubility, showing essentially the same dissolution behavior as the vendor material in the absence of cesium ion. The [Cs] is quickly reduced to the AA detection limit for both of the starting concentrations tested.

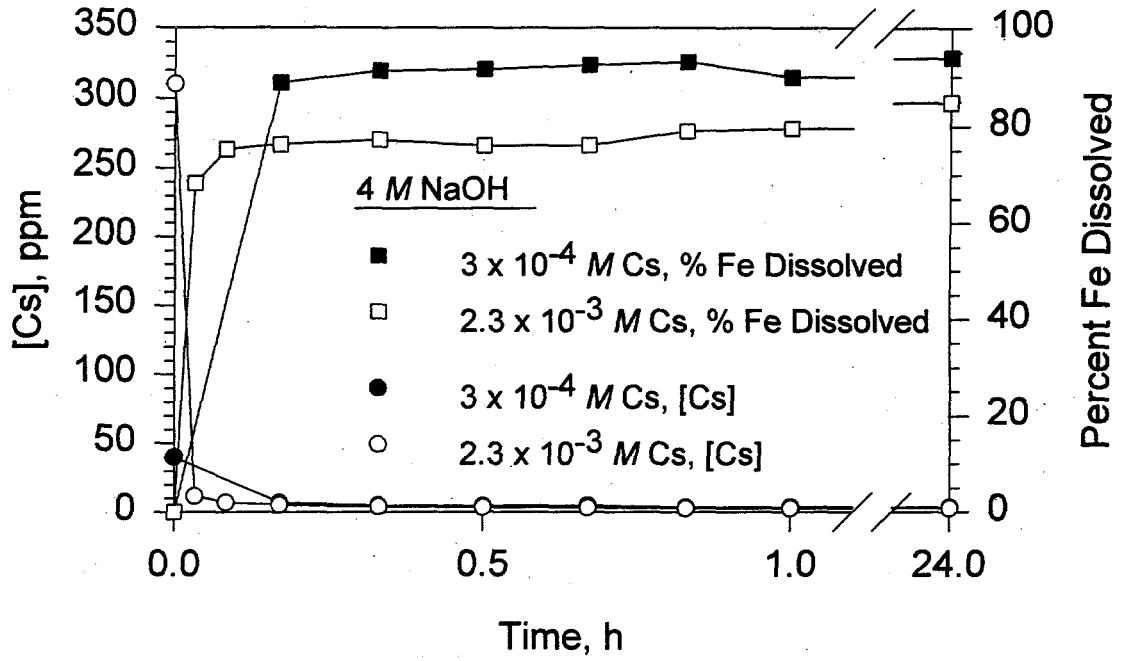

Figure 2.18. Dissolution and Cesium Ion Exchange in 4 *M* NaOH at 2.3 x 10^{-3} *M* and 3 x 10^{-4} *M* Initial Cesium Ion Concentration

These experiments using the vendor ferrocyanide simulant, which did not initially contain cesium, can be compared with dissolution experiments of the IF-1A flowsheet simulant, which was precipitated with cesium. Figure 2.19 illustrates the difference in dissolution behavior between the vendor material in the presence of soluble cesium and the IF-1A material containing cesium already incorporated in the solid phase. Cesium in the solid phase inhibited dissolution, making dissolution of the In-Farm material slow relative to materials not initially containing cesium. Dissolution of the vendor material was not inhibited initially, and dissolution was rapid. However, because cesium ion-exchanged into the solid phase, dissolution slowed and became incomplete. The rate of cesium ion exchange was apparently faster than the rate of ferrocyanide dissolution, since cesium was effectively removed from solution before dissolution was complete.

In addition, more insoluble ferrocyanide was present at the end of these experiments than might be predicted from the number of moles of cesium present. For a $Cs_2NiFe(CN)_6$ phase, the Fe/Cs mole ratio would be 0.5; for a $CsNaNiFe(CN)_6$ phase, this ratio would be 1.0. For IF-1A dissolution, the Fe/Cs mole ratio was found to be 3.3 (although dissolution may not have reached equilibrium at the end of this experiment, in which case, the ratio would be smaller). For the vendor material dissolutions, this ratio varied from 1.4 to about 8. These results are similar to results for the IF-1B material, discussed in Section 2.1.2, and are consistent with the formation of an insoluble cesium-rich ferrocyanide phase at the particle surface, encasing otherwise-soluble $Na_2NiFe(CN)_6$.

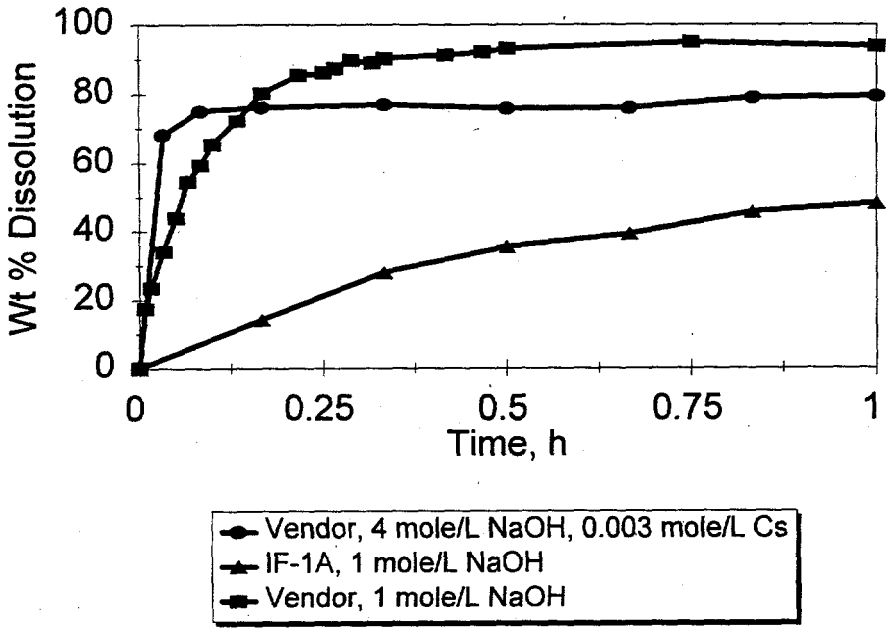

Figure 2.19. Dissolution Behavior of a Solid In-Farm Flowsheet Material Containing Cesium Ion Compared with a Solid Vendor-prepared Simulant Not Containing Cesium

2.3 Radiolysis of Ammonia and Formate Ion Under Hydrolysis Conditions

Hydrolysis of ferrocyanide ion present in IF-1B produces, along with other products, ammonia and formate ion. These products were found to be destroyed in the gamma field; and experiments were performed to estimate their rate of destruction under hydrolysis conditions. Experiments were conducted in which solutions containing 0.03 *M* formate ion or 0.03 *M* ammonia, along with 2 *M* NaOH containing $NaNO_3$ and $NaNO_2$, were heated to 90°C and exposed to gamma radiation. Starting concentrations of ammonia and formate ion were chosen to fall in the range of the concentrations present in IF-1B hydrolysis experiments. Vessels were individually pulled from the gamma tubes after various reaction times, then analyzed.

Because ammonia was destroyed with time, mole% conversion based on ammonia was only an estimate of the amount of cyanide or ferrocyanide hydrolyzed. Reported mole% conversion values (sometimes called apparent percent conversion in this report) do not take into account the amount of ammonia lost to radiolysis.

2.3.1 Radiolysis of Ammonia

Two series of experiments were conducted in which solutions containing 0.03 *M* ammonia (generated in situ from NH_4Cl), 2 *M* NaOH, 0.095 *M* $NaNO_3$, and 0.036 *M* $NaNO_2$ were irradiated at 90°C in a gamma field; one series at 1 x 10^5 rad/h, the other at 9 x 10^3 rad/h. Nitrate and nitrite were added because they are nitrogen-containing species present in the IF-1B flowsheet material that undergo radiolysis. An identical control solution containing 0.03 *M* ammonia was heated but not irradiated. Two more controls were prepared containing 2 *M* NaOH, 0.095 *M* $NaNO_3$, and 0.036 *M* $NaNO_2$ but no ammonia (NH_4Cl). One was placed in a gamma tube, heated to 90°C, and irradiated at 1 x 10^5 rad/h, while the other received identical treatment but was not irradiated. The purpose of these two controls was to determine whether ammonia was generated radiolytically or thermally from nitrate or nitrite. All three controls were sampled after 20 days.

The measured ammonia concentration in the control vessel containing ammonia, but not subjected to irradiation, was 0.029 *M*, the same as the starting concentration within experimental error. No ammonia was generated in either of the two controls not initially containing ammonia, indicating that ammonia was not generated either thermally or radiolytically from nitrate or nitrite under the conditions of the IF-1B hydrolysis experiments.

The results of ammonia radiolysis experiments conducted with applied gamma dose rates of 1 x 10^5 rad/h and 9 x 10^3 rad/h are shown in Figure 2.20. Destruction appears to be a zero-order

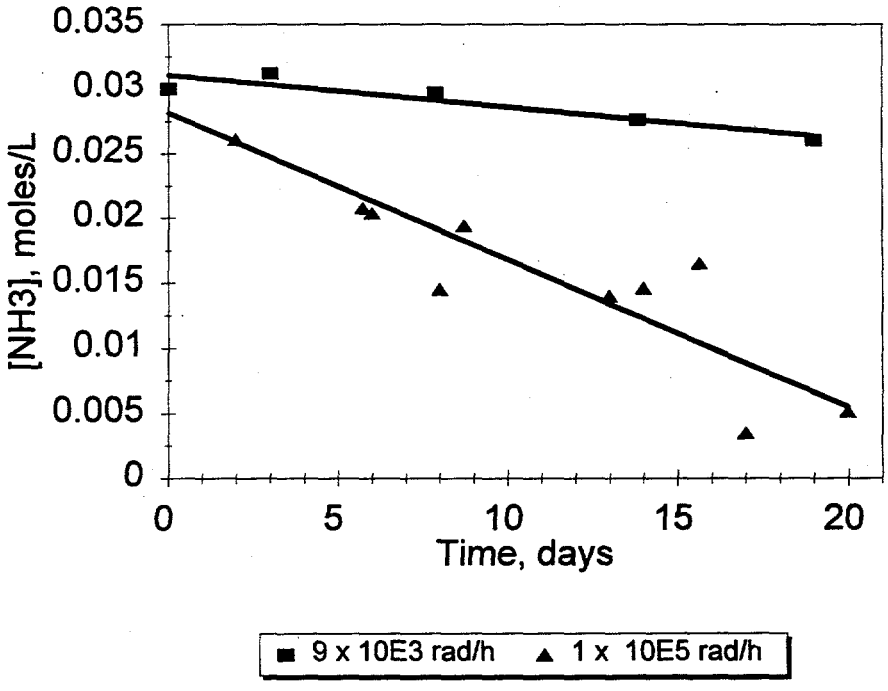

Figure 2.20. Radiolysis of Ammonia Under Hydrolysis Experiment Conditions at Gamma Dose Rates of 1 x 10^5 rad/h and 9 x 10^3 rad/h and Least Squares Fits to Data

process, but there is a great deal of scatter in the data, especially at the higher dose rate after long reaction times. Zero-order behavior is consistent with rate-limiting radical (hydroxyl or oxide radical) formation, followed by more rapid reaction of the radical with ammonia. Radiolysis was more rapid at the higher dose rate; assuming a zero-order relationship, the destruction rate constant at the incident dose rate of 1×10^5 rad/h was about 1.1×10^{-3} *M*/day and about 2.1×10^{-4} *M*/day at 9×10^3 rad/h.

2.3.2 Radiolysis of Formate

Formate ion radiolysis was more rapid than ammonia radiolysis. Radiolysis of 0.03 *M* formate ion in 2 *M* NaOH containing 0.095 *M* $NaNO_3$ and 0.029 *M* $NaNO_2$ was conducted at 1×10^5 rad/h and 90°C. Before 6 days of reaction, formate ion was completely destroyed (Figure 2.21). Assuming destruction occurs by a zero-order process, and using data from the first 4 days, a rate of 6.15×10^{-3} *M*/day, or over 5 times the rate of ammonia destruction, was calculated. This series of experiments, however, does not confirm zero-order destruction, and the mechanism is likely more complicated than this assumption implies (Goldstein et al. 1988; Singleton et al. 1988).

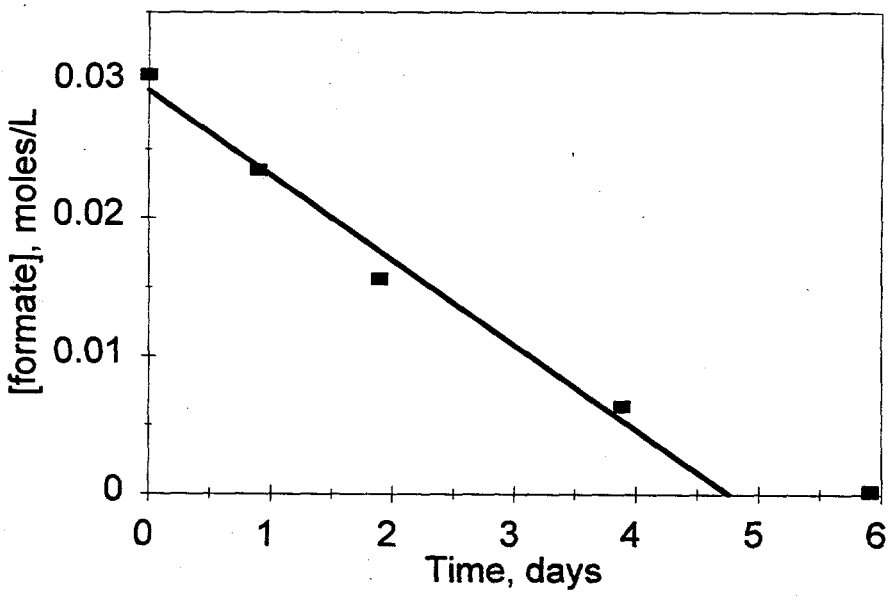

Figure 2.21. Radiolysis of Formate Ion Under Hydrolysis Experiment Conditions at a Gamma Dose Rate of 1×10^5 rad/h and 90°C

Similar results were obtained in nuclear magnetic resonance (NMR) experiments, which showed that radiolysis of formate ion forms carbonate ion (Figure 2.22). Experiments were conducted by irradiating NMR tubes containing 0.1 *M* $NaNO_3$, 0.03 *M* $NaNO_2$, and 0.03 *M* $NaH^{13}CO_2$ in 2 *M* NaOH solution at about 16°C and at a dose rate of about 1×10^5 rad/h. Again, formate ion decomposed in an

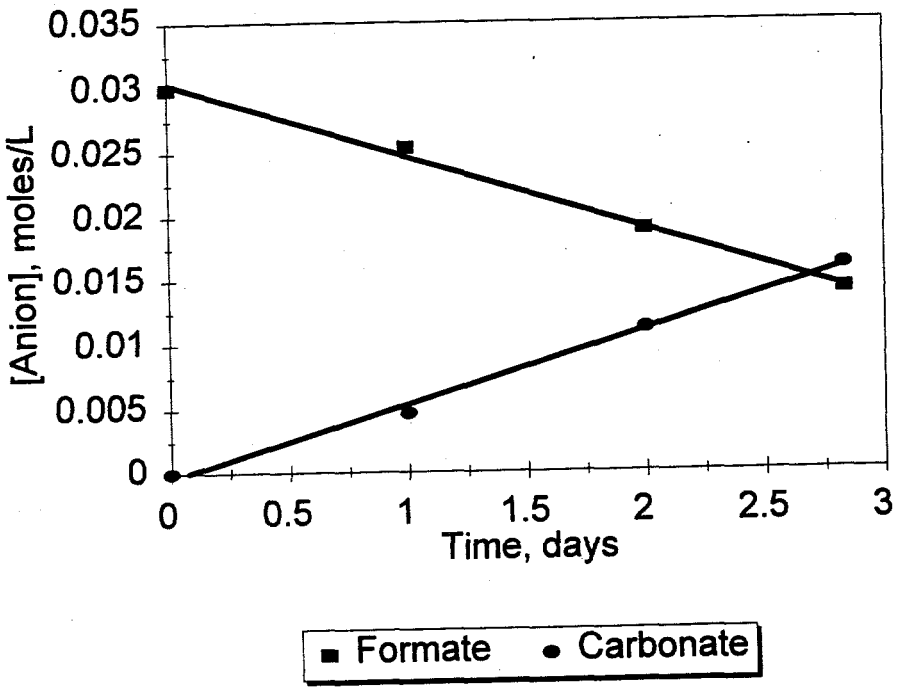

Figure 2.22. Radiolytic Conversion of ^{13}C-labeled Formate Ion to Carbonate Ion at a Gamma Dose Rate of 1 x 10^5 rad/h and at 25°C as Determined by NMR Spectroscopy

apparently zero-order fashion at a rate of 5.7 x 10^{-3} *M*/day, in good agreement with the experiment discussed above. Carbonate ion appeared at the same rate, and no other ions, including oxalate, were observed.

2.4 Hydrolysis of In-Farm Ferrocyanide Flowsheet Material in 2 *M* NaOH

Several experiments were conducted in 2 *M* NaOH solution to investigate the influence of temperature and gamma dose rate on the hydrolysis of IF-1B flowsheet material, the bottom layer of the In-Farm simulant. Table 2.7 outlines the experiments conducted and the conditions used. The temperature range investigated is representative of present and past conditions in most of the tanks (Meacham et al. 1994b).

All of the experiments discussed in this section were conducted in 2 *M* NaOH. The base concentration was not varied because it has been reported that for soluble ferrocyanide anion the rate of thermal hydrolysis is independent of hydroxide ion concentration above pH 9 (Kuhn and Rice 1977). For experiments reported in this section, the hydrolysis reaction conducted in a gamma field was also assumed to be zero-order in hydroxide ion concentration. Although hydroxide ion is consumed to precipitate nickel and iron, hydroxide ion is initially present in large excess. Experiments conducted at pH 10 in which $Na_2NiFe(CN)_6$ has low solubility are discussed in Section 2.8.

Table 2.7. Conditions for IF-1B Hydrolysis Experiments Investigating the Effects of Temperature and Gamma Dose Rate. Experiments were conducted with 0.5 g IF-1B in 25 mL of 2 *M* NaOH for 3 weeks.

Experiment Number	Incident Gamma Dose Rate (rad/h)	Temperature (°C)
H11	1×10^5	100
H1	1×10^5	90
H10	1×10^5	80
H2	1×10^5	70
H3	1×10^5	50
H4	4×10^4	90
H5	9×10^3	90
H12	9×10^3	100

2.4.1 Change in Ammonia and Formate Ion Concentrations with Aging

Figure 2.23 shows ammonia and formate produced by hydrolysis in the gamma-irradiated and thermal (control) experiments at 80°C (H10). The ammonia and formate data are typical and clearly show that both temperature and gamma radiation promote the hydrolysis reaction. For the 80°C experiment, ammonia yields after 19 days were found to be an order of magnitude higher in the gamma-irradiated samples compared with identical, but non-irradiated, controls. Based on the ammonia data and the solubility of IF-1B at the reaction temperature, the apparent percent conversion of ferrocyanide to ammonia in this experiment was at least 30%, not taking into account ammonia lost by radiolysis.

According to the stoichiometry of the thermal hydrolysis reaction (Eqs. 2 and 3), ammonia and formate should be formed in a 1:1 mole ratio. This ratio was observed in the non-irradiated control experiments in which only thermal hydrolysis occurred. However, although formate production paralleled ammonia production, ammonia concentrations in the 90°C experiment irradiated at 1×10^5 rad/h were on the order of 4 to 4.5 times higher than the measured formate ion concentrations. Data from gamma dependence studies showed that the disparity in ammonia and formate concentrations decreased as the applied gamma dose rate decreased. For example, at 4×10^4 rad/h (H4), the $[NH_3]/[HCO_2^-]$ ratio varied from about 2 to 3.8, and at 9×10^3 rad/h (H5), this ratio was between 1 and 1.5 for most samples (Figure 2.24). The difference in concentrations could result from stoichiometric formation of these products by radiolysis as discussed in Section 2.3. Formate ion radiolysis was more rapid than

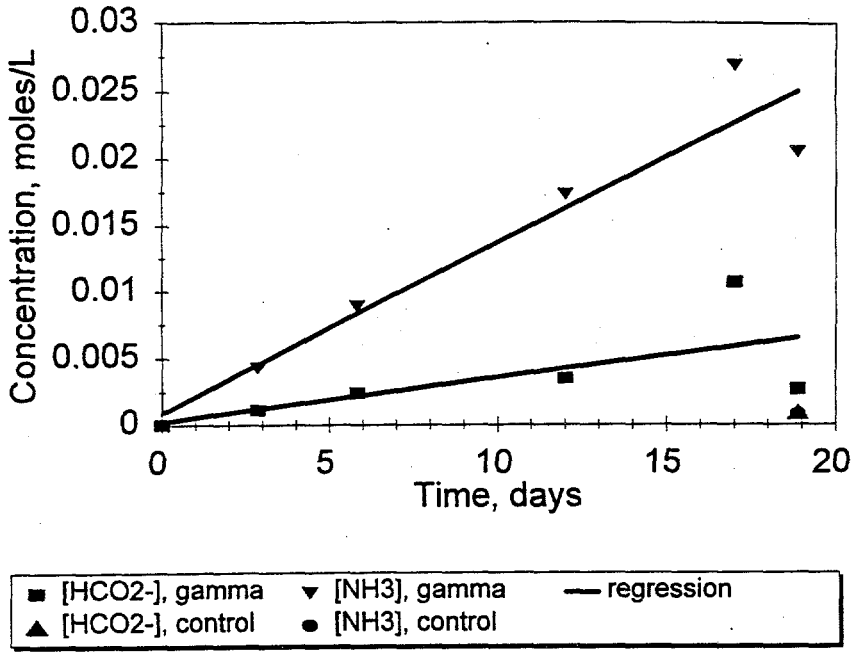

Figure 2.23. Ammonia and Formate Ion Production in the Hydrolysis of IF-1B in 2 *M* NaOH at 80°C and 1 x 10^5 rad/h (H10). Control experiments were identical but not irradiated.

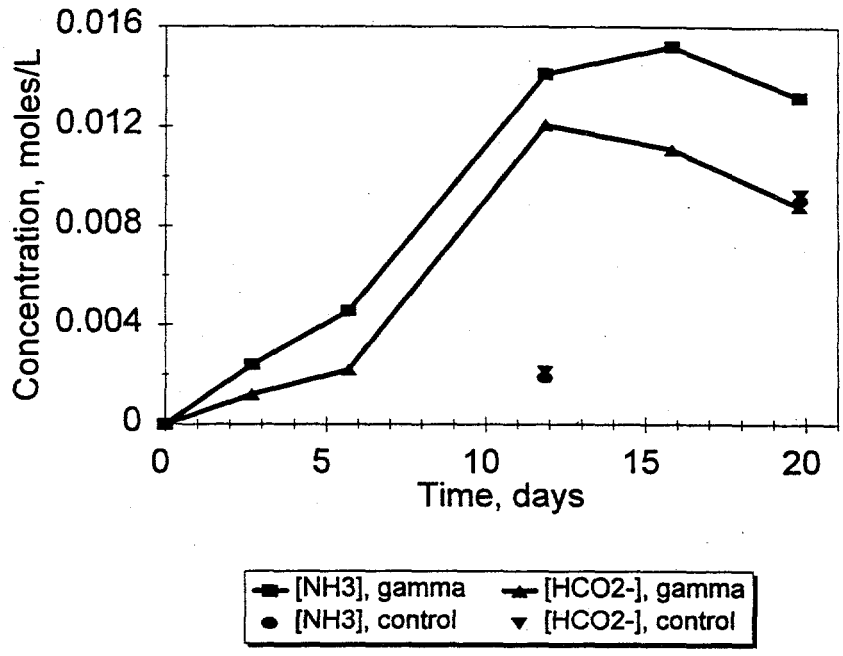

Figure 2.24. Ammonia and Formate Ion Production in the Hydrolysis of IF-1B in 2 *M* NaOH at 90°C and 9 x 10^3 rad/h (H5). Control experiments were identical but not irradiated.

ammonia radiolysis by about a factor of 5 at this dose rate. It is also possible that other parallel hydrolysis reactions that do not form formate occur in the gamma field, such as by oxidation of cyanide to cyanate, which would hydrolyze to ammonia and carbonate in the 2 *M* NaOH.

The results of hydrolysis of IF-1B at 90°C (H1) are comparable to those at 80°C. The curve for ammonia production at 90°C is shown in Figure 2.25. Also shown are results from a series of 12-day experiments to estimate the reproducibility of the aging experiments, conducted under conditions nearly identical to the H1 experiment, and the 95% confidence limits calculated from a linear regression of the data. In the reproducibility experiments, vessel/gamma access tube combinations were systematically varied to investigate the effects of vessel, gamma access tube, and sample preparation and analysis techniques. The average concentration of ammonia formed after 12 days in all experiments, including H1, was 0.0472 *M*. The relative standard deviation was 0.0038 *M* for a percent deviation of 8.0%. The results showed that there was very little error associated with sample preparation and analysis. More error was introduced when different vessels were used in the same gamma tube than when the same vessel was used in different gamma tubes. The relative sensitivity to vessel likely arises from slight differences in temperature control rather than variations in gamma dose rate or sample preparation and analysis.

Although gamma radiation promotes hydrolysis, the agreement between results of the duplicate experiments and the H1 experiment also indicates the relative insensitivity of aging to changes in applied gamma dose rate. The reproducibility data were collected about 2 years after the H1 data were

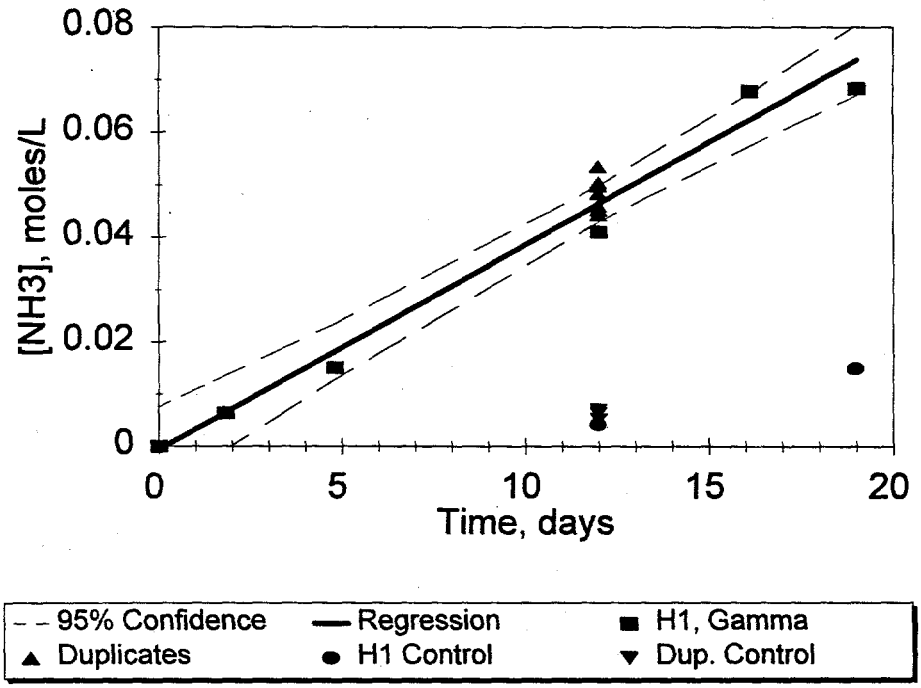

Figure 2.25. Ammonia Production and Reproducibility in the Hydrolysis of IF-1B in 2 *M* NaOH at 90°C and 1 x 10^5 rad/h (H1)

collected. In that time, the gamma dose rate decayed about 20%, i.e., reproducibility experiments received a 20% lower dose rate than in the H1 experiment, yet no discernible effect on the hydrolysis results was seen.

Data for ammonia production at various temperatures are compared in Figure 2.26. Overall, the ammonia concentration increased approximately linearly with hydrolysis time. This behavior was different from published thermal hydrolysis rate data, which indicated that hydrolysis was first order in total cyanide (Robuck and Luthy 1989). The linear approximation was made (Figure 2.26) as an approach toward developing a mathematical model, and global rate constants calculated from the slopes of the lines (Table 2.8). The Eyring plot of these rate data, shown in Figure 2.27, was linear, and an activation energy of $\Delta H = 145$ kJ/mole was calculated. Rate constants for ammonia production at a given temperature at a gamma dose rate of 1×10^5 rad/h may be calculated with use of Eq. (6). The calculated rate constants do not directly represent the rate of ferrocyanide hydrolysis because the rate of ammonia radiolysis is included; rate constants underestimate the actual extent of aging that occurred. Rate constants predicted from this equation are generally within a factor of about 2 of the observed rate constants.

$$\ln(k_T/T) = 36.3 - 1.74 \times 10^4 \cdot 1/T \qquad (6)$$

In three sets of experiments to study the effects of applied radiation, the gamma dose rate was varied over one order of magnitude. While dose rates used in aging studies were higher than those experienced by waste in SSTs, the integrated dose was about the same (see Section 2.1.3). The gamma dose rates used and other conditions of each experiment were summarized in Table 2.7.

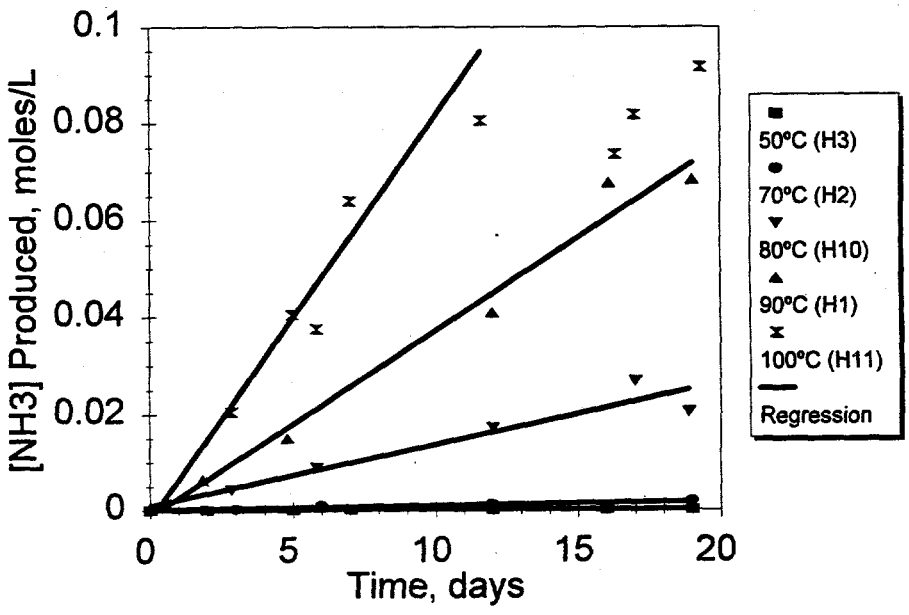

Figure 2.26. Linear Approximation to the Temperature Dependence of Ammonia Production in the Hydrolysis of IF-1B (0.5 g) at a Gamma Dose Rate of 1×10^5 rad/h

Table 2.8. Rate Constants for Ammonia Production and Iron Loss in Hydrolysis Experiments at Various Temperatures and Applied Gamma Dose Rates

Experiment Number	Temperature (°C)	Applied Gamma Dose Rate (Rad/h)	NH_3 Production Rate Constant (*M*/day)	Iron Loss Rate Constant (day^{-1})
H3	50	1×10^5	7.76×10^{-6}	--
H2	70	1×10^5	8.87×10^{-5}	0.022
H10	80	1×10^5	1.28×10^{-3}	0.078
H1	90	1×10^5	3.83×10^{-3}	0.11
H11	100	1×10^5	4.47×10^{-3}	0.22
H4	90	4×10^4	1.99×10^{-3}	0.060
H5	90	9×10^3	1.05×10^{-3}	0.0025

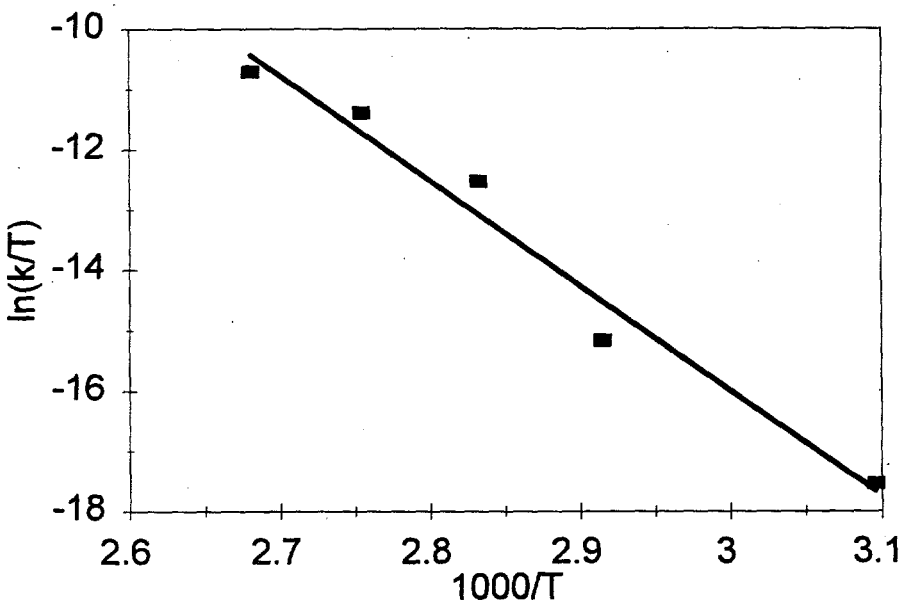

Figure 2.27. Eyring Plot for Ammonia Production in the Hydrolysis of IF-1B Flowsheet Material

At each dose rate, conversion was enhanced by the gamma field as compared with the thermal controls, as previously discussed. At Day 12, the amounts of ammonia produced in solutions irradiated at 4×10^4 rad/h (H4) and 9×10^3 rad/h (H5) were about 11 and 8 times more, respectively, than in the associated controls. Conversions in thermal controls for H1, H4, and H5 were comparable.

As the dose rate increases, the rate of ammonia production also increases. As in the temperature-dependence experiments, the change in ammonia concentration with time is approximately linear (Figure 2.28). Global rate constants calculated from the slopes of the linear regression lines through the data are given in Table 2.8. A plot of rate constant as a function of gamma dose rate is linear (Figure 2.29) with a slope of 2.8×10^{-8} $M \cdot h \cdot rad^{-1} \cdot day^{-1}$. The intercept gives a rate constant consistent with results of the non-irradiated control experiments at 90°C if the linear approximation is made, although this is not necessarily the best model for the thermal data (Tan and Teo 1987). The gamma dose rate dependence of hydrolysis, therefore, can be described by Eq. (7), where γ is the incident gamma dose rate and $k_{\gamma,90}$ is the predicted hydrolysis rate constant at 90°C.

$$k_{\gamma,90} = 2.8 \times 10^{-8} \cdot \gamma + 7.88 \times 10^{-4} \quad (7)$$

A hydrolysis experiment was conducted at 100°C and 9×10^3 rad/h to test the use of Eqs. (5) and (6) to predict reaction rates. Ammonia production observed in this experiment is compared with other related experiments in Figure 2.30. As expected, the extent of hydrolysis was greater than in the 90°C experiment at the same dose rate, and was less than that obtained in the higher dose rate experiment at the same temperature.

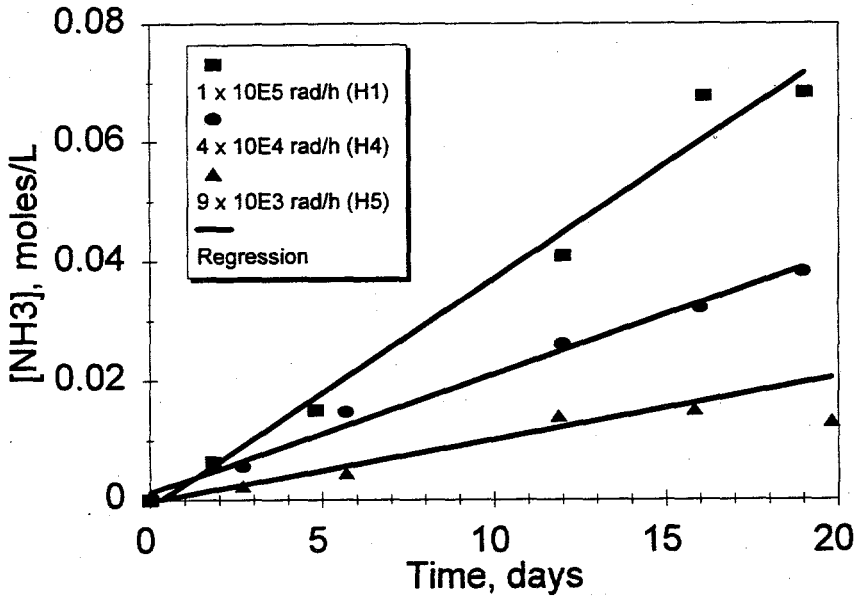

Figure 2.28. Linear Approximation to the Applied Gamma Dose Rate Dependence of Ammonia Production in the Hydrolysis of IF-1B (0.5 g) at 90°C

It is not known why the Day-21 data point in Experiment H12 indicates a drop in ammonia produced, but the ammonia concentration shown in Figure 2.30 is lower than the ammonia concentration in the thermal control run under the same conditions (not shown), suggesting the Day-21 data point is in error. Ammonia radiolysis does occur, and, if hydrolysis slowed for some reason, such

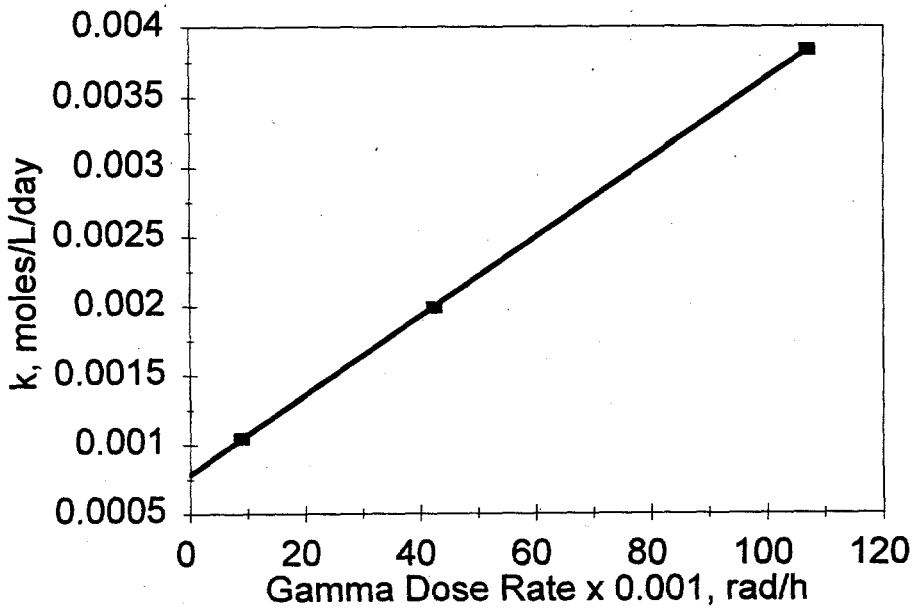

Figure 2.29. Ammonia Production Rate Constant as a Function of Applied Gamma Dose Rate in the Hydrolysis of IF-1B (0.5 g) at 90°C

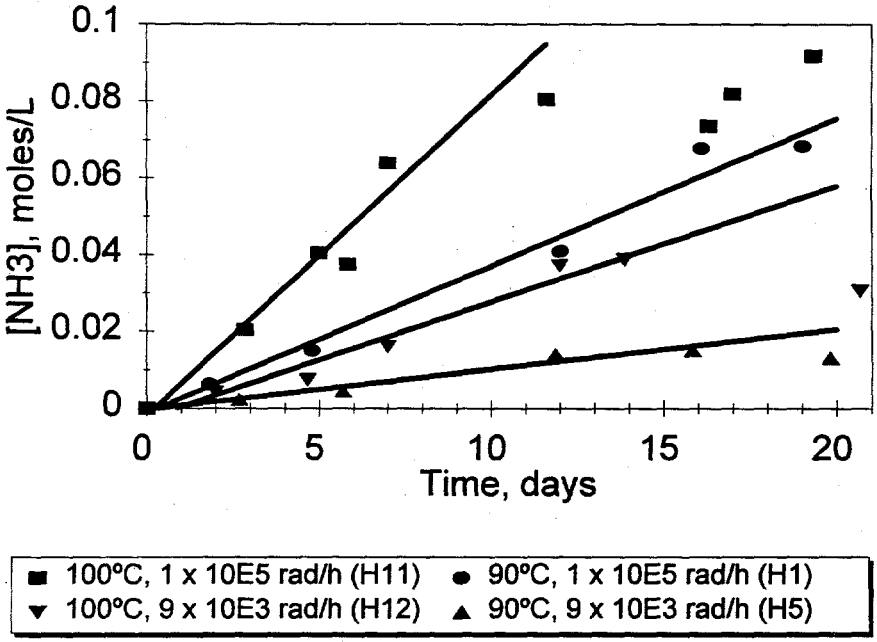

Figure 2.30. Ammonia Production During Hydrolysis of IF-1B in an Experiment in Which Both the Applied Gamma Dose Rate and Temperature Were Varied

as if a more stable intermediate was formed, the ammonia concentration could drop. However, FTIR analysis of the Day-21 supernate shows that, like most other samples tested, only $Fe(CN)_6^{-4}$ and $Ni(CN)_4^{-2}$ are present, and does not offer an explanation for a decreased rate of conversion. Further discussions of FTIR results are found in Sections 2.4.2 and 2.6.

If the linear approximation is made using all data except the Day-21 data, a rate constant for ammonia production of 3.0×10^{-3} *M*/day is obtained. This rate constant is in very good agreement with the predicted value of 3.6×10^{-3} *M*/day. The latter value was calculated by first using Eq. (7) to obtain a calculated rate constant at 90°C at the incident gamma dose rate, then adjusting to 100°C assuming that the temperature relationship of Eq. (6) holds for the different gamma dose rate. This assumption is valid as illustrated by Figure 2.31, which shows that the slopes of lines in Eyring plots are about the same for available temperature data at different gamma dose rates.

Figure 2.32 plots the observed ammonia concentrations at 90°C as a function of integrated dose (rad) for Experiments H1, H4, and H5. The plot appears to indicate that production of ammonia at the lower dose rates is more efficient than at the higher dose rates; i.e., more ammonia is produced for the amount of gamma absorbed. However, the plot actually illustrates the relative effects of temperature and gamma radiation. At low dose rates, the relative contribution of gamma dose is small and thermal hydrolysis produces most of the ammonia. Therefore, more ammonia is observed at a given dose as

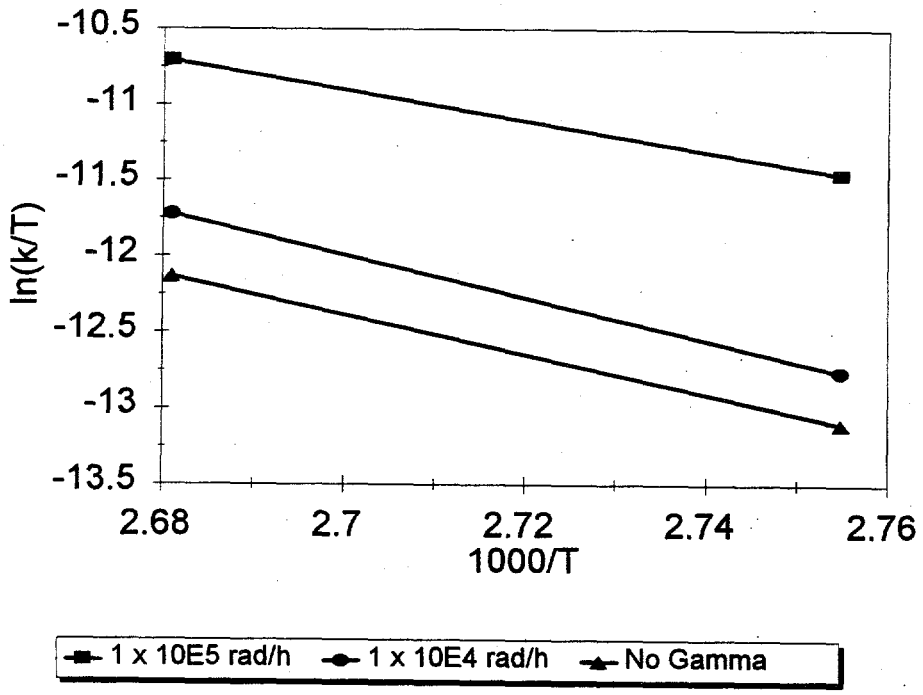

Figure 2.31. Eyring Plots for IF-1B Hydrolysis at Various Gamma Dose Rates

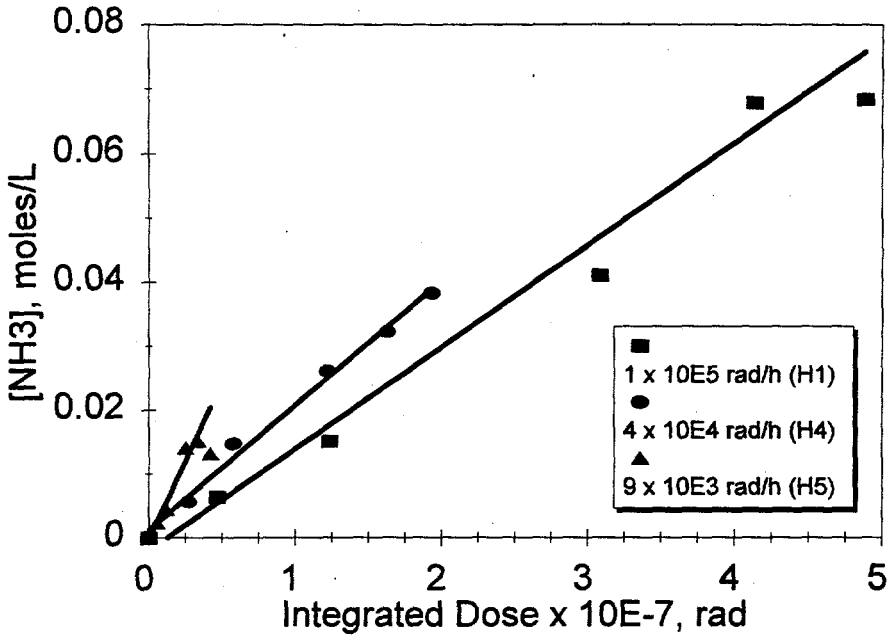

Figure 2.32. Ammonia Production for IF-1B Hydrolysis as a Function of Integrated Dose

dose rate decreases because of the thermal contribution. Figure 2.32 also is complicated by an inconsistent time component. Integrated dose, and therefore the portion of the hydrolysis arising from radiolysis, is independent of time; i.e., the abscissa is not a function of time. However, the portion of the hydrolysis arising from thermal pathways are dependent on time, yet are plotted in Figure 2.32 as if they are not.

A better representation is obtained if the thermal component of hydrolysis is first subtracted to give the amount of ammonia formed by the radiolytic pathway. The thermal rate was determined from a pseudo zero-order fit to the control data (Figure 2.25), subtracted from the linear fit to the observed ammonia data from gamma-irradiated experiments, and plotted in Figure 2.33 as a function of integrated dose. The concentration of ammonia arising from the radiolytic pathway is directly proportional to dose and independent of dose rate.

2.4.2 Change in Iron Concentration with Aging

During aging, caustic added to materials containing $Na_2NiFe(CN)_6$ dissolves the $Fe(CN)_6^{-4}$ anion, which then undergoes hydrolysis. The iron precipitates during the course of the reaction as oxides or hydroxides. The change in total soluble iron concentration was monitored by AA, a measure of all soluble iron species. In some cases FTIR was used to determine the nature of the dissolved cyano species.

Infrared spectra of gamma-irradiated supernates from selected experiments showed that the only detected iron cyanide was the $Fe(CN)_6^{-4}$ anion (2037 cm^{-1}). Figure 2.34 shows the presence of this anion in a supernate solution from the 80°C experiment. Also present is $Ni(CN)_4^{-2}$, an intermediate

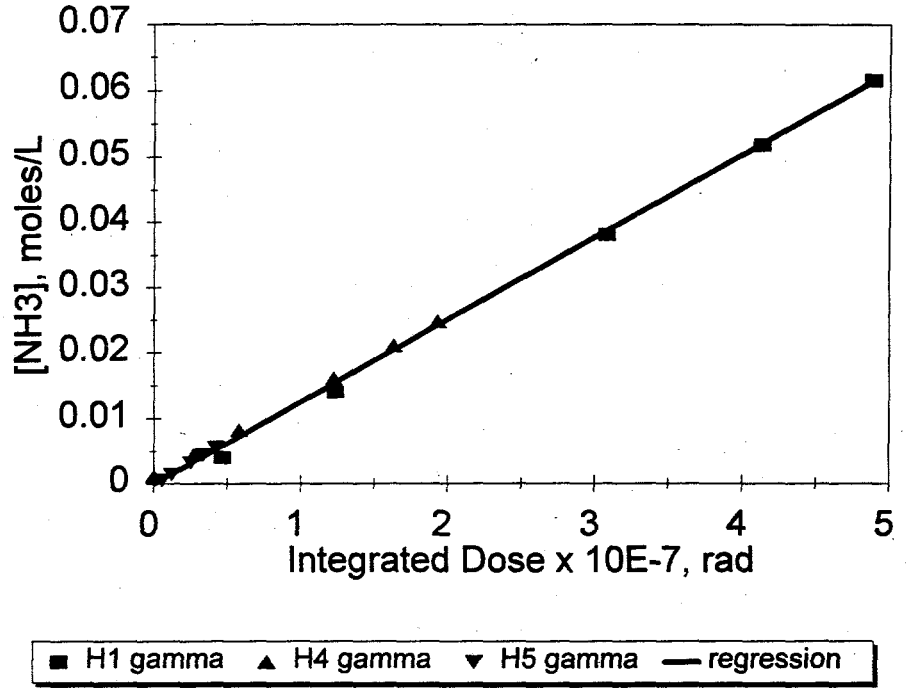

Figure 2.33. Radiolytic Component of Ammonia Production as a Function of Integrated Dose

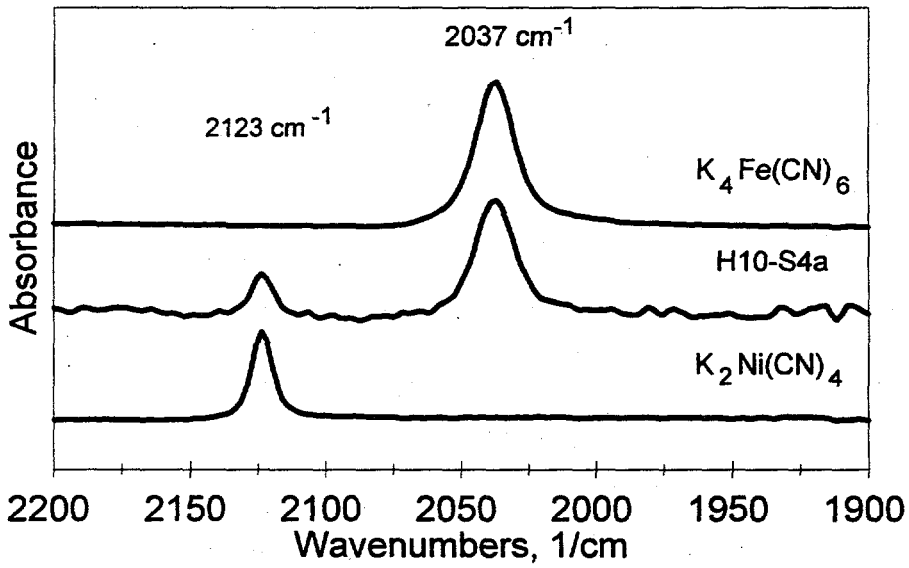

Figure 2.34. FTIR Spectra of an 80°C Hydrolysis Supernate Solution, $Ni(CN)_4^{-2}$, and $Fe(CN)_6^{-4}$

aging product whose formation and aging are discussed in more detail in Section 2.6. The concentrations of ferrocyanide ion from the FTIR results were in very good agreement with the total iron concentrations determined by AA analysis, on average within about 10%. Thus, it appears that essentially all of the soluble iron is ferrocyanide anion and that substitution products formed by sequential cyanide ion displacement during aging are short-lived or only present in very low concentrations. No ferricyanide anion was detected.

Identification of soluble iron as $Fe(CN)_6^{-4}$ and soluble nickel as $Ni(CN)_4^{-2}$ allows a determination of the approximate cyanide balance. The sum of the moles of cyanide bound to nickel and iron, using FTIR results, combined with the moles of ammonia measured, accounts for the starting cyanide within 2%, on the average, for the 11 samples analyzed (% cyanide found ranges from 89% to 109%). For example, in Sample H1-S4 (Day 12) conducted at 90°C, the initial ferrocyanide concentration is 0.0166 *M*, giving a total cyanide concentration of 0.0996 *M*. By FTIR, $[Ni(CN)_4^{-2}]$ was 0.0085 *M*, $Fe(CN)_6^{-4}$ was 0.00385 *M*, and $[NH_3]$ was 0.041 *M*. These concentrations account for a cyanide concentration of 0.0981 *M*, or 98.5% of theoretical. The amount of ammonia destroyed by radiolysis is not included in these calculations.

A typical change in total soluble iron concentration as a function of hydrolysis time is illustrated by the experiment at 80°C and 1 x 10^5 rad/h (H10), shown in Figure 2.35. The observed decrease in concentration (shown as data points) can be described as pseudo-first-order, and the line represents the fit

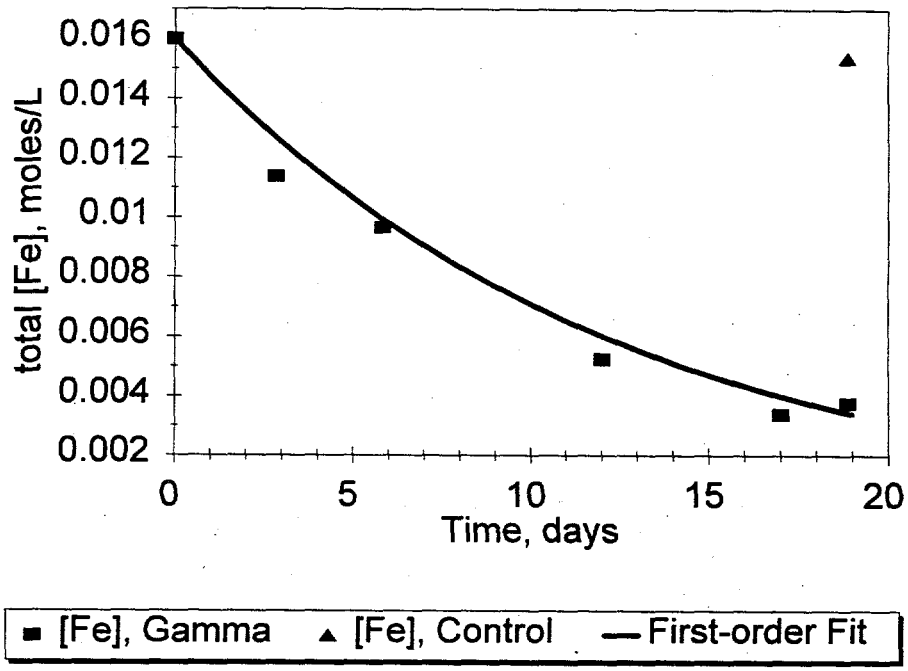

Figure 2.35. Total Iron Concentration in the Hydrolysis of IF-1B (0.5 g) at 80°C and at a Gamma Dose Rate of 1 x 10^5 rad/h (H10)

to all of the data from the gamma-irradiated experiments. The rate constant of 0.081 day^{-1} was determined from the slope of the line in a plot of ln[Fe] versus time (Figure 2.36). The rate constant is a pseudo-first-order rate constant since the loss of soluble iron from solution likely involves reaction with hydroxide, present in large excess, to precipitate iron hydroxides or oxides. Calculated pseudo-first-order rate constants at all temperatures investigated were shown in Table 2.8. The Eyring plot is linear, as shown in Figure 2.37, and the activation energy for iron loss from solution is 74 kJ/mole with gamma irradiation. For the thermal control experiments, assuming pseudo-first-order behavior, the activation energy is approximately 89 kJ/mole, in very good agreement with the value of 94.1 kJ/mole reported by Tan and Teo (1987).

The rate constant of iron loss (Table 2.8) increased linearly with increasing incident dose rate, as shown in Figure 2.38. The slope is 1.3 x 10^{-6} $day^{-1}\cdot h\cdot rad^{-1}$ at 90°C. The intercept (no applied dose) is in very good agreement with the average observed rate of thermal iron loss from control solutions at 90°C.

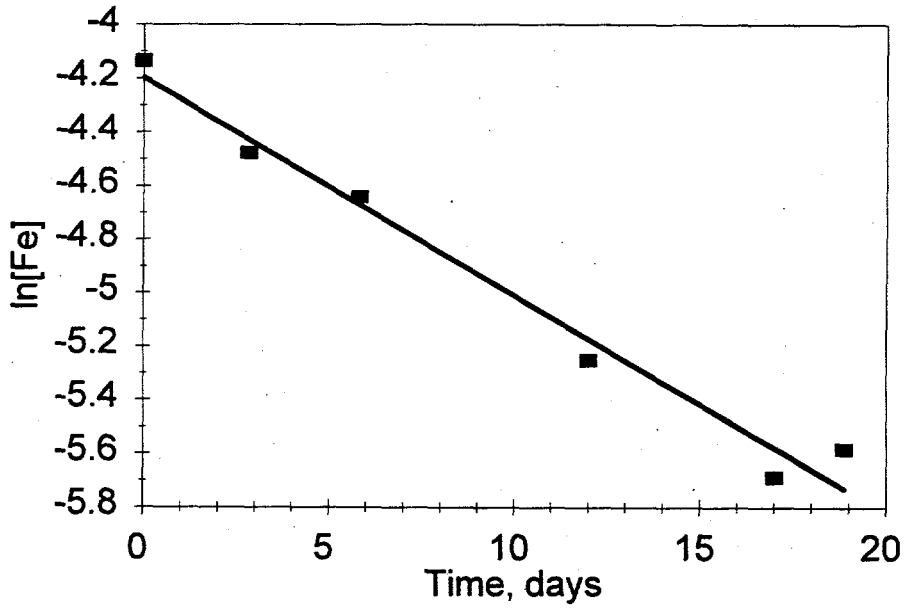

Figure 2.36. First-Order Plot for the Change in Iron Concentration in the Hydrolysis of IF-1B (0.5 g) at 80°C and at a Gamma Dose Rate of 1 x 10^5 rad/h (H10)

2.4.3 Change in Nitrate and Nitrite Concentrations with Aging

In a typical hydrolysis experiment, dissolution of 0.5 g of the dried IF-1B flowsheet material gave a solution with an initial $[NO_2^-]$ of 0.030 *M* and an initial $[NO_3^-]$ of 0.10 *M*. No additional nitrate or nitrite was added to the aging solutions. The changes in nitrate and nitrite concentrations in gamma irradiated solutions, the sum of these two concentrations, and concentrations in the thermal controls for Experiment H1 (90°C, 1 x 10^5 rad/h) are shown in Figure 2.39. Nitrate ion concentrations decreased

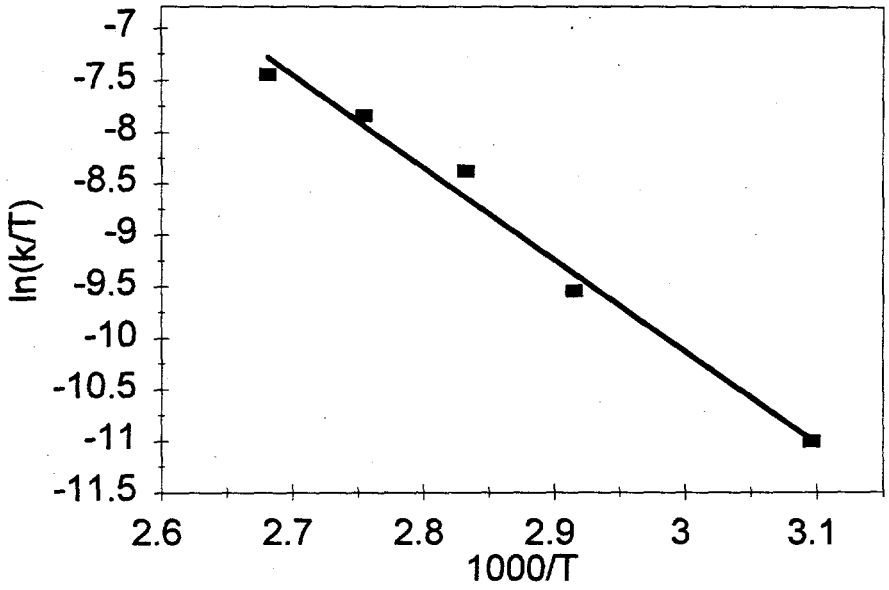

Figure 2.37. Eyring Plot for Iron Concentration Decrease in the Hydrolysis of IF-1B Flowsheet Material

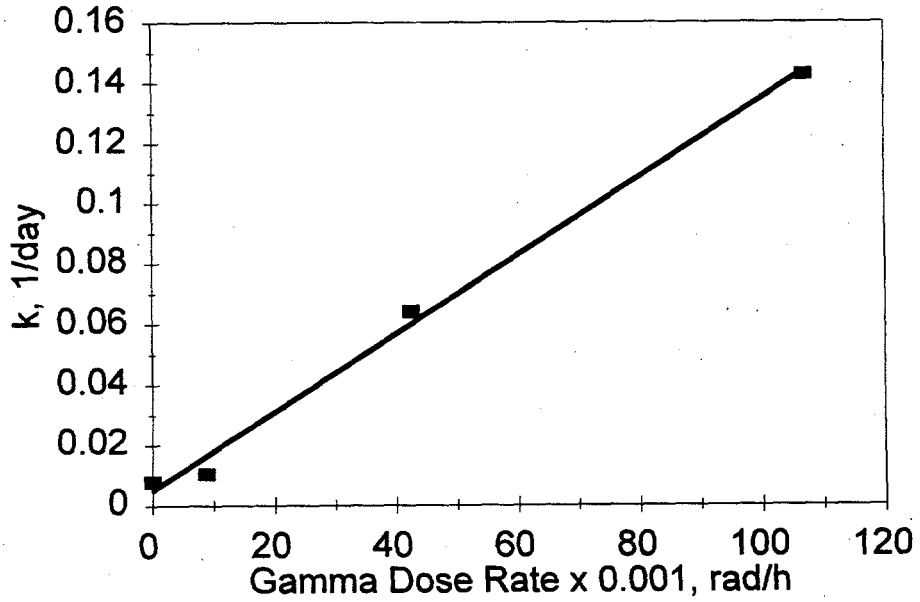

Figure 2.38. Iron Loss Rate Constant as a Function of Applied Gamma Dose Rate in the Hydrolysis of IF-1B (0.5 g) at 90°C

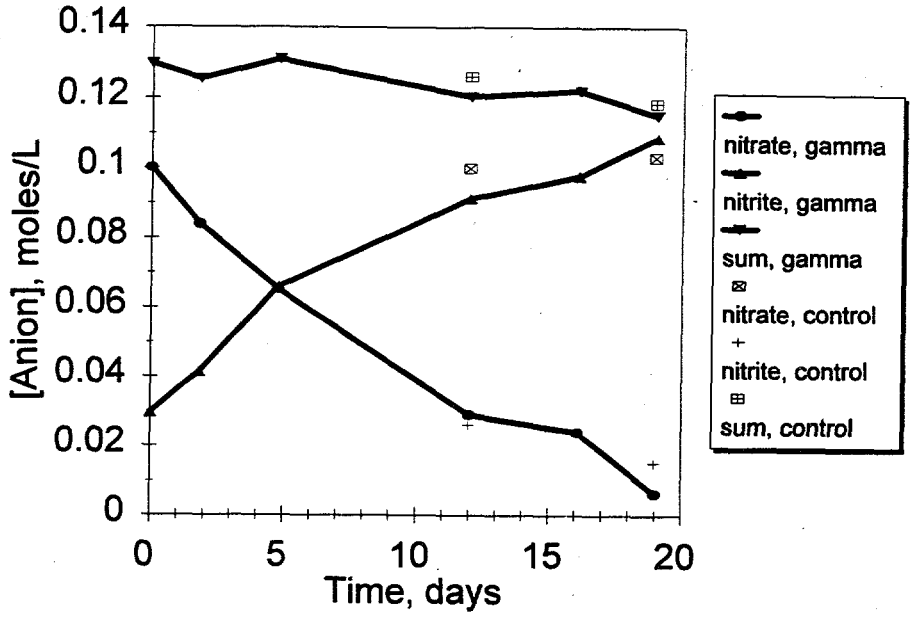

Figure 2.39. Changes in Nitrate and Nitrite Ion Concentrations in a Gamma Field, the Sum of These Concentrations, and Concentrations in Thermal Controls in the Hydrolysis of IF-1B (0.5 g) at 90°C and at a Gamma Dose Rate of 1 x 10^5 rad/h (H1)

and nitrite ion concentrations increased during the course of this experiment and all other hydrolysis experiments in the gamma field. The rate of nitrate decrease was seen to be about the same as the rate of nitrite increase. Also, the sum of these concentrations is about constant for each series of experiments, suggesting that nitrate is radiolytically converted to nitrite. Very little N_2O was detected in the gas phase for these experiments. For controls (not irradiated), nitrate and nitrite ion concentrations remained largely unchanged from the starting concentrations, and N_2O levels were higher.

Figures 2.40 through 2.43 illustrate that the rates of nitrate destruction and nitrite formation increased with increasing applied temperature and gamma dose rate. Curvature in these plots becomes apparent at the higher temperatures tested, and it is possible to fit the data with a first-order model. First-order rate constants for nitrate destruction are shown in Table 2.9. However, the radiation chemistry of NO_3^-/NO_2^- is complicated, and rate constants likely do not represent elementary reactions; mechanistic conclusions should not be drawn without further data. Nevertheless, an Eyring plot of first-order nitrate destruction rate constants at an applied dose rate of 1 x 10^5 rad/h was linear, yielding an activation energy of 30 kJ/mole (Figure 2.44). The gamma dose rate dependence at 90°C was also linear (Figure 2.45). The temperature and gamma dependences can be described by Eqs. (8) and (9), respectively, where k_T is the rate constant at temperature T(K) and at a dose rate of 1 x 10^5 rad/h, and $k_{\gamma,363}$ is the rate constant at 90°C (363K) at a gamma dose rate of γ.

$$\ln(k_T/T) = 1.35 - 3.55 \times 10^3 \cdot 1/T \quad (8)$$

$$k_{\gamma,363} = 8.7 \times 10^{-7} \cdot \gamma + 2.57 \times 10^{-4} \quad (9)$$

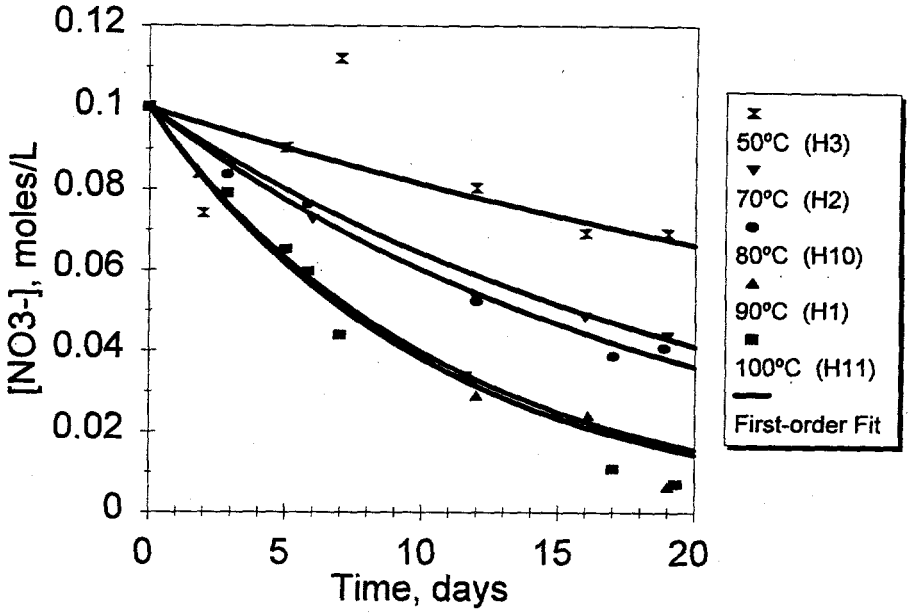

Figure 2.40. Temperature Dependence of Nitrate Destruction in the Hydrolysis of IF-1B (0.5 g) at a Gamma Dose Rate of 1 x 10^5 rad/h

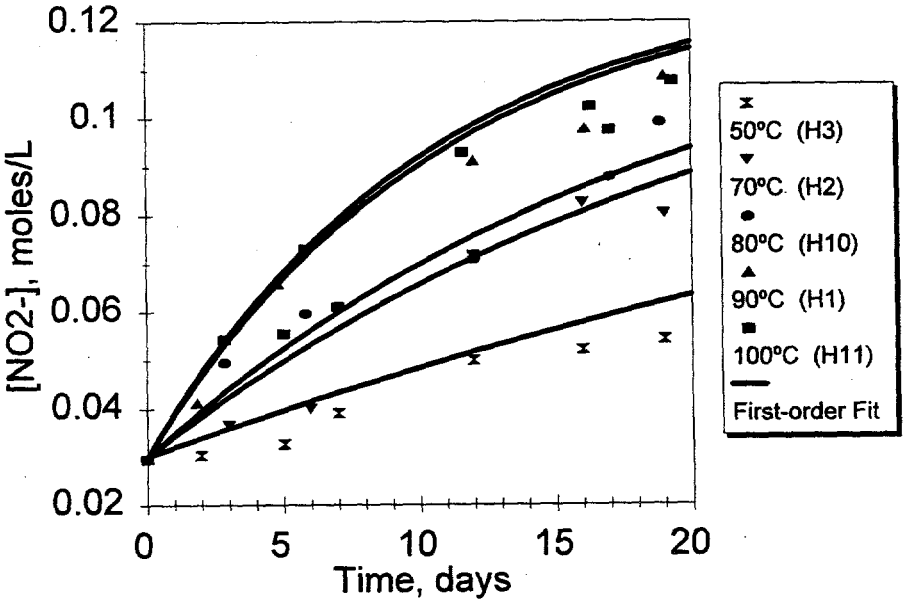

Figure 2.41. Temperature Dependence of Nitrite Formation in the Hydrolysis of IF-1B (0.5 g) at a Gamma Dose Rate of 1 x 10^5 rad/h

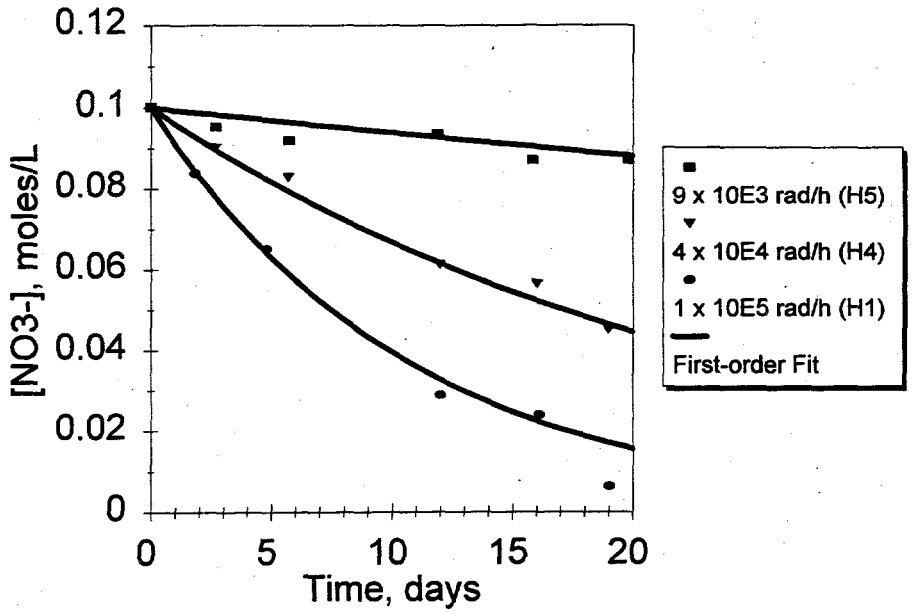

Figure 2.42. Gamma Dose Rate Dependence of Nitrate Destruction in the Hydrolysis of IF-1B (0.5 g) at 90°C

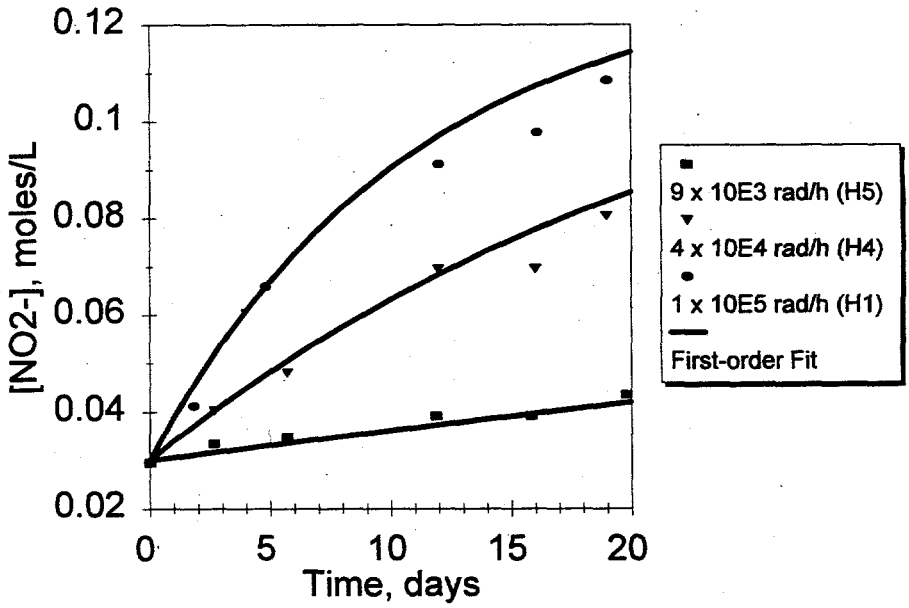

Figure 2.43. Gamma Dose Rate Dependence of Nitrite Formation in the Hydrolysis of IF-1B (0.5 g) at 90°C

Table 2.9. First-Order Rate Constants for Nitrate Destruction in Hydrolysis Experiments at Various Temperatures and Applied Gamma Dose Rates

Experiment Number	Temperature (°C)	Applied Gamma Dose Rate (rad/h)	NO_3^- Destruction Rate Constant (day^{-1})
H3	50	1×10^5	0.020
H2	70	1×10^5	0.044
H10	80	1×10^5	0.051
H1	90	1×10^5	0.093
H11	100	1×10^5	0.097
H4	90	4×10^4	0.040
H5	90	9×10^3	0.0063

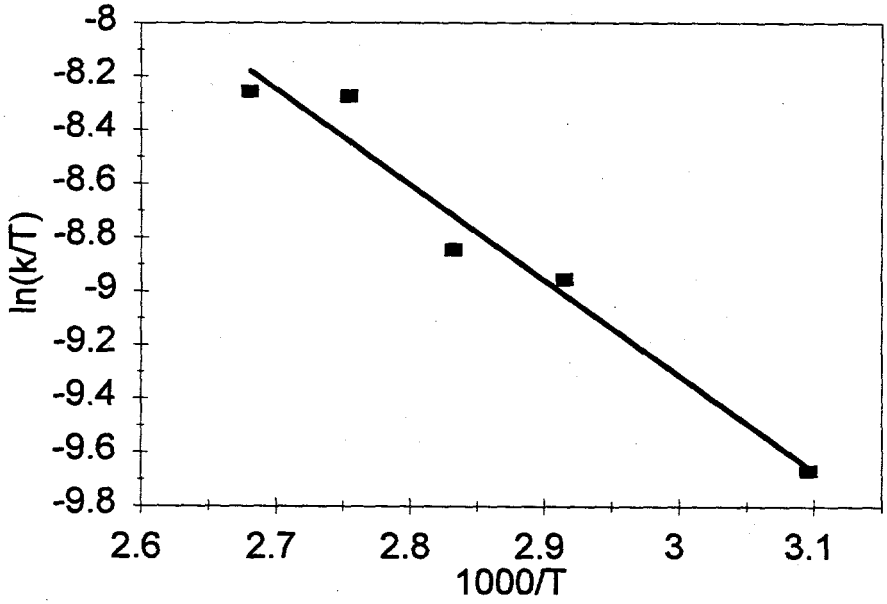

Figure 2.44. Eyring Plot for Nitrate Ion Destruction at a Gamma Dose Rate of 1×10^5 rad/h

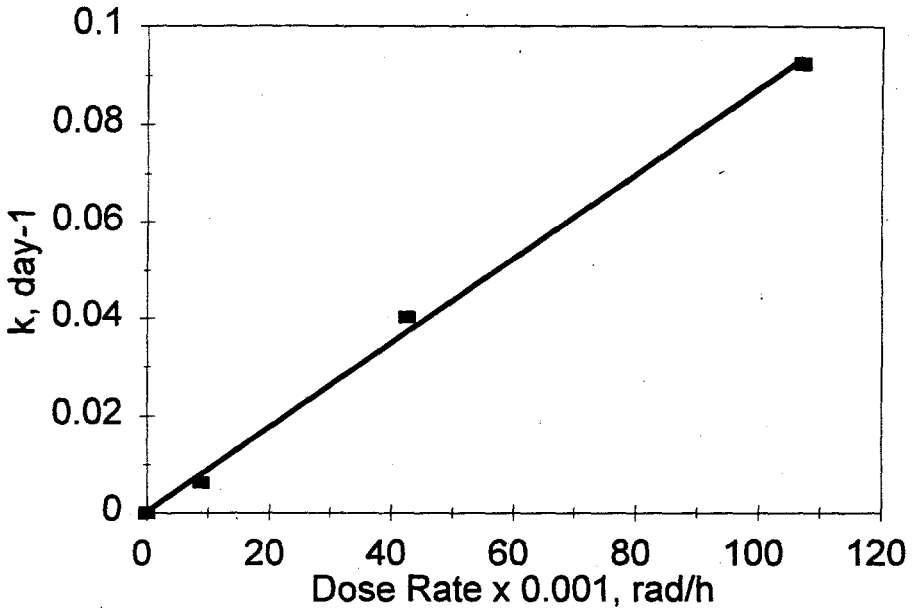

Figure 2.45. Rate Constants for Nitrate Ion Destruction as a Function of Gamma Dose Rate

While the rate of change in nitrate and nitrite concentrations was seen to be dependent on the applied gamma dose rate, the concentrations of these ions at a given integrated dose are independent of dose rate. Figures 2.46 and 2.47 show the changes in concentration of nitrate and nitrite, respectively, as a function of dose (rad) at 90°C. All of the data fall on the same curves regardless of dose rate. Apparently, recombination and termination reactions of radical precursors are not significant prior to reaction with nitrate, and all nitrate reactions eventually form nitrite.

2.5 Hydrolysis of Free Cyanide Ion

The hydrolysis of 0.03 *M* cyanide ion was studied in one set of experiments in 25 mL of 2 *M* NaOH at 90°C and 1 x 10^5 rad/h. The reaction solutions also contained 0.1 *M* $NaNO_3$ and 0.03 *M* $NaNO_2$ to match concentrations in IF-1B hydrolyses. The data points in Figure 2.48 show the concentrations of ammonia formed in the gamma-irradiated solutions and in the one control that was run. The cyanide in the control was completely hydrolyzed after 20 days. In the gamma field, the concentration of ammonia is a function of the rate of production by hydrolysis and the rate of destruction by radiolysis. The rate of production was conservatively estimated by a first-order fit to the initial concentration data, as shown in the figure. The first-order rate constant for ammonia production was estimated to be 0.36 day^{-1}, giving a half life of, at most, 1.9 days under the conditions tested.

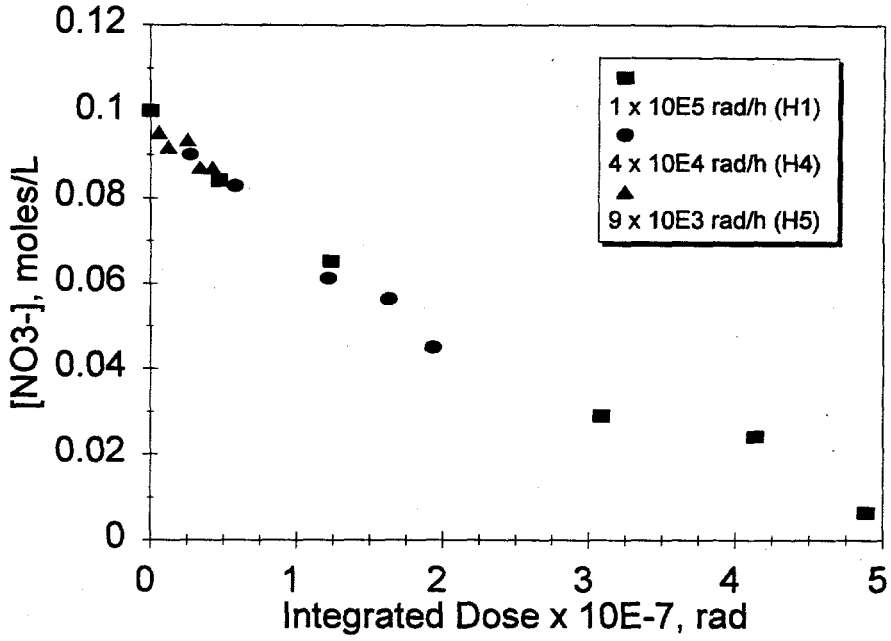

Figure 2.46. Change in Nitrate Ion Concentration as a Function of Gamma Dose at 90°C

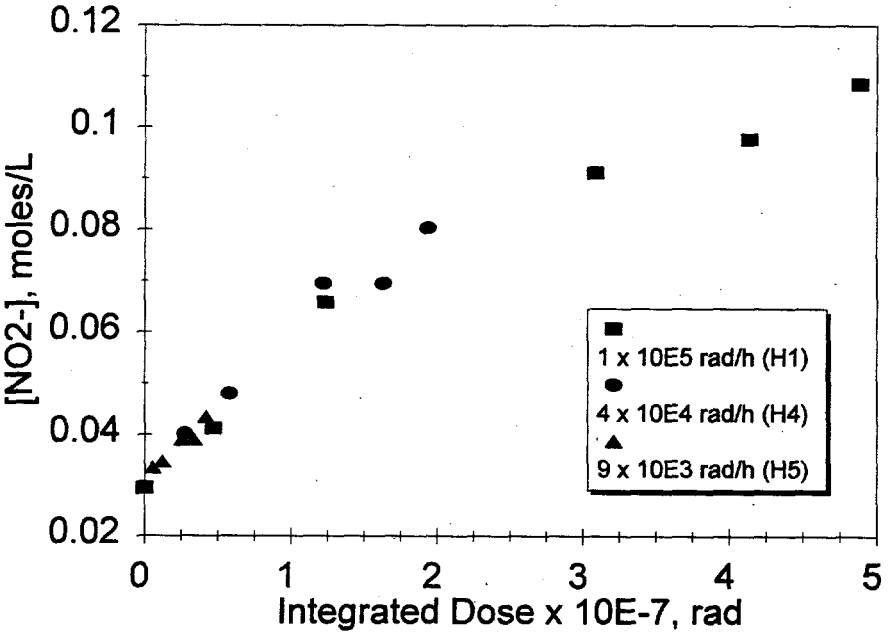

Figure 2.47. Change in Nitrite Ion Concentration as a Function of Gamma Dose at 90°C

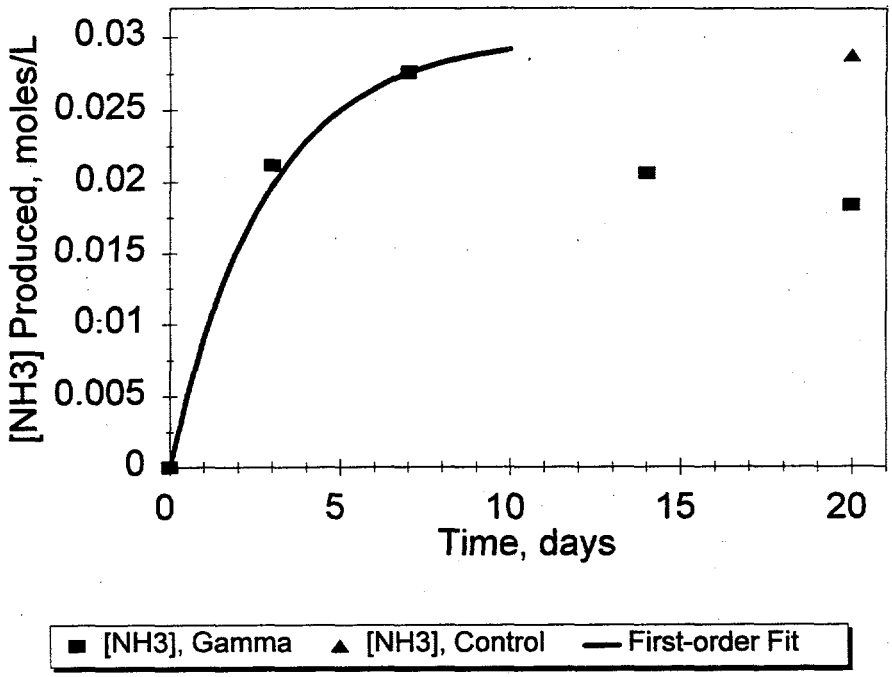

Figure 2.48. Cyanide Hydrolysis at 90°C In and Out of a 1 x 10^5 rad/h Gamma Field and a First-Order Fit

2.6 Dissolution and Hydrolysis of $Ni(CN)_4^{-2}$

Analyses of supernate solutions showed that the nickel concentration increased during aging. For example, the nickel concentration in Experiment H1 (90°C, 1 x 10^5 rad/h), shown in Figure 2.49, increased to a maximum on Day 12, then decreased. The maximum corresponded to about 70 mole% of the nickel initially precipitated as $Ni(OH)_2$ when IF-1B was contacted with 2 *M* NaOH at 90°C, assuming the expected 1:1 stoichiometry between precipitated nickel and dissolved $Fe(CN)_6^{-4}$.

FTIR spectroscopy was used to identify the soluble nickel species. Spectra of supernate samples from selected experiments showed the presence of $Ni(CN)_4^{-2}$ (2123 cm^{-1}). This species was identified by comparison of its spectrum with that of a commercial sample (see Figure 2.34). In addition, the calculated concentrations of this species by FTIR matched the total nickel concentrations determined by AA.

Initially, $Ni(OH)_2$ precipitates when aqueous base is added to the flowsheet material containing $Na_2NiFe(CN)_6$. As hydrolysis takes place, cyanide ion is liberated from iron. Some of the cyanide is converted to ammonia and formate ion, and some survives to redissolve nickel as $Ni(CN)_4^{-2}$. Cyanide

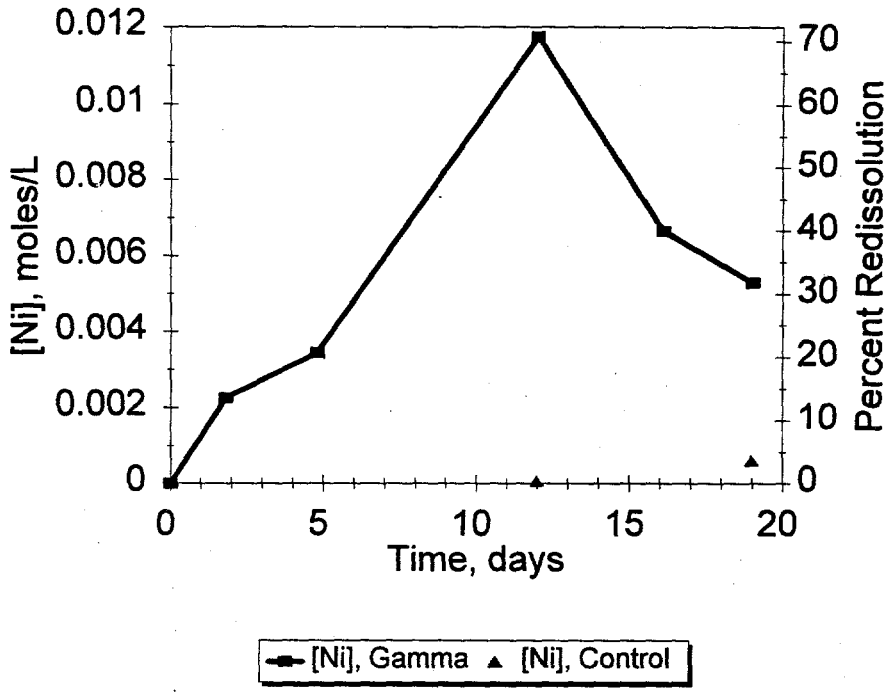

Figure 2.49. Total Nickel Concentration in the Hydrolysis of IF-1B (0.5 g) at 90°C and at a Gamma Dose Rate of 1 x 10^5 rad/h (H1)

redissolution of $Ni(OH)_2$ is consistent with known equilibrium data (Butler 1964; Christensen et al. 1963). Equations (10) through (12) indicate that the formation of $Ni(CN)_4^{-2}$ should be highly favored even in solutions containing several orders of magnitude more hydroxide ion than cyanide ion. Using these reported equilibrium data, the overall equilibrium constant for the formation of $Ni(CN)_4^{-2}$ (Eq. 12) was calculated to be 7.95 x 10^{12} M^{-1}.

$$Ni(OH)_{2\,(s)} \rightleftarrows Ni^{+2} + 2\,OH^- \qquad K_{sp} = 6.31 \times 10^{-18}\ M^{-3} \qquad (10)$$

$$Ni^{+2} + 4\,CN^- \rightleftarrows Ni(CN)_4^{-2} \qquad \beta_4 = 1.26 \times 10^{30}\ M^{-4} \qquad (11)$$

$$Ni(OH)_{2\,(s)} + 4\,CN^- \rightleftarrows Ni(CN)_4^{-2} + 2\,OH^- \qquad K_{eq} = 7.95 \times 10^{12}\ M^{-1} \qquad (12)$$

The feasibility of this series of reactions in the aging solutions was demonstrated in separate control experiments in which excess $Ni(OH)_2$ was stirred with aqueous 2 *M* NaOH solutions containing cyanide ion at concentrations ranging from 0 to 0.1 *M*. More nickel dissolved as the cyanide ion concentration of the reactant solution increased. Figure 2.50 shows the increase in equilibrium nickel concentration versus the measured equilibrium free cyanide ion concentrations, determined by ISE without dilution, in each of the solutions. The equilibrium concentrations are consistent with free cyanide ion, possibly displaced by hydroxide ion or water (L), in equilibrium with a nickel-cyanide complex. Such an equilibrium has the general form of Eq. (13). If the total nickel concentration is much greater than the

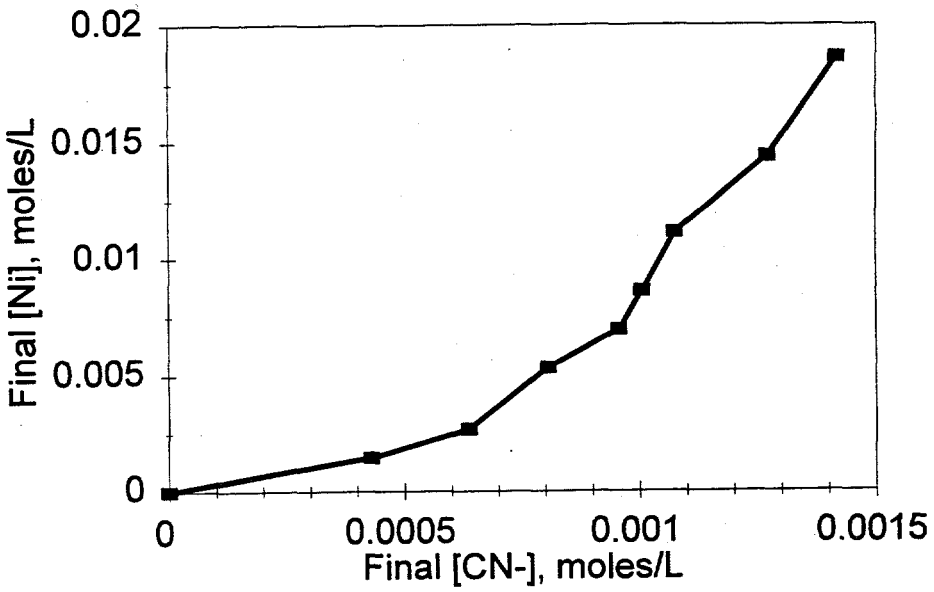

Figure 2.50. Equilibrium Free Cyanide Ion Versus Nickel Concentrations for the Nickel Redissolution Control Experiments

free cyanide ion concentration (a valid assumption), the equilibrium constant is predicted to be proportional to $[CN^-]^2/[Ni]$. Figure 2.51 shows that this relationship holds, meaning that in aging experiments, the free cyanide ion concentration is buffered by nickel cyanide equilibria.

$$Ni(CN)_4^{-2} + L^{-n} \rightleftarrows Ni(CN)_3(L)^{-1-n} + CN^- \quad (13)$$

The hydrolysis of $Ni(CN)_4^{-2}$ was studied because of the importance of this intermediate to the aging process. Experiments were conducted to mimic conditions in IF-1B hydrolysis studies for direct comparison of results. In a typical experiment, hydrolysis of 0.0128 *M* $K_2Ni(CN)_4$ was conducted in 25 mL of 2 *M* NaOH containing 0.1 *M* $NaNO_3$ and 0.03 *M* $NaNO_2$. In one set of experiments, the NO_2^- and NO_3^- were not added and, in another set, the concentration of these ions was increased by a factor of five. The temperature and gamma dose rate conditions tested are listed in Table 2.10.

Ammonia production was linear with time, in some cases to nearly complete conversion. When ammonia production slowed and radiolysis dominated, the measured concentration decreased. As in IF-1B hydrolysis, rate constants were calculated from the slopes of the ammonia production curves (Table 2.10). The rate constants for $Ni(CN)_4^{-2}$ aging are essentially identical to those for IF-1B aging.

Identical rate constants for the hydrolyses of the Ni and Ni/Fe systems are not caused by a rate-determining, free-cyanide hydrolysis step. This is a more facile reaction as indicated by a half life of 1.9 days compared with 9.4 days in $Ni(CN)_4^{-2}$ hydrolysis. Rather, the rate-limiting step is either associated with the reactions that liberate free cyanide (or, less likely, activate bound cyanide) or

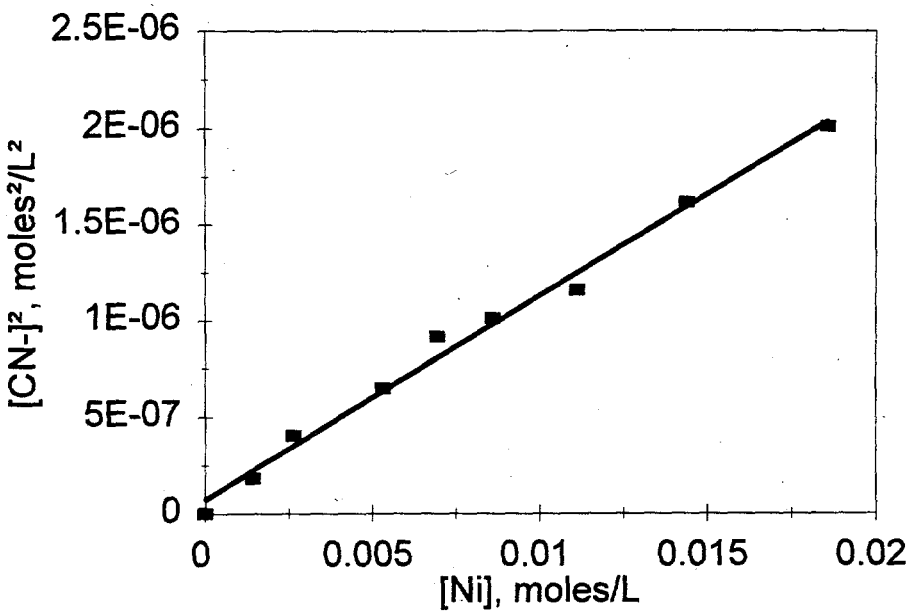

Figure 2.51. Plot of $[CN^-]^2$ Versus [Ni] for Nickel Redissolution Control Experiments at Equilibrium. Data points and linear regression shown.

Table 2.10. Summary of Rate Constants for $Ni(CN)_4^{-2}$ and In-Farm-1B Aging

Temperature (°C)	Dose Rate (rad/h)	$Ni(CN)_4^{-2}$		In-Farm 1B	
		Exp. #	k, *M*/day	Exp. #	k, *M*/day
90	1×10^5	Ni5	5.3×10^{-3}	H1	4.0×10^{-3}
90	1×10^4	Ni3	1.0×10^{-3}	H5	1.1×10^{-3}
100	1×10^5	Ni4	8.6×10^{-3}	H11	8.4×10^{-3}
90	1×10^5	Ni8[a]	4.1×10^{-3}		
90	1×10^5	Ni1[b]	1.9×10^{-3}		

(a) Experiment contained a 5-fold excess of nitrate and nitrite.
(b) Experiment did not contain nitrate or nitrite.

reactions that generate a reactive intermediate involved in ammonia production. Such reactions could involve thermal dissociation of cyanide from the metal complexes or radiolytic generation of oxidizing radicals. It has been reported that nickel cyanide and ferrocyanide have similar thermal hydrolysis behavior (Robuck and Luthy 1989; Tan and Teo 1987).

The $Ni(CN)_4^{-2}$ hydrolysis data also indicate that nitrate and/or nitrite play a role in ammonia production. When these anions were present, ammonia was produced about three times faster than when they were absent (Figure 2.52). The rate constants are given in Table 2.10. The role of NO_3^-/ NO_2^- may be to generate a higher concentration of radical species able to promote aging. For example, in the absence of these ions the main oxidizing species are ·OH and O^-. With these species present, however, the oxidizing $\cdot NO_2$ radical can form from ·OH/O^- by reaction with nitrite (Eq. 14) and from electron scavenging by nitrate (Eq. 15), giving a higher yield of oxidant (Meisel et al. 1991). One possible aging mechanism might involve oxidation of cyanide to cyanogen, which disproportionates in basic solution to form cyanate ion, which in turn hydrolyzes to ammonia (Eqs. 16 through 18). Intermediates such as cyanogen or cyanate were not detected in aged solutions.

$$\cdot OH + NO_2^- \rightarrow \cdot NO_2 + OH^- \quad (14)$$

$$e^-_{(aq)} + NO_3^- + H_2O \rightarrow \cdot NO_2 + 2\,OH^- \quad (15)$$

$$2\,\cdot NO_2 + 2\,CN^- \rightarrow (CN)_2 + 2\,NO_2^- \quad (16)$$

$$(CN)_2 + 2\,OH^- \rightarrow NCO^- + CN^- + 2\,H_2O \quad (17)$$

$$NCO^- + 2\,H_2O \rightarrow NH_3 + HCO_3^- \quad (18)$$

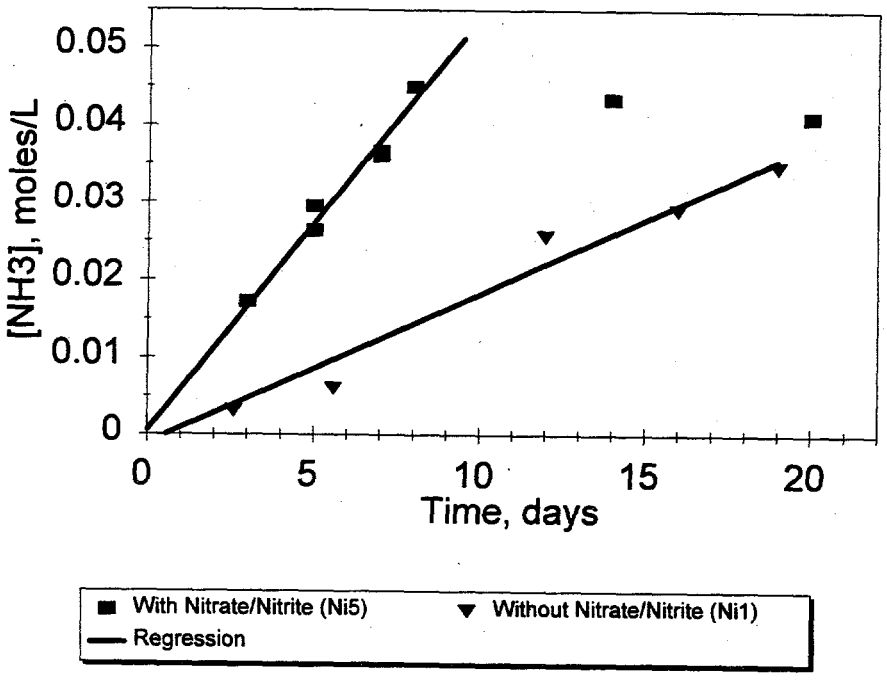

Figure 2.52. Hydrolysis of $Ni(CN)_4^{-2}$ With and Without NO_3^- and NO_2^-

2.7 Hydrolysis of In-Farm Ferrocyanide Flowsheet Material in the Presence of Added Metal Ions

Ferrocyanide tank waste contains many ions that could catalyze or inhibit the aging reactions. For testing these effects on IF-1B aging, some of the more concentrated metal-ions present in the waste were added to reaction solutions, and ammonia production monitored. Metal ions tested were aluminum, bismuth, lead, zinc, and chromium.

2.7.1 Influence of Added Aluminum Cladding Waste Simulant on IF-1B Hydrolysis

Aluminum cladding waste accounted for much of the waste added after ferrocyanide was precipitated in the tanks. A typical composition for neutralized aluminum coating waste generated by the bismuth phosphate process is shown in Table 2.11. A similar waste stream generated in PUREX processing was also added to tanks containing ferrocyanide waste.

The effect of aluminum on the hydrolysis reaction was investigated by preparing a simulant, see Table 2.11, and contacting it with IF-1B. The simulant is similar to one bismuth phosphate process stream; however, concentrations in the tanks would be different depending on the compositions of other waste streams added, and on the composition of the tank contents at the time of addition. Actual aluminum concentrations were probably less than that used in this experiment.

Table 2.11. Neutralized Aluminum Coating Waste Composition Estimated from the Bismuth Phosphate Process and Composition of the Simulant Solution Used for Hydrolysis

Component	Bismuth Phosphate Process Estimated Composition (mole/L)	Composition of Simulant Solution (mole/L)
$NaAlO_2$	1.6	1.6
NaOH	1.5	1.5
$NaNO_3$	0.9	0.9
$NaNO_2$	1.2	1.2
Na_2SiO_3	0.01	0

Besides the aluminum content, the simulant solution differed from solutions used for the IF-1B aging experiments discussed above. The hydroxide ion concentration was lower (1.5 *M* vs. 2 *M*), and the nitrate (0.9 *M* vs. 0.1 *M*) and nitrite ion (1.2 *M* vs. 0.03 *M*) concentrations were higher. The temperature and dose rate were the same as in Experiment H1; i.e., 25 mL of solution were added to IF-1B (0.5 g), heated to 90°C, and irradiated at 1 x 10^5 rad/h for 3 weeks.

Figure 2.53 shows the ammonia production for this experiment in comparison with Experiment H1. The initial stages of reaction appear identical until after about Day 11 when ammonia production in the cladding waste simulant experiment apparently levels off. However, in a separate experiment, aluminum was found to interfere with the ammonia analysis.

The ISE ammonia determination in the presence of aluminum was tested by adding ammonium chloride (0.1 *M* aqueous solution) to basic stock solutions, similar to the neutralized aluminum coating waste simulant used in Experiment H9, to generate five solutions containing ammonia concentrations ranging from 0.2 to 0.8 *M*. The resulting diluted stock solutions also contained aluminum, nitrate, and nitrite, each at concentrations about five times less than in the analogous diluted H9 solutions that were analyzed for ammonia. Results of the ISE determination of ammonia in these five solutions (plus a blank not containing ammonia) are shown in Figure 2.54. The measured [NH_3] was found to be lower than the known concentration by up to 33%, the suppression in electrode reading increasing with increasing [NH_3]. The electrode response was seen to saturate at an observed [NH_3] of about 0.05 *M*. This behavior was very similar to what was observed in Experiment H9; the measured [NH_3] plateaus at about 0.045 *M*. Thus, it appears that the leveling-off in ammonia produced in Experiment H9 was an analytical artifact and not a suppression in hydrolysis activity by aluminum. This behavior may also be due to association of NH_3 with aluminum or precipitation of an aluminum/ammonia complex (Seidell 1958).

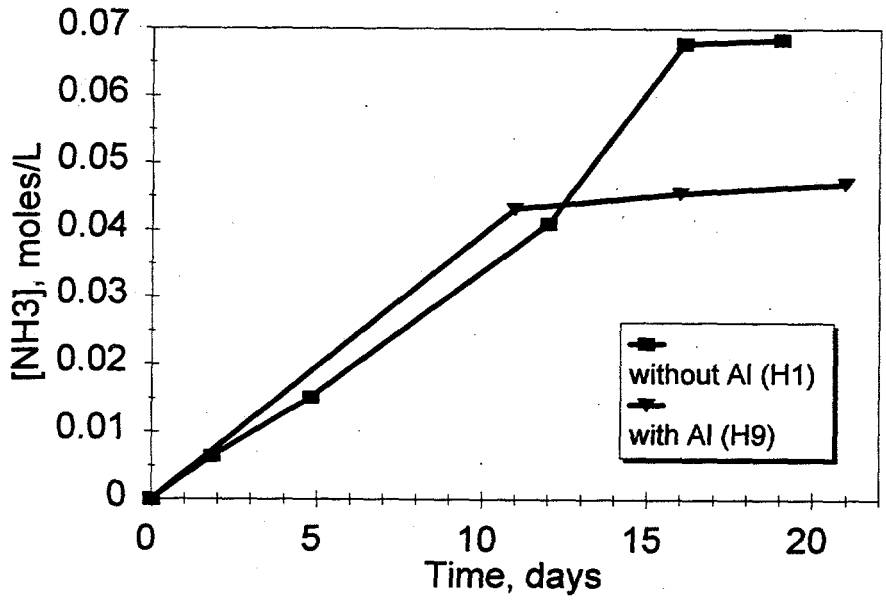

Figure 2.53. Ammonia Production in Hydrolysis of IF-1B (0.5 g) at 90°C and at a Gamma Dose Rate of 1 x 10^5 rad/h in the Absence (H1) and in the Presence (H9) of Aluminum

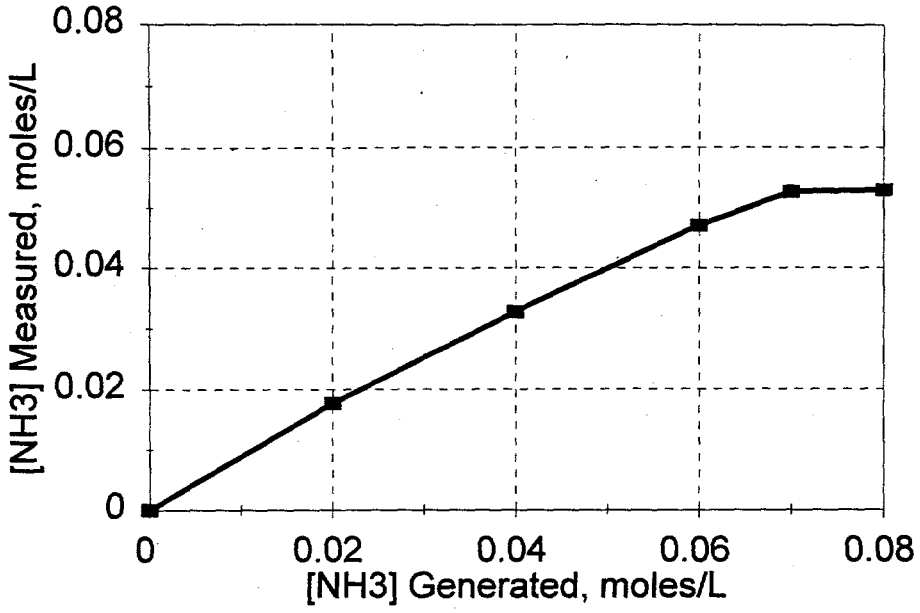

Figure 2.54. Measured Versus Known Ammonia Concentrations in Standard Solutions Containing Aluminum

The conclusion that aluminum does not suppress hydrolysis is supported by the formate concentration, which continued to increase until Day 16, after which the concentration decreased. The continued increase after Day 11, when the measured ammonia concentration plateaued, indicated that hydrolysis was continuing. The same type of behavior was also seen when aluminum was not present at 90°C (Experiment H1) and at other temperatures (see Figure 2.23). The formate concentration data indicated the same or greater extent of aging when aluminum was present.

The changes in total dissolved iron and nickel with time are also consistent with what was observed in Experiment H1 and the reproducibility experiments. The rate constant for the decrease in iron concentration in Experiment H9 was calculated to be 0.088 day^{-1}, very similar to the analogous Experiment H1, in which the rate constant was calculated to be 0.11 day^{-1}.

2.7.2 Influence of Bismuth, Lead, Zinc, and Chromium Ions on IF-1B Hydrolysis

Experiments were conducted to evaluate the influence of several other metal ions present in tank waste on In-Farm flowsheet material hydrolysis. The metal ions investigated were bismuth, lead, zinc, and chromium because analyses of samples from Tanks C-112 and C-109 showed these ions to be present in more than trace level concentrations (Simpson et al. 1993a, b). The maximum average concentrations of chromium and zinc in acid-digested core composite analyses were 241 and 314 $\mu g/g$, respectively. Lead was present in higher concentrations with a maximum average concentration of

9238 μg/g reported for acid-digested C-109 Core 47 composite. In hydrolysis studies, the concentration of the metal ion used was 0.01 g/0.5 g simulant, or over 100 times the measured chromium and zinc concentrations and about twice the measured lead concentration. The metal ions were added here as $BiPO_4$, $Pb(NO_3)_2$, $Cr(NO_3)_3$, and $Zn(OH)_2$.

The experiments were conducted using a similar methodology as experiments discussed in the previous sections, except thick-wall stainless steel vessels (0.93-cm wall thickness) were used and experiments were terminated and sampled after 13 days. Vessels were charged with 0.5 g of IF-1B ferrocyanide simulant, the metal to be tested, and 25 mL of 2 *M* NaOH solution. The vessels were purged with argon, sealed, irradiated at an applied gamma dose rate of about 1 x 10^5 rad/h, and heated to 90°C. Controls in this set of experiments were prepared and handled identically, including gamma irradiation, except they did not contain the added metal ion.

Figure 2.55 shows the results of the 13-day hydrolysis experiments with and without each individually added metal ion, along with data showing the time dependence of hydrolysis, collected under identical conditions in the same vessels. Bismuth, lead, zinc, and chromium ions did not affect the extent of aging of the ferrocyanide flowsheet simulant, as indicated by the amount of ammonia produced after about 13 days in a gamma field. Results of experiments containing these ions were statistically the same as results from identical control experiments, which did not contain additives. Overall, metal ion and control data had a relative standard deviation of about 11%, which indicates that the reproducibility of these experiments was similar to that seen previously.

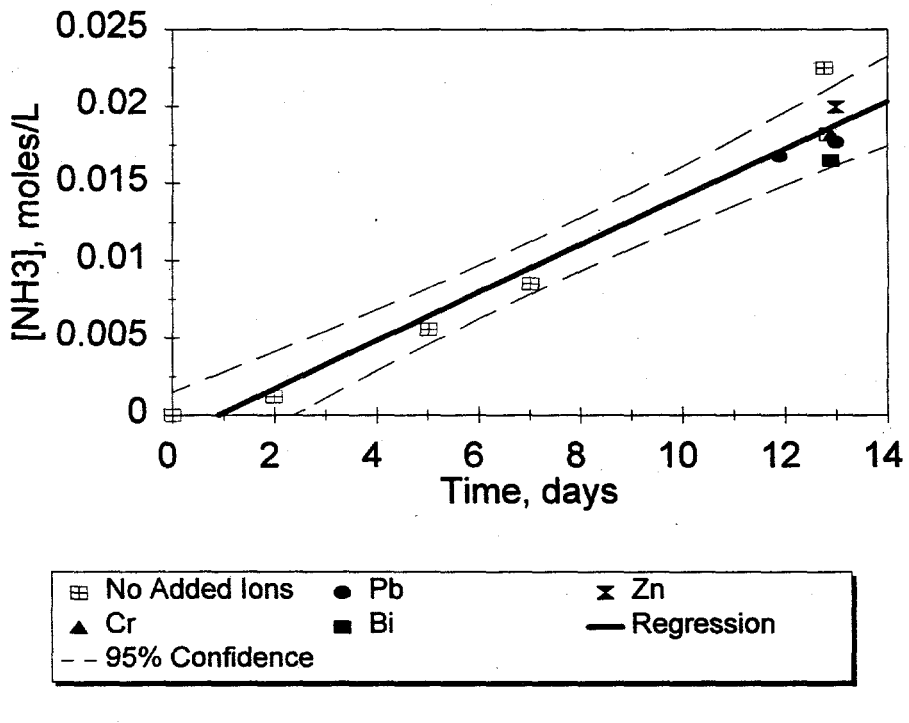

Figure 2.55. Influence of Added Metal Ions on Hydrolysis of IF-1B at 90°C with an Applied Gamma Dose Rate of 1 x 10^5 rad/h

Analyses of the supernate solutions of the metal ion experiments showed that the metal ions were soluble to different extents (Bi, 2%; Cr, 16%; Pb, 67%; and Zn, 81% of the added metal ion dissolved), but the nature of the soluble species is not known. Zinc cyanide is reported to be more easily hydrolyzed than either nickel or iron cyanides (Robuck and Luthy 1989; Tan and Teo 1987) and, if formed, may have no observable influence. The observation that the metal ions were in the solution phase and yet had no appreciable effect on hydrolysis further suggests that these ions play no significant role in aging.

2.8 Aging of IF-1B at 60°C and pH 10

Cesium scavenging was performed at a pH in the range of 8 to 10. If waste added subsequently did not mix thoroughly, or did not contact the sludge through convection (McGrail et al. 1993; McGrail 1994), areas within the ferrocyanide waste might never have been exposed to high pH and may not have been heated to a high temperature. The lower pH may not greatly affect the hydrolysis of dissolved metal cyanides, since it is reported that thermal hydrolysis is unaffected by pH above 9 (Kuhn and Rice 1977). However, the IF-1B flowsheet material has very low solubility in pH 8 to 10 solutions.

In the experiments used to investigate the behavior of such waste, IF-1B (0.5 g) was contacted with a pH 10 carbonate buffer (25 mL) containing 0.77 *M* $NaNO_3$ (to give a 1 *M* [Na^+] solution), gamma-irradiated at an incident dose rate of 4.5 x 10^4 rad/h and heated to 60°C. Four identically prepared solutions were irradiated and sampled individually over a 5.3-month period. Monel vessels were used in this series.

Results of this experiment suggest that even ferrocyanide sludge that did not come into direct contact with highly basic wastes may have aged significantly over decades of storage. The change in ammonia concentration over the course of this experiment is shown in Figure 2.56. Based on the concentration in the 161-day sample, an apparent cyanide conversion of about 18 mole% was seen, not accounting for ammonia radiolysis. A global rate constant for ammonia production of 8.0 x 10^{-5} *M*/day was calculated using the assumption that ammonia production was linear with time, as assumed above.

It is interesting to note that if Eq. (7) is used to calculate a rate constant at the applied gamma dose rate used in this experiment, then adjusted to 60°C using the relationship in Eq. (6), a rate constant of 3.3 x 10^{-5} *M*/day is calculated. Considering that Eqs. (6) and (7) were developed for hydrolysis of dissolved ferrocyanide and that the solubility of IF-1B in pH 10 solution is very low, the agreement is remarkably close. Also surprising is that the measured rate constant for hydrolysis of the insoluble material is larger than that predicted for dissolved IF-1B at the same dose rate and temperature. The effect of gamma radiation leading to higher reactivity of the solids is unknown, but might be caused by direct radiolysis of the solid phase resulting in reactive intermediates at the interface or the formation of more reactive soluble species. If this is so, the extent of aging of solid ferrocyanide materials should be dependent on the applied gamma dose.

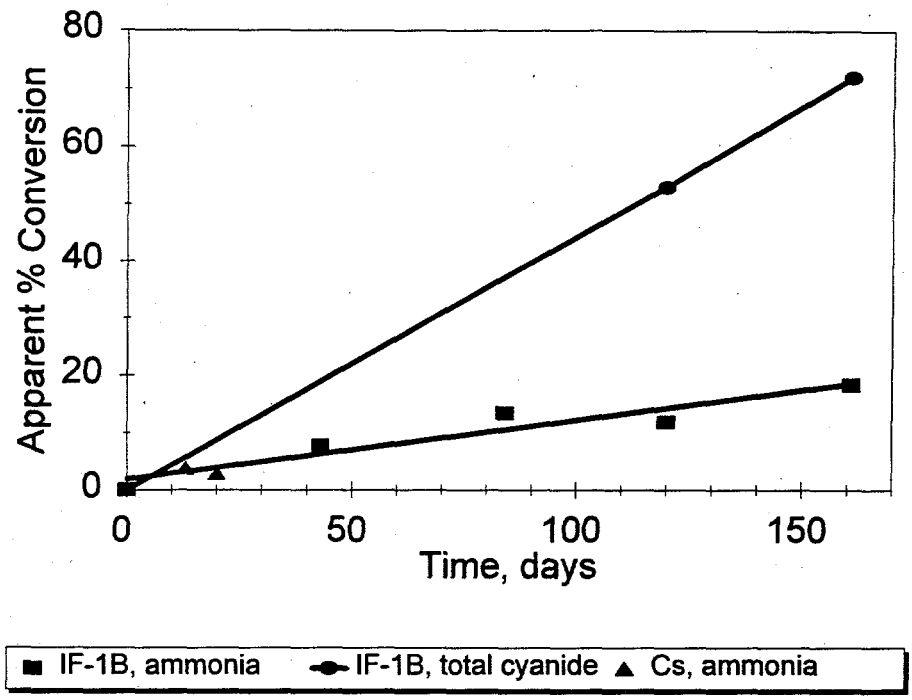

Figure 2.56. Apparent Percent Conversion During Hydrolysis of IF-1B (pH 10, 60°C, 4.5 x 10^4 rad/h) and $Cs_2NiFe(CN)_6$ (2 *M* NaOH, 90°C, 1 x 10^5 rad/h) as Estimated by the Soluble Ammonia Concentration and Total Cyanide Content of the Remaining Solids

Total cyanide analyses of the remaining solids show that the actual conversion was higher than 18% determined from the ammonia data. After 161 days, total cyanide analyses indicated 72% destruction had occurred (Figure 2.56). A rate constant of 3.4 x 10^{-4} *M*/day, or about four times larger than that estimated from the solution ammonia data, was calculated. Radiolysis significantly decreased the solution ammonia concentration over the long reaction time, giving the lower apparent conversion.

2.9 Aging of $Cs_2NiFe(CN)_6$

A majority of the ferrocyanide in the flowsheet materials is in the disodium form with only a small fraction containing cesium, about 0.1% to 0.2% calculated as $Cs_2NiFe(CN)_6$. Aging of $Cs_2NiFe(CN)_6$, which has very low solubility in the 2*M* NaOH solutions used in these, and most other, aging experiments (Bryan et al. 1993; Lilga et al. 1993), was investigated at 90°C and 1 x 10^5 rad/h applied gamma irradiation using the normal procedure described in the experimental section. A "pure" $Cs_2NiFe(CN)_6$ material (0.5 g) was used in these experiments (Rai et al. 1994).

Irradiated simulant solutions contained up to twice the ammonia concentrations as the non-irradiated control. After 20 days, the highest conversion, based on solution ammonia concentration

and on the molecular weight of $Cs_2NiFe(CN)_6$, corresponded to about 4% hydrolysis. This apparent conversion was similar to that observed in IF-1B hydrolysis in pH 10 solution at 60°C, discussed above (Figure 2.56), which, like the cesium compound, is also insoluble in the reaction solution.

2.10 Aging of T-Plant and U-Plant-2 Ferrocyanide Simulants

T-Plant-24 and U-Plant-2-19 ferrocyanide simulants were aged at 90°C in 2*M* NaOH with an applied gamma dose rate of 1 x 10^5 rad/h. Figure 2.57 compares apparent percent conversions based on reported ferrocyanide concentrations in the dried starting materials, T-Plant = 0.278 mmoles $Fe(CN)_6^{-4}$/g dry simulant, U-Plant-2 = 0.26 mmoles $Fe(CN)_6^{-4}$/g dry simulant, and In-Farm = 0.635 mmoles $Fe(CN)_6^{-4}$/g dry simulant. On an apparent percent conversion basis, the reactivity of the T-Plant material is comparable to the In-Farm material aged under the same conditions. The U-Plant-2 flowsheet material is destroyed more rapidly than either of the In-Farm and T-Plant materials, being nearly completely hydrolyzed by Day 13. The decrease in ammonia concentration from Day 13 to Day 20 is caused by radiolysis of the ammonia product. The rate of ammonia radiolysis observed in this experiment (1.3 x 10^{-3} *M*/day) corresponds well with the independently determined rate (1.1 x 10^{-3} *M*/day).

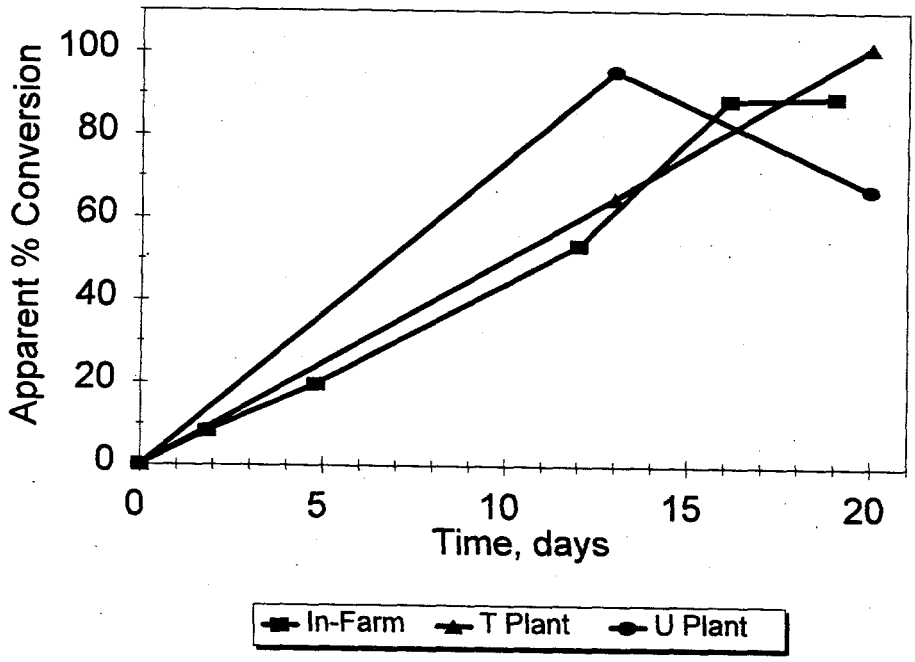

Figure 2.57. Comparison of Apparent Percent Conversion as Indicated by Ammonia Production During Hydrolysis of IF-1B, U-Plant-2, and T-Plant Simulants in 2 *M* NaOH at 90°C with an Applied Gamma Dose Rate of 1 x 10^5 rad/h

3.0 Conclusions

Results of these studies show that aging of simulated wastes in contact with highly caustic solutions does occur, resulting in the dissolution and hydrolysis of ferrocyanide ion. Therefore, any ferrocyanide-bearing sludge in the Hanford Site high-level waste tanks that came in contact with highly caustic waste would have undergone similar aging and should now be significantly depleted of ferrocyanide ion. The results also show that ferrocyanide waste not contacted by a highly caustic solution should also degrade, depending on the strength of the gamma field.

The ultimate products of ferrocyanide aging are ammonia (which is slowly radiolyzed), carbonate, and oxides or hydroxides of iron and nickel. Thus, most of the fuel value in the solid phase is consumed in the process. These studies show that any ferrocyanide tank waste that contacted highly caustic waste also would undergo similar aging processes. The rate of aging is primarily a function of the waste temperature. Tank records indicate that most tanks were at a sufficiently high temperature for a sufficiently long time that significant aging would be expected. Waste samples from C-Farm tanks contained very little, if any, ferrocyanide and may be the best evidence that aging occurs in ferrocyanide tanks.

In general, aging can be described by the following equations. In addition, both ammonia and formate undergo radiolysis. Other reactions and intermediates thought to play a role in aging are discussed below. The complexity of the aging reactions precluded a determination of many mechanistic details, such as the nature of intermediate iron cyanide species and the exact nature of the cyanide hydrolysis reaction itself.

$$Na_2NiFe(CN)_{6\,(s)} + 2\,OH^- \rightleftarrows Fe(CN)_6^{-4} + 2\,Na^+ + Ni(OH)_{2\,(s)}$$

$$Fe(CN)_6^{-4} + x\,L^n \rightleftarrows Fe(CN)_{6-x}L^{-4+x(n+1)} + x\,CN^-$$

$L^n = OH^-, H_2O$, etc.

$$Ni(OH)_{2\,(s)} + 4\,CN^- \rightleftarrows Ni(CN)_4^{-2} + 2\,OH^-$$

$$CN^- + 2\,H_2O \rightleftarrows HCO_2^- + NH_3$$

Sodium nickel ferrocyanide, $Na_2NiFe(CN)_6$, dissolved in aqueous base to give primarily insoluble $Ni(OH)_2$ and soluble $Na_4Fe(CN)_6$. The rate of dissolution of the vendor-prepared material in aqueous base increased with increasing pH. At pH 14, 95% dissolution was observed after 0.5 h. Addition of sodium ion in the form of Na_2SO_4 or $NaNO_3$ suppressed dissolution at pH 13. However, 1 *M* Na^+ in the form of Na_2CO_3, Na_3PO_4, or SST simulant salts (mixed sodium salts of phosphate, carbonate, nitrate, nitrite, sulfate, and hydroxide) resulted in an enhancement of the rate of solubilization. At pH 14 these effects were not seen, dissolution being rapid even in the presence of 4 *M* sodium ion. The rate of dissolution was influenced most by the base concentration.

Dissolution of IF-1A, containing 4.51×10^{-2} moles Cs/moles ferrocyanide, took place more slowly than the vendor material under identical conditions at both pH 13 and pH 14. A material containing a $Cs_2NiFe(CN)_6$ phase (2.3 moles Cs/moles ferrocyanide) was found to be insoluble in up to 4 *M* NaOH after stirring for 144 h. The inhibition of IF-1A dissolution may be caused by an insoluble (or less soluble) $Cs_2NiFe(CN)_6$ or $NaCsNiFe(CN)_6$ phase concentrating at the particle surface as the bulk $Na_2NiFe(CN)_6$ dissolves.

Gamma radiation promoted the destruction of ferrocyanide anion by hydrolysis to ammonia and formate ion. Yields of ammonia were found to be higher in reaction solutions exposed to gamma radiation than in identical solutions that were not irradiated. As the gamma dose rate increased, the rate of hydrolysis also increased. Similarly, increasing temperature increased the rate of ammonia production. As an approximation, ammonia production with time was described as being linear, and rate constants for ammonia production were obtained from the slope of the lines. A linear Eyring relationship was obtained. The change in rate constant with applied gamma dose rate was also found to be linear. The temperature and dose rate relationships were used to predict rate constants for ammonia production at other conditions.

The presence of aluminum did not inhibit ferrocyanide aging. Similarly, no significant effect on aging could be detected when lead, chromium, bismuth, and zinc were present. These metals are found in ferrocyanide tank waste in higher than trace concentrations.

The total concentrations of all soluble iron species decreased in most gamma-irradiated solutions, apparently following a pseudo-first-order rate law. The calculated rate constants for this decrease correlated linearly with temperature and gamma dose rate. For both gamma-irradiated and control solutions, total iron concentrations determined by AA correlated well with ferrocyanide ion concentrations determined by FTIR, indicating that soluble iron was in the form of ferrocyanide ion.

Nickel, initially precipitated as $Ni(OH)_2$ when the flowsheet simulant reacts with aqueous base, redissolved when free cyanide ion, liberated by dissociation from ferrocyanide ion during aging, formed the $Ni(CN)_4^{-2}$ anion. This anion was identified in FTIR spectra of supernate solutions. $Ni(CN)_4^{-2}$ was found to hydrolyze at the same rate as ferrocyanide anion at several temperatures and gamma dose rates tested. Also, the hydrolysis rate was found to be about three times slower in the absence of NO_3^- and NO_2^-, but unaffected by a five-fold increase in initial concentration of these ions.

These results illustrate the importance of NO_3^- and NO_2^- in the aging chemistry and suggest that their function may be to increase the concentration of oxidizing radicals by converting both $\cdot OH/O^-$ and $e^-_{(aq)}$ to $\cdot NO_2$ as shown below. In the absence of these anions, only $\cdot OH/O^-$ will form $\cdot NO_2$. This radical is a good oxidant and will oxidize CN^- to cyanogen, which will disproportionate to cyanate ion in base. Cyanate ion hydrolyzes to form ammonia and bicarbonate or carbonate. Neither cyanogen nor cyanate have been directly observed, but their lifetimes are expected to be short in these solutions.

The following reactions symbolize some of these proposed processes:

$$\cdot OH + NO_2^- \rightarrow \cdot NO_2 + OH^-$$

$$e^-_{(aq)} + NO_3^- + H_2O \rightarrow \cdot NO_2 + 2\,OH^-$$

$$2\,\cdot NO_2 + 2\,CN^- \rightarrow (CN)_2 + 2\,NO_2^-$$

$$(CN)_2 + 2\,OH^- \rightarrow NCO^- + CN^- + 2\,H_2O$$

$$NCO^- + 2\,H_2O \rightarrow NH_3 + HCO_3^-$$

Hydrolysis occurred faster than expected at 60°C in a pH 10 solution. In the gamma field, an ammonia yield of at least 18 mole% was obtained, which is biased low because ammonia radiolysis was not taken into account. Using total cyanide analyses of the remaining unreacted solids, the actual percent destruction was found to be 72%. The rate constant obtained by assuming linear ammonia production could be reasonably approximated using temperature and dose rate relationships developed from experiments conducted in 2 *M* NaOH with dissolved ferrocyanide. The rate constant obtained is unexpectedly high, considering the low solubility of $Na_2NiFe(CN)_6$ at this pH, and indicates that even ferrocyanide sludge that did not come into direct contact with highly basic wastes would also have aged significantly, depending on the gamma field.

Cesium ion generally was not liberated in the hydrolysis experiments and presumably remains associated with ferrocyanide in the form of insoluble cesium-containing nickel ferrocyanide compounds. The exception is in cases where hydrolysis was driven to completion. For example, at 100°C, about 40% of the cesium ion was found in solution.

In competition experiments, cesium uptake by a ferrocyanide simulant not initially containing cesium was found to be more rapid than dissolution. Assuming that caustic waste added to the SSTs contacted the ferrocyanide solids, these results suggest that cesium in the waste probably was immobilized in an insoluble ferrocyanide phase, even though much of the ferrocyanide was likely dissolved by such additions.

4.0 References

Anderson, J. D. 1990. *A History of the 200 Area Tank Farms.* WHC-MR-0132, Westinghouse Hanford Company, Richland, Washington.

Babad, H., D. M. Camaioni, M. A. Lilga, W. D. Samuels, and D. M. Strachan. 1993. *Tank Waste Chemistry - A New Understanding of Waste Aging.* WHC-SA-1694-FP, Westinghouse Hanford Company, Richland, Washington.

Borsheim, G. L., and B. C. Simpson. 1991. *An Assessment of the Inventories of the Ferrocyanide Watchlist Tanks.* WHC-SD-WM-ER-133 Rev. 0, Westinghouse Hanford Company, Richland, Washington.

Bryan, S. A., K. H. Pool, S. L. Bryan, R. L. Sell, and L.M.P. Thomas. 1993. *Ferrocyanide Safety Program. Cyanide Speciation Studies FY 1993 Annual Report.* PNL-8887, Pacific Northwest National Laboratory, Richland, Washington.

Burger, L. L. 1984. *Complexant Stability Investigation, Task 1 - Ferrocyanide Solids.* PNL-5441, Pacific Northwest National Laboratory, Richland, Washington.

Burger, L. L., and R. D. Scheele. 1988. *Interim Report - Cyanide Safety Studies.* PNL-7175, Pacific Northwest National Laboratory, Richland, Washington.

Burger, L. L., and R. D. Scheele. 1991. *The Reactivity of Cesium Nickel Ferrocyanide Towards Nitrate and Nitrite Salts - A Status Report.* PNL-7550, Pacific Northwest National Laboratory, Richland, Washington.

Burger, L. L., D. A. Reynolds, W. W. Schulz, and D. M. Strachan. 1991. *A Summary of Available Information on Ferrocyanide Tank Wastes.* PNL-7822, Pacific Northwest National Laboratory, Richland, Washington.

Burgeson, I. E., S. A. Bryan, and L. E. Burger. 1994. *Cesium Uptake Capacity of Simulated Ferrocyanide Tank Waste.* PNL-10160, Pacific Northwest National Laboratory, Richland, Washington.

Butler, J. N. 1964. *Ionic Equilibrium, A Mathematical Approach.* Addison-Wesley Publishing Company, Inc., Reading, Massachusetts.

Cady, H. H. 1993. *Evaluation of Ferrocyanide/Nitrate Explosive Hazard.* LA-12589-MS, Pacific Northwest National Laboratory, Richland, Washington.

Campbell, D. O., D. D. Lee, and T. A. Dillow. 1990. "Low-Level Liquid Waste Decontamination by Ion Exchange." *Waste Management '90*, ed. R. G. Post. 2:389-398.

Cash, R. J., and J. E. Meacham. 1996. *Quarterly Report on the Ferrocyanide Safety Program for the Period Ending March 31, 1996.* WHC-EP-0474-20, Westinghouse Hanford Company, Richland, Washington.

Christensen, J. J., R. M. Izatt, J. D. Hale, R. T. Pack, and G. D. Watt. 1963. "Thermodynamics of Metal Cyanide Coordination. II. $\Delta G°$, $\Delta H°$, and $\Delta S°$ Values for Tetracyanoniccolate(II) Ion Formation in Aqueous Solution at 25°C." *Inorg. Chem.* 2:337-339.

Crowe, R. D., M. Kummerer, and A. K. Postma. 1993. *Estimation of Heat Load in Waste Tanks Using Average Vapor Space Temperatures.* WHC-EP-0709, Westinghouse Hanford Company, Richland, Washington.

Deaton, D. E. 1990. *Unusual Occurrence-Unreviewed Safety Questions Regarding Tanks Containing Ferrocyanide.* WHC-90-B003-R1, Update 10-22-90, Westinghouse Hanford Company, Richland, Washington.

Dodds, J. N., and W. J. Thompson. 1994. "DXRD Studies of Sodium Nickel Ferrocyanide Reactions with Equimolar Nitrate/Nitrite Salts." *Environ. Sci. Technol.* 28(5):882-889.

Edwards, T. J., G. Maurer, J. Newman, and J. M. Prausznitz. 1978. "Vapor-Liquid Equilibria in Multicomponent Aqueous Solutions of Volatile Weak Electrolytes." *American Institute of Chemical Eng. Journal* 24:966.

Epstein, M., H. K. Fauske, M. D. Crippen, D. R. Dickinson, J. D. McCormack, R. J. Cash, J. E. Meacham, and C. S. Simmons. 1994. *Ferrocyanide Safety Program: An Assessment of the Possibility of Ferrocyanide Sludge Dryout.* WHC-EP-0816, Westinghouse Hanford Company, Richland, Washington.

Goldstein, S., G. Czapski, H. Cohen, and D. Meyerstein. 1988. "Formation and Decomposition of Iron-Carbon σ-Bonds in the Reaction of Iron(III)-Poly(amino carboxylate) Complexes with CO_2^- Free Radicals. A Pulse Radiolysis Study." *J. Am. Chem. Soc.* 110(12):3903-3907.

Hallen, R. T., L. L. Burger, R. L. Hockey, M. A. Lilga, R. D. Scheele, and J. M. Tingey. 1992. *Ferrocyanide Safety Project FY 1991 Annual Report.* PNL-8165, Pacific Northwest National Laboratory, Richland, Washington.

Hepworth, J. L., E. D. McClanahan, and R. L. Moore. 1957. *Cesium Packaging Studies - Conversion of Zinc Ferrocyanide to a Cesium Chloride Product.* HW-48832, Hanford Atomic Products Operation, Richland, Washington.

Jeppson, D. W., and J. J. Wong. 1993. *Ferrocyanide Waste Simulant Characterization.* WHC-EP-0631, Westinghouse Hanford Company, Richland, Washington.

Kuhn, A., and C. Rice. 1977. "Alkaline Hydrolysis of Cyanides, Cyanates, and Dicyan." *Oberflache-Surface* 18:119-123.

Lilga, M. A., M. R. Lumetta, W. F. Riemath, R. A. Romine, and G. F. Schiefelbein. 1992. *Ferrocyanide Safety Project, Subtask 3.4, Aging Studies FY 1992 Annual Report.* PNL-8387, Pacific Northwest National Laboratory, Richland, Washington.

Lilga, M. A., M. R. Lumetta, and G. F. Schiefelbein. 1993. *Ferrocyanide Safety Project, Task 3 Ferrocyanide Aging Studies FY 1993 Annual Report.* PNL-8888, Pacific Northwest National Laboratory, Richland, Washington.

Lilga, M. A., E. V. Alderson, D. J. Kowalski, M. R. Lumetta, and G. F. Schiefelbein. 1994. *Ferrocyanide Safety Project, Task 3 Ferrocyanide Aging Studies FY 1994 Annual Report.* PNL-10126, Pacific Northwest National Laboratory, Richland, Washington.

Lilga, M. A., E. V. Alderson, R. T. Hallen, M. O. Hogan, T. L. Hubler, G. L. Jones, D. J. Kowalski, M. R. Lumetta, G. F. Schiefelbein, and M. R. Telander. 1995. *Ferrocyanide Safety Project, Ferrocyanide Aging Studies FY 1995 Annual Report.* PNL-10713, Pacific Northwest National Laboratory, Richland, Washington.

Loewenschuss, H. 1982. "Metal-Ferrocyanide Complexes for the Decontamination of Cesium from Aqueous Radioactive Waste." *Radioactive Waste Management* 2(4):327-341.

Loos-Neskovic, C., and M. Fedoroff. 1989. "Fixation Mechanisms of Cesium on Nickel and Zinc Ferrocyanides." *Solvent Extraction and Ion Exchange* 7(1):131-158.

Loos-Neskovic, C., M. Fedoroff, and E. Garnier. 1989. "Preparation, Composition and Structure of Some Nickel and Zinc Ferrocyanides: Experimental Results." *Talanta* 36(7):749-759.

Loos-Neskovic, C., M. Fedoroff, E. Garnier, and P. Gravereau. 1984. "Zinc and Nickel Ferrocyanides: Preparation, Composition and Structure." *Talanta* 31(12):1133-1147.

Loos-Neskovic, C., M. Fedoroff, and G. Revel. 1976. "Influence of Sodium Content of Nickel Ferrocyanides on the Retention of Alkaline Ions." *Radiochem. Radioanal. Letters* 26(1):17-26.

Loos-Neskovic, C., M. Fedoroff, and M. O. Mecherri. 1990. "Ion Fixation Kinetics and Column Performance of Nickel and Zinc Hexacyanoferrates(II)." *Analyst* 115:981-986.

McGrail, B. P. 1994. *Computational Analysis of Coupled Fluid, Heat, and Mass Transport in Ferrocyanide Single-shell Tanks: FY 1994 Interim Report. Ferrocyanide Tank Safety Project.* PNL-10163, Pacific Northwest National Laboratory, Richland, Washington.

McGrail, B. P., D. S. Trent, G. Terrones, J. D. Hudson, and T. E. Michener. 1993. *Computational Analysis of Fluid Flow and Zonal Deposition in Ferrocyanide Single-shell Tanks.* PNL-8876, Pacific Northwest National Laboratory, Richland, Washington.

McLaren, J. M. 1993. *Ferrocyanide Safety Program: Updated Thermal Analysis Model for Ferrocyanide Tanks with Application to Tank 241-BY-104.* WHC-EP-0669, Westinghouse Hanford Company, Richland, Washington.

McLaren, J. M. 1994. *Ferrocyanide Safety Program: Thermal Analysis of Ferrocyanide Tanks, Group I.* WHC-EP-0729, Westinghouse Hanford Company, Richland, Washington.

McLaren, J. M., and R. J. Cash. 1993. *Ferrocyanide Safety Program: Heat Load and Thermal Characteristics Determination for Selected Tanks.* WHC-EP-0638, Westinghouse Hanford Company, Richland, Washington.

Meacham, J. E., R. J. Cash, D. R. Dickinson, F. R. Reich, J. M. Grigsby, A. K. Postma, and M. A. Lilga. 1996. *Assessment of the Potential for Ferrocyanide Propagating Reaction Accidents.* WHC-SD-WM-SARR-038, Rev. 1, Westinghouse Hanford Company, Richland, Washington.

Meacham, J. E., R. J. Cash, and G. T. Dukelow. 1994a. *Quarterly Report on the Ferrocyanide Safety Program for the Period Ending June 30, 1994.* WHC-EP-0474-13, Westinghouse Hanford Company, Richland, Washington.

Meacham, J. E., R. J. Cash, G. T. Dukelow, H. Babad, and J. W. Buck. 1994b. *Data Requirements for the Ferrocyanide Safety Issue Developed Through the Data Quality Objectives Process.* WHC-SD-WM-DQO-007, Westinghouse Hanford Company, Richland, Washington.

Meisel, D., H. Diamond, E. P. Horwitz, C. D. Jonah, M. S. Matheson, M. C. Sauer, Jr., and J. C. Sullivan. 1991. *Radiation Chemistry of Synthetic Waste.* ANL-91/40, Argonne National Laboratory, Argonne, Illinois.

Norton, J. D., and L. R. Pederson. 1994. *Ammonia in Simulated Hanford Double-shell Tank Wastes: Solubility and Effects on Surface Tension.* PNL-10173, Pacific Northwest National Laboratory, Richland, Washington.

Parra, S. A. 1994. *Integrated Beta and Gamma Radiation Dose Calculations for the Ferrocyanide Waste Tanks.* WHC-SD-WM-TI-634, Rev. 0, Westinghouse Hanford Company, Richland, Washington.

Peach, J. D. 1990. "Consequences of Explosion of Hanford's Single-shell Tanks Are Understated." Letter B-241479 dated October 1990 to M. Synar, GAO/RCED-91-34, General Accounting Office, Washington, D.C.

Postma, A. K., J. E. Meacham, G. S. Barney, G. L. Borsheim, R. J. Cash, M. D. Crippen, D. R. Dickinson, J. M. Grigsby, D. W. Jeppson, M. Kummerer, J. M. McLaren, C. S. Simmons, and B. C. Simpson. 1994. *Ferrocyanide Safety Program: Safety Criteria for Ferrocyanide Watch List Tanks*. WHC-EP-0691, Westinghouse Hanford Company, Richland, Washington.

Rai, D., A. R. Felmy, S. C. Smith, and J. L. Ryan. 1994. *Solubility of Ferrocyanide Compounds*, PNL-10150, Pacific Northwest National Laboratory, Richland, Washington.

Robuck, S. J., and R. G. Luthy. 1989. "Destruction of Iron-Complexed Cyanide by Alkaline Hydrolysis." *Wat. Sci. Tech.* 21:547-558.

Rocklin, R. D., and E. L. Johnson. 1983. "Determination of Cyanide, Sulfide, Iodide, and Bromide by Ion Chromatography with Electrochemical Detection." *Anal. Chem.* 55:4-7.

Scheele, R. D., and H. H. Cady. 1992. *Preliminary Safe-handling Experiments on a Mixture of Cesium Nickel Ferrocyanide and Equimolar Sodium Nitrate/Nitrite*. PNL-7928, Pacific Northwest National Laboratory, Richland, Washington.

Scheele, R. D., L. L. Burger, J. M. Tingey, S. A. Bryan, G. L. Borsheim, B. C. Simpson, R. J. Cash, and H. H. Cady. 1991. "Ferrocyanide-containing Waste Tanks: Ferrocyanide Chemistry and Reactivity." PNL-SA-19924, presented at *Environmental Restoration 1991*, University of Arizona, Tucson, Arizona.

Scheele, R. D., L. L. Burger, J. M. Tingey, R. T. Hallen, and M. A. Lilga. 1992. "Chemical Reactivity of Potential Ferrocyanide Precipitates in Hanford Tanks with Nitrates and Nitrites." In *Proceedings of Waste Management '92*, Tucson, Arizona.

Seidell, A. 1958. *Solubilities of Inorganic and Metal Organic Compounds, 4th Edition*, Vol. 1, American Chemical Society, Washington, D.C.

Sheridan, T. R. 1994. *Closure of the Ferrocyanide Unreviewed Safety Question*, (letter 9401180B/94-SST-052 to A. L. Trego, WHC, March 4), U.S. Department of Energy, Richland, Washington.

Simpson, B. C., G. L. Borsheim, and L. Jensen. 1993a. *Tank Characterization Report: Tank 241-C-112*. WHC-EP-0640, Rev. 1, Westinghouse Hanford Company, Richland, Washington.

Simpson, B. C., G. L. Borsheim, and L. Jensen. 1993b. *Tank Characterization Report: Tank 241-C-109*. WHC-EP-0668, Westinghouse Hanford Company, Richland, Washington.

Singleton, D. L., G. Paraskevopoulos, R. S. Irwin, G. S. Jolly, and D. J. McKenney. 1988. "Rate and Mechanism of the Reaction of Hydroxyl Radicals with Formic and Deuteriated Formic Acids." *J. Am. Chem. Soc.* 110(23):7786-7790.

Tan, T. C., and W. K. Teo. 1987. "Destruction of Cyanides by Thermal Hydrolysis." *Plating and Surface Finishing* 74:70-73.

U.S. Department of Energy (DOE). 1987. *Final Environmental Impact Statement, Disposal of Hanford Defense High-Level, Transuranic, and Tank Wastes.* DOE-EIS-0113, Washington, D.C.

Distribution

No. of Copies

OFFSITE

Charles S. Abrams
1987 Virginia
Idaho Falls, ID 83404

Shirley Campbell-Grizzel
U.S. Department of Energy
EH-15, Trevion II
12800 Middlebrook Road
Germantown, MD 20874

Cynthia Hilland
U.S. Department of Energy
656 Quince Diamond Road
Room 235, EM-20.1
Gaithersburg, MD 20879

George E. Schmauch
Air Products & Chemicals, Inc.
7201 Hamilton Blvd.
Allentown, PA 18195-1501

Kamal K. Bandyopadhyay
Brookhaven National Laboratory
Upton, NY 11973

David O. Campbell
102 Windham Road
Oak Ridge, TN 37830

Fred N. Carlson
6965 North 5th West
Idaho Falls, ID 83401

No. of Copies

Gary Powers
Design Science, Inc.
163 Witherow Road
Sewickley, PA 15143

2 Fauske and Associates, Inc.
16W070 W. 83rd St.
Burr Ridge, IL 60521
Attn: Hans K. Fauske
Michael Epstein

Gregory R. Choppin
Florida State University
Department of Chemistry B-164
Tallahassee, FL 32306

Melvin W. First
Harvard University
295 Upland Avenue
Newton Highlands, MA 02161

Chester Grelecki
Hazards Research Corporation
200 Valley Road, Suite 301
Mt. Arlington, NJ 07856

Billy Hudson
202 Northridge Court
Lindsborg, KA 67456

Thomas S. Kress
102-B Newridge Road
Oak Ridge, TN 37839

No. of Copies

2 Los Alamos National Laboratory
P.O. Box 1663
Los Alamos, NM 87545
Attn: Steve F. Agnew
Thomas E. Larson

Mujid S. Kazimi
MIT/Dept of Nuclear Eng.
77 Massachusetts Avenue
Room 24-102
Cambridge, MA 02139

J. Louis Kovach
Nuclear Consulting Services, Inc.
P.O. Box 29151
Columbus, OH 43229-0151

2 Oak Ridge National Laboratory
P.O. Box 2008
Oak Ridge, TN 37831
Attn: Emory D. Collins, MS-6385
Charles W. Forsberg, MS-6495

2 Arlin K. Postma
G & P Consulting, Inc.
3640 Ballard Road
The Dalles, OR 97338

William R. Prindle
1556 Crestline Drive
Santa Barbara, CA 93105

Andrew S. Veletsos
Rice University
5211 Paisley
Houston, TX 77096

No. of Copies

2 Sandia National Laboratory
P.O. Box 5800
Albuquerque, NM 87185
Attn: Scott E. Slezak, MS-0741
Dana Powers, MS-0744

Alfred Schneider
5005 Hidden Branches Drive
Dunwoody, GA 30338

3 Paul Hogroian
Science Applications International Corporation
20300 Century Blvd., Suite 200-B
Germantown, MD 20874

Robert C. King
State of Washington
Department of Ecology
P. O. Box 47600
Olympia, WA 98504-7600

Alex Stone
1315 W. 4th Avenue
Kennewick, WA 99336

6 U.S. Department of Energy
EM-36, Trevion II
12800 Middlebrook Road
Germantown, MD 20874
Attn: Harry Calley (4)
Maureen Hunemuller
Ken Lang

No. of Copies

U.S. Department of Energy
Forrestal Building
1000 Independence Avenue SW
Washington, DC 20585
Attn: Shirley Campbell, EH-71
John Kaysak, EM-25

Thomas C. Temple
U.S. Department of Energy
Savannah River Operations Office
P.O. Box A
Aiken, SC 29808

Bruce R. Kowalski
University of Washington
Center for Process Analytical Chemistry
Chemistry Department BG-10
Seattle, WA 98195

Joseph S. Byrd
University of South Carolina
Department of Electrical and Computer Engineering
Swearingen Engineering Center
Columbia, SC 29208

Frank L. Parker
Vanderbilt University
P.O. Box 1596, Station B
Nashville, TN 37235

Donald T. Oakley
Waste Policy Institute
555 Quince Orchard Road,
Suite 600
Gaithersburg, MD 20878-1437

No. of Copies

FOREIGN

Claude Musikas
Consultant
5, Avenue Moissan,
91440 Bures/Yvette,
FRANCE

ONSITE

10 **Richland Operations Office**

W. F. Hendrickson	S7-54
D. H. Irby (2)	S7-54
M. F. Jarvis (2)	K8-50
A. G. Krasopoulos	A4-81
J. C. Peschong	S7-54
Public Reading Room	H2-53
RL Docket File (2)	B1-17

32 **Westinghouse Hanford Company**

H. Babad	S7-14
J. B. Billetdeaux	S7-15
W. S. Callaway	S3-90
R. J. Cash (5)	S7-14
M. D. Crippen	L5-31
R. D. Crowe	H0-32
M. L. Dexter	R1-51
D. R. Dickinson	L5-31
G. T. Dukelow	S7-14
S. J. Eberlein	R2-12
J. M. Grigsby	A3-37
M. N. Islam	R3-08
D. W. Jeppson	L5-31
N. W. Kirch	R2-11
C. A. Kuhlman	B3-30

No. of Copies		No. of Copies	
L. L. Lockrem	S3-90	D. M. Camaioni	K2-44
J. E. Meacham (2)	S7-14	J. A. Campbell	P8-08
N. J. Milliken	A3-37	S. D. Colson	K9-62
S. R. Moreno	B3-06	S. R. Gano	P8-38
F. R. Reich	L5-55	S. C. Goheen	P8-08
E. F. Riedel	S3-90	R. T. Hallen (2)	P8-38
B. C. Simpson	R2-12	M. O. Hogan	P8-38
Central Files	A3-88	T. L. Hubler	P8-38
Correspondence Processing	A3-01	M. A. Lilga (10)	P8-38
EDMC	H6-08	M. R. Lumetta	P8-38
OSTI (2)	G3-11	L. G. Morgan	K9-62
		L. R. Pederson	K2-44
36 **Pacific Northwest National Laboratory**		R. A. Romine	K2-40
		R. D. Scheele	P7-25
E. G. Baker	P8-38	C. W. Stewart	K7-15
J. W. Brothers	K9-20	M. R. Telander	P8-15
S. A. Bryan	P7-25	Information Release (7)	